



MICROFRACTURING OF ROCK
IN COMPRESSION

by

CHRISTOPHER HENRY SCHOLZ

B.S. Geol. Eng., University of Nevada
(1964)

SUBMITTED IN PARTIAL FULFILLMENT OF THE
REQUIREMENTS FOR THE DEGREE OF
DOCTOR OF PHILOSOPHY

at the

MASSACHUSETTS INSTITUTE OF TECHNOLOGY

September, 1967

Signature of Author
Department of Geology and Geophysics
August 21, 1967

Certified by
Thesis Supervisor

Accepted by
Chairman,
Departmental Committee on Graduate Students

ABSTRACT

TITLE: Microfracturing of Rock in Compression

AUTHOR: Christopher H. Scholz

Submitted to the Department of Geology and Geophysics on August 21, 1967 in partial fulfillment of the requirement for the degree of Doctor of Philosophy at the Massachusetts Institute of Technology.

When rock is deformed in compression, small scale cracking, i.e. microfracturing, occurs. Each microfracture event radiates elastic energy in a manner analogous to earthquakes. A broad study of many aspects of the microfracturing process was made by detecting and analyzing these radiations with a new type of instrumental system. Microfracturing activity was compared with macroscopic strain measurements and it was found that it is closely related to the inelastic stress-strain properties of brittle rock. Dilatancy could be entirely attributed to microfracturing. The microfracturing that occurs during fractional sliding or ductile deformation are very similar but differ markedly from that which occurs in brittle rock. Marble was found to undergo a transition from cataclastic to fully plastic flow as the confining pressure was increased in triaxial tests. A statistical model of rock deformation which treats rock as an inhomogeneous brittle material was developed and found to predict the observed microfracturing behavior. Because the statistics of microfractures are very similar to that of earthquakes, the theory was generalized to describe crustal deformation as well. The frequency-magnitude relation of microfractures was found to be similar to that of earthquakes. The b parameter in the Gutenberg and Richter relation was studied as a function of rock type, stress, and confining pressure and found to depend primarily on stress. The propagation properties of fractures were introduced into the model and the frequency-magnitude relation deduced. Evidence suggest that creep in brittle rock at low temperature is produced by time dependent microfracturing. Based on a model of static fatigue in an inhomogeneous medium, a transient creep law for rock was derived and found to agree with all present observations. In order to study rock fracture, 22 of the largest microfractures were located in space with a multi-transducer array. It was found that just prior to fracture, where a rapid acceleration of activity occurs, microfractures cluster on the plane which corresponds to the

eventual fault.

Thesis supervisor: William F. Brace

Title: Professor of Geology

TABLE OF CONTENTS

ABSTRACT	2
INTRODUCTION	6
CHAPTER 1 Microfracturing and the Inelastic Deformation of Rock	
Introduction	19
Experimental Technique	20
Observations	27
Theory and Discussion	51
CHAPTER 2 The Mechanism of Creep in Brittle Rock	
Introduction	65
Analysis	69
Discussion	85
CHAPTER 3 The Frequency-Magnitude Relation of Microfracturing and its Relation to Earthquakes	
Introduction	90
Experimental Technique	93
Experimental Observations	95
Theory	113
Conclusions	124
CHAPTER 4 An Experimental Study of the Fracturing Process in Brittle Rock	

Introduction	129
Experimental Technique	132
Experimental Observations	137
Discussion	149
CONCLUSIONS	152
ACKNOWLEDGEMENTS	155
BIBLIOGRAPHY	156
APPENDIX I End Effects	165
APPENDIX II Pulse Shaper	168
APPENDIX III Method for Calculating Event Locations	171
APPENDIX IV Creep Experiments	174
BIOGRAPHY OF THE AUTHOR	177

INTRODUCTION

The processes which have and are now occurring within the earth are of profound interest, yet our understanding of them will not be full until a more fundamental knowledge of the mechanical properties of rock is obtained. Of particular interest are the processes which occur within the crust, and affect man directly, such as earthquakes. The properties of rock under crustal conditions have been extensively studied, since crustal temperatures and pressures are readily accessible in the laboratory.

Under shallow crustal temperature and pressure conditions, silicate rocks have in general been found to be brittle materials. That is, they fail by sudden catastrophic fracture resulting in total loss of cohesion after undergoing a very small elastic strain. Although rock strength has been extensively studied, the actual processes which occur during deformation and fracture of brittle rock are poorly understood. The strength of rock, as of all brittle solids, is anomalous in that it is several orders of magnitude less than the theoretical strength, or stress required to break atomic bonds. The classical approach of Griffith [1924] was that cracks within the body produce very high stress concentrations, so that the theoretical strength will be reached at the tip of such a crack even when the applied stresses are a great deal less. He then

proposed that failure occurs when the theoretical strength is thus first exceeded. Essentially, then, brittle fracture should occur by the propagation of a single crack through the body.

Although the Griffith fracture criterion has been to a large extent verified for such brittle materials as glasses, a large body of evidence has recently been found to suggest that rock in the brittle range behaves in quite a different manner.

Unlike many brittle materials, rocks are not usually linearly elastic up to fracture. The stress-strain behavior of most silicate rocks at low temperatures and pressures is typically nonlinear and inelastic, and generally shows the same basic properties. Figure 1a is an idealized axial stress-strain curve for rock under uniaxial compression. At low stress, the curve is concave upwards; that is, the modulus increases with stress. Walsh [1965a, 1965b, 1965c] has made an extensive theoretical study of this behavior and found that it is due to the closing of pre-existing cracks. After a few hundred bars, the effective cracks are all closed and the rock becomes essentially linearly elastic. At stresses above about half the breaking strength, however, the modulus decreases and the curve is concave downwards until fracture. Concurrent with this latter behavior, the strains normal to the stressed direction begin increasing to a

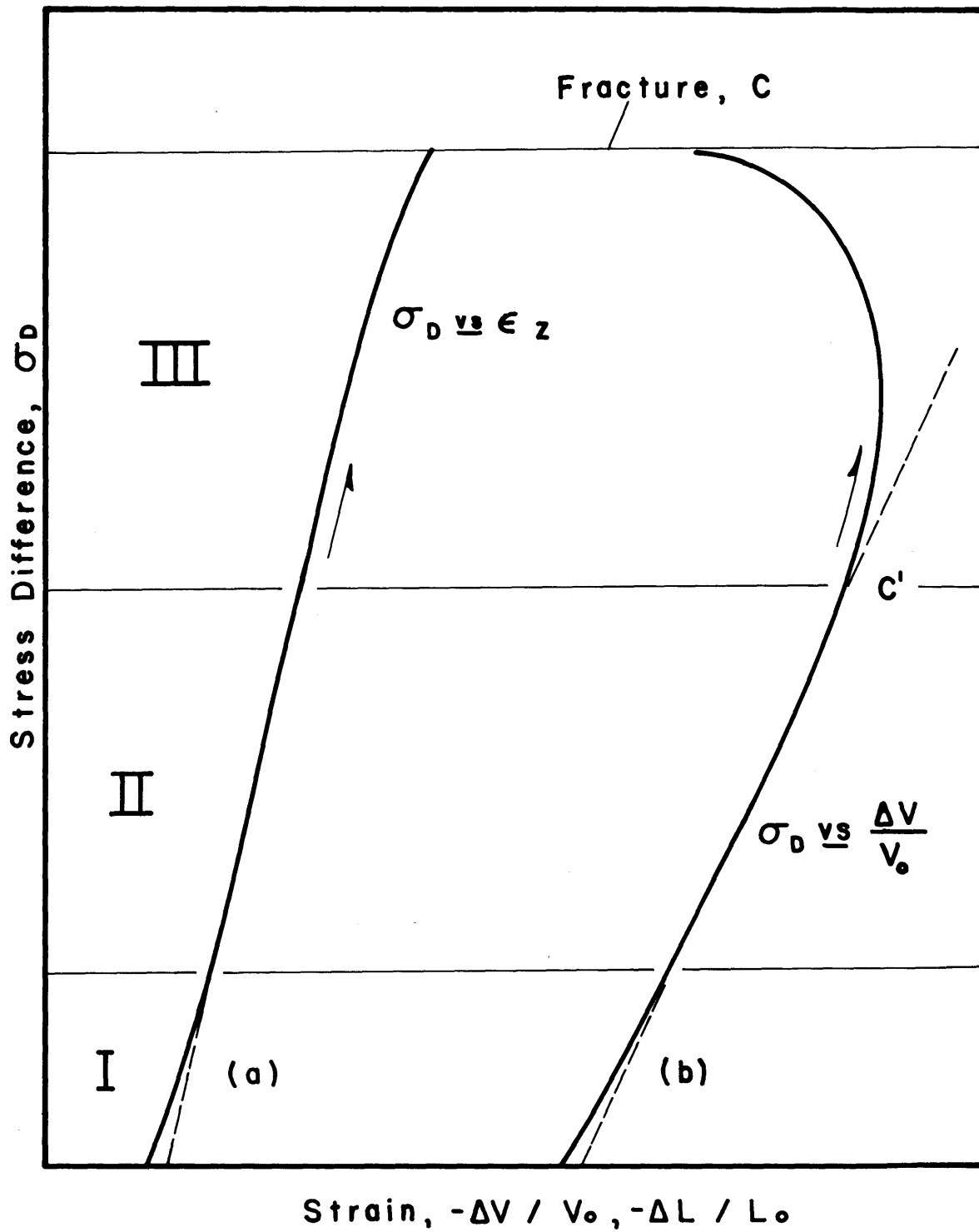


FIGURE 1. Stages in the stress-axial strain and stress-volumetric strain behavior preceding fracture. Modified after Brace et al. (1966).

remarkable extent. Disregarding elastic compression, this behavior constitutes an inelastic volumetric increase, or dilatancy, of the rock. Figure 1b shows a typical volumetric strain curve corresponding to the axial stress-strain curve of Figure 1a. If the rock were linearly elastic, it would be expected to follow the linear portion of the curve in a manner indicated by the dashed line. The deviation of the actual behavior from this elastic extrapolation indicates dilatancy, which is first detectable at about half the fracture stress and steadily increases until failure. Brace, Paulding, and Scholz [1966] studied this behavior and concluded that dilatancy is due to the creation of new pore space within the body due to the propagation of cracks.

The viewpoint that this inelasticity is produced by small cracks propagating in the rock is supported by considerable evidence, some of which is collected in Figure 2. Matsushima [1960a] found that the velocity of dilatational elastic waves measured parallel and perpendicular to the major direction of stress during a fracture test decreases markedly as fracture is approached (Figure 2a). This behavior is consistent with the idea that open cracks are being formed in the region of dilatancy. Similarly, Brace and Orange [1966] explained anomalous changes in electrical resistivity of stressed water saturated rock by an increase of porosity as stress is increased to fracture. Robertson [1955, 1960] found that specimens of Solenhofen limestone

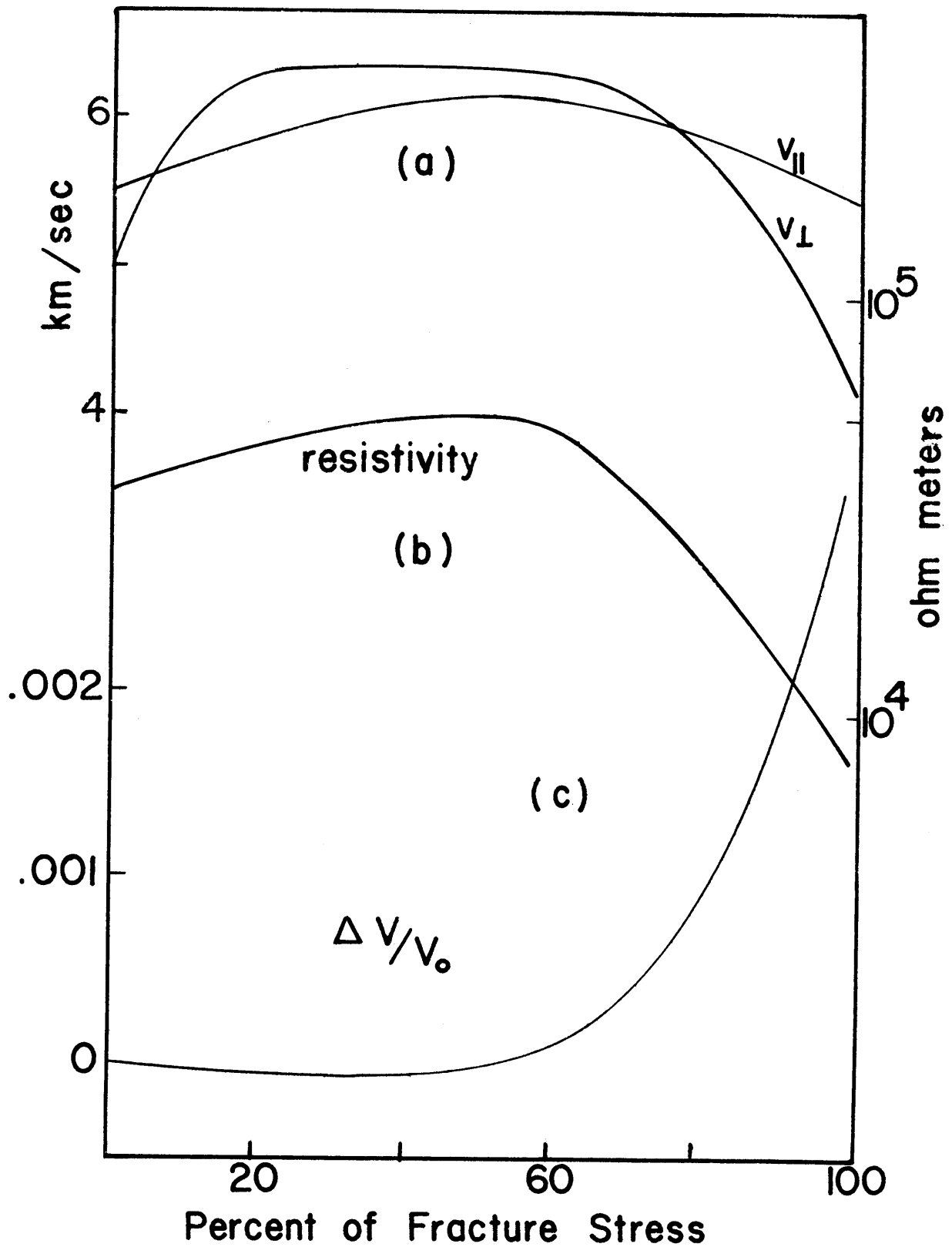


FIGURE 2. The behavior of several physical properties during compression of rock. (a) P wave velocity parallel and perpendicular to the stress direction. (b) Electrical resistivity. (c) Volumetric strain. Sources are cited in the text.

which had been subjected to creep had decreased in density.

The observations that cracking occurs over a large region of the stress-strain curve contradicts the concepts of Griffith's theory of brittle fracture. The first crack to propagate does so at a stress considerably lower than the fracture strength of the rock itself, and the strength is reached only after a great deal of cracking has occurred. The brittle fracture of rock, then, appears to be a much more complicated process than that proposed by Griffith. The cracking which occurs prior to fracture, which we shall refer to as microfracturing, seems to be a fundamental property of brittle rock, and is probably closely related to the fracture process. In addition, the inelastic rheological properties of rock at high stresses are likely to be closely related to microfracturing in much the same way that rock inelasticity at low stresses is related to crack closure. The purpose of this investigation was to delineate the general microfracturing behavior of rock, and to determine the relation of this behavior to the fracture and deformation processes.

A crack propagating in a brittle fashion would be expected to radiate elastic waves, which provides an excellent means for studying microfracturing directly, since such radiations can be detected and analysed. In fact, it has been known for a long time that rocks and certain other materials emit noises during deformation, and a considerable

amount of work has been done in studying this behavior.

The earliest investigations of the phenomena, using piezoelectric crystals for detection, were those of Obert [1941], and Obert and Duval [1942, 1945a, 1945b, 1957, 1961]. They studied the pattern of noises emitted during compression tests on rock, and from direct observation of cracking were able to conclude that the noise was due to small cracks being formed within the specimen. The main intent of their work was to develop a method for predicting rockburst in mines. By monitoring microfracturing in mines with similar equipment, they were able to demonstrate that noises preceeding rockbursts are somewhat similar to those observed prior to fracture in laboratory tests. The possibility of this application stimulated a considerable amount of further work on microfracturing activity and its relation to rockbursts, notably by Vinogradov [1957, 1959a, 1959b, 1962, 1963] and Konstantinova [1959a, 1959b, 1960, 1962, 1966]. The latter was particularly interested in noises accompanying gas explosions in coal mines, and her work dealt primarily with the behavior of coal and models with very soft materials such as talc.

Somewhat more detailed studies of the pattern of microfracturing activity in uniaxial compression were done by Franklin [1965] and Malone [1965]. They found that the number of noises which they detected increased strongly as fracture was approached. The microfracturing behavior in

uniaxial tension was studied by Brown [1965], who found that it is similar to that observed in compression. He also did static fatigue tests, and found that microfracturing occurs during creep. A close relationship between microfracturing and creep had been previously observed in compression by Watenabe [1963], and in bending by Mogi [1962a]. Gold [1960] observed similar behavior in ice.

The systems used by the previous workers have all had the same general characteristics. The microfracturing events were detected with a piezoelectric transducer, amplified, recorded on tape, and the results read out with an oscillograph or pen recorder. A great drawback of these systems is that they have all been limited to the audio frequency range or less. The present investigations have revealed that most of the energy radiated by microfracturing is in the low Mhz range, almost entirely above the frequency response of earlier experimental systems. Therefore, a system capable of responding to these high frequencies was designed, with the result that the sensitivity of measurement of microfracturing was increased by several orders of magnitude over that of previous workers. A second advantage is that the data reduction time of this system is very low.

The previous investigations were sufficient to outline the basic pattern of microfracturing, but were not precise or systematic enough to demonstrate the important parameters

involved in the process or to relate it clearly to the physical processes occurring.

It was therefore decided that a thorough and systematic investigation of microfracturing be made. The bulk of the investigations deal with the statistical analysis of large numbers of microfracturing events and the correlation of this with stress-strain behavior. The behavior of a variety of rocks deformed in uniaxial compression was studied, and triaxial compression tests were performed on both a brittle and a ductile rock. In these experiments, strains in two perpendicular directions were measured as well as microfracturing activity, so that microfracturing could be compared directly with volumetric strain. The time dependence of microfracturing was also studied and compared with strains in creep tests.

The results of these investigations showed that many thousands of cracking events occur prior to actual fracture of the specimen, and that the inelastic properties of brittle rock can be adequately explained by the contributions to strain of these newly formed cracks. Such statistical work, however, is not sufficient to clarify the formation of the fault and ultimate fracture of the specimen. In order to study the fracture process directly, a system was developed to study in detail individual microfracturing events during the course of an experiment. With a multi-transducer array, the foci of individual events were located

throughout the progress of a fracture experiment in order to trace out the formation of the terminal fault.

An additional incentive for these investigations was spurred by the work of Mogi. In a particularly significant series of papers, Mogi [1962a, 1962b, 1962c, 1963a, 1963b, 1963c] was able to show that in many ways microfracturing activity resembles seismicity in the statistics of events emitted during bending tests, and noted the similarities between these events and foreshocks. He also studied the frequency-magnitude relation of microfracturing events, as did Vinogradov [1959, 1962], and found that this relation is also the same as that found for earthquakes. By treating microfracturing as a stochastic process, he was able to determine some of the characteristics of the process, although this was not related directly to a physical model. In later experiments, he reproduced foreshock and aftershock sequences in models and related the characteristics of the sequences qualitatively to the heterogeneity of the model material.

Although the earthquake mechanism is evidently some sort of rock fracture process, the relation between earthquakes and rock fracture in the laboratory is not clear. Mogi's contention that microfracturing in the laboratory is essentially a scale model of regional seismicity leads to some rather intriguing questions. Perhaps the most interesting is that of the physical mechanism of microfracturing, and the reasons for its similarity with earthquakes. We

would like, in particular, to know how far this similarity can be carried.

In order to answer some of these questions, investigations were performed along the lines of Mogi's work. The purpose of these studies was to find if Mogi's results could be confirmed under the more geologically realistic conditions of compressive stress, and to extend these observations in considerable more detail. Very precise determinations of the frequency-magnitude relation were made, and this relation was studied systematically as a function of rock type, stress, and confining pressure. In the light of the stick-slip hypothesis of earthquakes [Brace and Byerlee, 1966] the microfracturing behavior during frictional sliding was observed and compared to that occurring during fracture.

In conjunction with the experimental work, theoretical studies of the microfracturing process were undertaken to clarify and to relate it to earthquake behavior. It was first recognized that in considering a microscopic process such as microfracturing, the inhomogeneity of the stress field within the body due to elastic and structural heterogeneities had to be taken into account. Consequently, a statistical model of rock deformation and fracture was developed. The theory is kept as general as possible in order to describe the basic properties of deformation of an inhomogeneous medium, so that the basic relations between

rock and crustal deformation could be brought out.

The work is divided into four main sections. In the first section, the general microfracturing behavior in uniaxial and triaxial compression tests is described, together with the introduction of the basic theoretical model. The microfracturing behavior during frictional sliding and during deformation of a ductile rock are also described, and compared with the behavior in brittle rock.

The second section is mostly theoretical in content and discusses the time dependence of microfracturing and relates this to creep.

In the third section, the frequency-magnitude relation of microfracturing events is described under a wide range of conditions. The theory is extended to predict a frequency-magnitude relation which is found to be in close agreement with the experimental results. The implications of this work is discussed with respect to earthquake behavior.

Detailed studies of individual microfracturing events are the subject of the last chapter. The location of selected events in space were determined, and the implications discussed with respect to rock fracture and earthquake prediction.

Each chapter is designed to be read as a unit, and contains a brief introduction and description of the experimental technique involved. More detailed discussions of the

experimental procedures are contained in the appendices.

CHAPTER 1

MICROFRACTURING AND THE INELASTIC DEFORMATION
OF ROCK IN COMPRESSION

Introduction

For many geophysical applications the stress-strain behavior of rock at low temperature and pressure has been approximated by linear elasticity. It is well known, however, that at very low stresses the closure of pre-existing cracks within rock profoundly affects physical properties like elasticity [Walsh and Brace, 1966]. Although these effects usually disappear at a confining pressure of a few hundred bars, Brace et al. [1966] recently demonstrated that brittle rock is nonelastic at higher stresses, even at high confining pressure. This effect (Figure 1), which is noticeable at stresses greater than about half the compressive strength, is characterized by a decrease in modulus and by dilatancy. Dilatancy refers here to an increase in volumetric strain relative to what would be expected if the material were linearly elastic. The dilatancy was traced to the formation of small cracks within the rock.

This cracking was first detected indirectly by Obert and Duval [1942]. They found that small noises were emitted from rock during loading in compression and attributed them to cracking. These small cracking events, which we shall

refer to as microfractures in order to distinguish them from fracture of the test specimen itself, seem generally to accompany the deformation of brittle rock. However, it would be interesting to know if dilatancy can be accounted for solely by microfracturing, or if other processes are involved. We would also like to know how this behavior agrees with our ideas of brittle fracture of rock, and whether microfracturing also plays a significant role in frictional sliding or deformation of ductile rock.

If microfractures propagate in a brittle manner, we would expect that each event would radiate elastic waves of the sort detected by Obert and Duval and later workers. The study of the elastic radiations associated with microfracturing offers an excellent way of observing directly the microscopic processes which occur during deformation. These processes can then be correlated with the observed macroscopic stress-strain properties. In this investigation, microfracturing was observed and a precise and systematic study of the influence of it on the macroscopic stress-strain behavior of brittle rock was made. These observations were then compared with the microfracturing observed during frictional sliding of rock and during deformation of a ductile rock.

Experimental Technique

Microfracturing detection. Previous investigators of

microfracturing used the same basic technique. Events were detected with a piezoelectric transducer; the amplified signal was recorded with an audio-frequency tape recorder and displayed on an oscillograph or pen recorder. My investigations with a wideband system [see Chapt. 4] have revealed, however, that most of the microfracturing radiation emitted is in the 100 khz to 1 Mhz range. Consequently, the limited frequency response of the systems used in previous work severely limited the observations.

The experimental system used in the present study is shown schematically in Figure 3. The essential component is a TMC model 102 pulse height analyzer. This analyzer has 100 channels and was operated for these experiments as a multiscaler. In this mode, each channel operates as a scaler for a predetermined time (dwell time). The analyzer thus counts the number of pulses above a certain threshold that occur during the dwell time, then switches to the next channel and repeats the procedure until all channels are used. The number of events per channel is stored in a magnetic core memory and read out digitally after the experiment. A direct measurement of the number of events that occurred per unit time versus time is thus obtained. The dwell times used were 5 or 10 seconds and were regulated by an external timing clock.

Preliminary investigations showed that typical microfracturing signals are in the form of decaying sinusoids

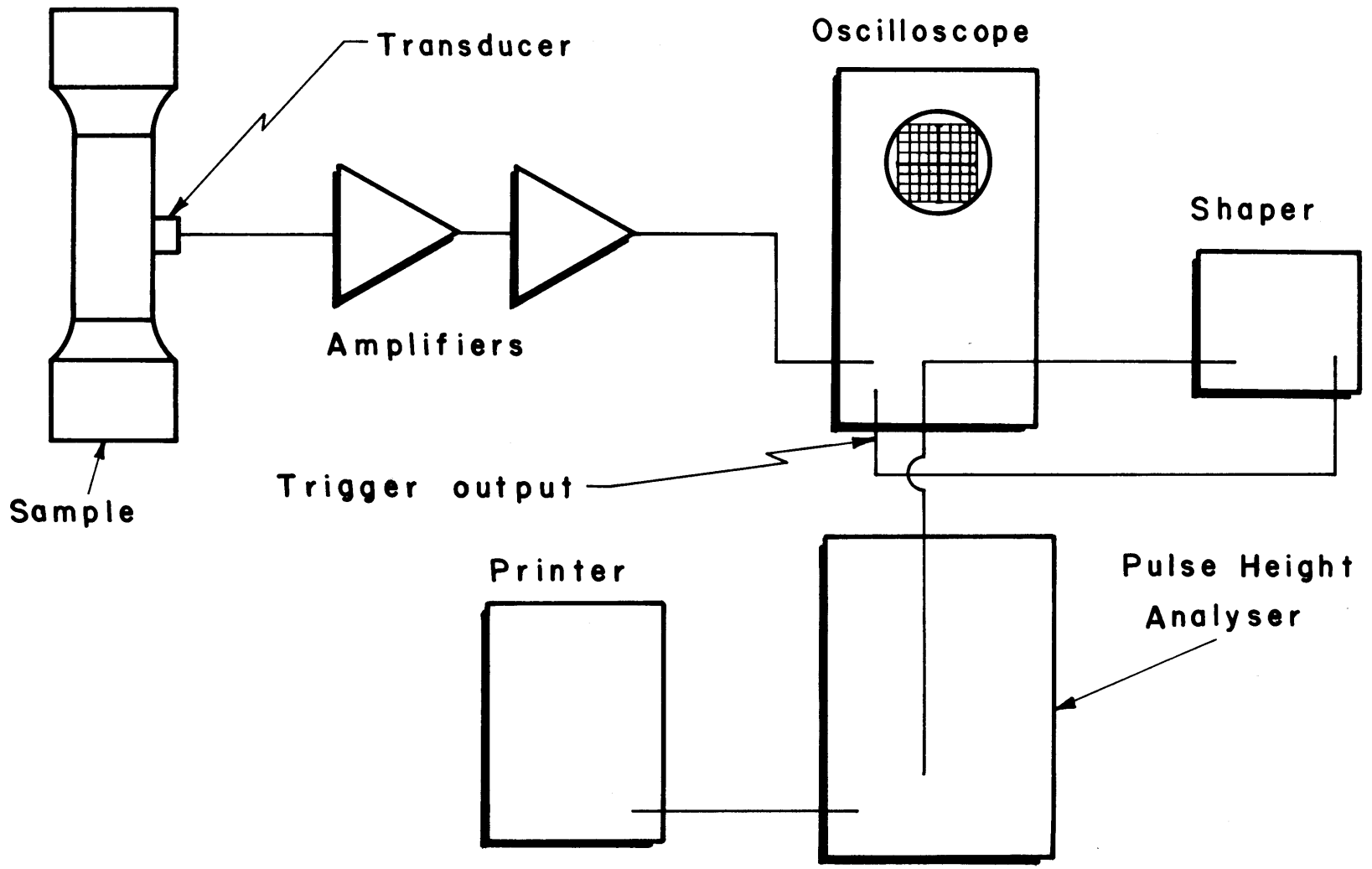


FIGURE 3. The experimental system for the detection and analysis of microfracturing signals.

of period of a few microseconds and trainlength 10 to 100 μ sec. Consequently, the signals could not be admitted directly to the analyzer since more than one count would be actuated. Instead, the wave trains were shaped after amplification in such a way that the input to the analyzer was the envelope of the negative part of the wavetrain, which was found to give very satisfactory results. The design of the shaping circuit is described more fully in **Appendix II.**

Amplification was achieved in three stages. The first stage was a Hewlett-Packard model 465 amplifier, which has a 40 db gain and served as an impedance match, with 10 megohms input and 50 ohms output impedance. A HP 461 amplifier was used as the second stage. A variable gain third stage was obtained simply by using the trigger output from the monitoring oscilloscope, a dual trace Textronix 545 B, which was used to monitor both the signal after the second amplifier and the shaped signal. The shaper input is into a diode, so the system noise in a particular experiment could be held below the diode cutoff by adjusting the third stage gain, and noise discriminated. The noise counted as events by the analyzer was in most cases reduced to a negligible level by means of this technique.

The transducers used in the experiments were barium titanate compressional mode discs, 6 mm in diameter and 2.5 mm thick. Copper foil electrodes were attached to the

faces of the discs with conductive epoxy and the package cemented to a rubber pad and brass backing. Overall frequency response of the amplification system was flat from 100 hz to 1 Mhz. This system was found to be extremely well suited to microfracturing studies. By simply increasing the frequency response, I found that the measurement of microfracturing activity with this system was two to three orders of magnitude more sensitive than that of the previous workers. At the same time, the data processing time was negligible, so that a much more detailed and systematic study was possible.

Compression tests. The sample designs used in the experiments were of three types. Samples for uniaxial compression tests were of the form designed by Mogi [1966] to eliminate end effects. End effects seriously alter microfracturing behavior [Appendix I]. These samples were right cylinders 1.6 cm in diameter by 5 cm long, attached to steel end caps by epoxy fillets. In the same paper, Mogi found that end effects were negligible at confining pressures above a few hundred bars, so that specimens used for triaxial experiments were straight cylinders of the same size. Jacketing was .13 mm thick copper.

Specimens for frictional sliding experiments have been described by Byerlee [1967]. Briefly, they were straight cylinders in which a flat ground sliding surface had been introduced at 45° to the axis. The two pieces were fitted

together inside a .13 mm thick copper jacket, and the ends were sealed with rubber tubing to steel end plugs. To allow the surface to undergo more than one stick-slip displacement without bursting the jacket, the copper jacket was strengthened around the margins of the sliding surface with a strip of RTV 102 silicone rubber sealant. The transducer was attached to a section of bare copper left exposed between this seal and the end seal. In all cases the transducers were clamped directly to the side of the specimens with rubber O-rings, with a film of Dow 276-V9 resin at the interface to insure good coupling.

Volumetric strains were measured with strain gages as described elsewhere [Brace et al., 1966]. The loading machine has a ball screw loading mechanism which imparts a high stiffness (about 10^6 kg/cm). All experiments were done at a constant strain rate of 10^{-5} sec⁻¹ which was achieved by driving the ball screw with a constant speed motor.

Due to the very high frequencies of the microfracturing signals and the design of the loading system, mechanical noise presented no problems during the experiments. Electrical noise was eliminated by shielding the sample, in uniaxial experiments, with .025 mm thick copper. The pressure vessel itself served as a shield for tests under confining pressure.

Rocks studied. Six rocks were selected for the study.

TABLE 1. Descriptions of Rocks

d is the average grain diameter. The total porosity η was determined by immersion in CCl_4 .

Rock	Density, g/cm^3	d, mm	η	Modal Analysis
Westerly granite	2.646	0.75	0.009	27.5 qu, 35.4 mi, 31.4 an ₇ , 4.9 mica
Rutland quartzite	2.643	0.30	0.005	91 qu, 7 or, 2 mi
Marble	2.688	0.20	0.013	99 ca
Colorado rhyolite tuff	1.77	0.01	0.41	20 qu, 20 gl, 60 an ₁₀
Pottsville sandstone	2.541	0.20	0.030	46.4 qu, 41.0 or, 10.9 mica
San Marcos gabbro	2.813	1.00	0.002	69.7 an ₄₂ , 8.2 au, 7.4 ho, 11.7 mica

Abbreviations: qu quartz ca calcite
 mi microcline gl glass
 or orthoclase ho hornblende
 an plagioclase with anorthite content
 mica muscovite, biotite, chlorite
 au augite-hypersthene

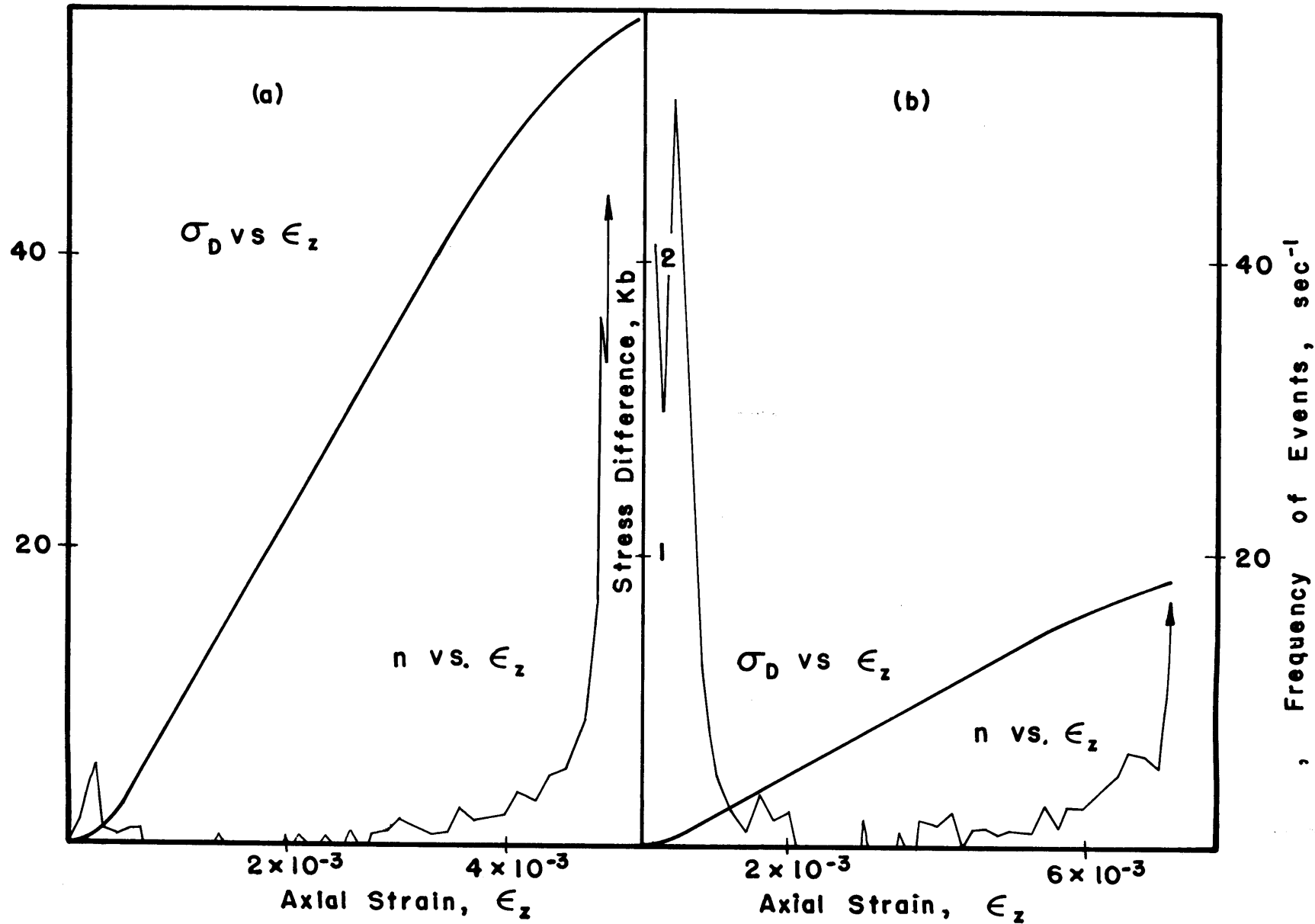
One, a medium grained pure calcite marble, was described in the earlier study [Brace et al., 1966]. This rock was ductile even at room pressure. The other rocks were all brittle under the testing conditions. One of these, Colorado rhyolite tuff, had an extremely high porosity of 40%, mostly due to open vesicles. Of the other rocks, San Marcos gabbro and Rutland quartzite were very compact whereas Westerly granite and Pottsville sandstone had appreciable crack porosity. Petrographic descriptions of the rocks are given in Table 1.

Observations

Uniaxial compression tests. Unconfined compression tests were done on six rocks to determine the effect of mineralogy and texture on microfracturing behavior. Figure 4 shows the frequency n of occurrence of microfracturing events vs axial strain for Westerly granite and Colorado rhyolite tuff. For comparison, the axial stress-strain curves are also shown.

The pattern of microfracturing for all rocks tested was very characteristic. The similarity in behavior for the two rocks shown in Figure 4 for example, is remarkable considering their strong disparity in physical properties, including strength. At low stress, a flurry of activity occurs; this soon dies down to a very low level. At stresses near approximately half the fracture strength, microfracturing

FIGURE 4. Stress vs strain and microfracturing frequency vs strain for two rocks in uniaxial compression. (a) Westerly granite. (b) Colorado rhyolite tuff.



activity begins to build up once more, and steadily increases until just before fracture, when a very rapid acceleration of activity occurs.

This pattern correlates closely with the stress-strain behavior. At low stresses, in the region in which the first activity occurs, the stress-strain curve is nonlinear and concave upwards. At higher stresses, where microfracturing activity is very low, the rock is nearly linearly elastic, and the resumption of activity corresponds with the beginning of nonlinearity of the upper part of the stress-strain curve.

The only significant difference in behavior among the various rocks is in the amount of activity that occurs in the low stress region relative to that occurring above half the fracture strength. It was found that the relative amount of activity detectable in the first region is roughly proportional to the porosity of the rock. Thus in Figure 4, the amount of activity in the low stress region of the compact Westerly granite is very slight relative to that which occurs later, whereas the activity in the first region of the highly porous Colorado rhyolite tuff reaches a very significant level. This observation is quite in accord with our knowledge of the behavior of rock in this portion of the stress-strain curve. The inelasticity of rock at low stress is due primarily to the closing of pre-existing cracks and pores (for a review of this behavior, see Walsh and Brace

[1966]). Such adjustment of the void spaces would be expected to be accompanied by inelastic processes such as crushing of pores and frictional sliding on crack faces and are probably responsible for the microfracturing activity in this region. Consequently, a high degree of activity in this region would be expected from a high porosity rock, as observed.

The nonlinear part of the stress-strain curve above about half the fracture strength is the region in which dilatancy occurs [Brace et al., 1966]. Microfracturing was observed in this region, but we wished to test more quantitatively the hypotheses that dilatancy is due to the introduction of new void space produced by cracking. If it is assumed that the average size of microfracturing events remains constant throughout this region, then the accumulated frequency of events, N , should be directly proportional to the inelastic part of the volumetric strain, Δ^* , if this hypothesis holds. In this case, each event can be thought to contribute a small increment, η , to the volumetric strain. It is found [see Chapt. 3] that the assumption of constant event size is not strictly true, but for this application the results will not be appreciably affected by its use.

In Figure 5 is shown the results of three different uniaxial experiments on Westerly granite. The ordinate is Δ^* , which is obtained by subtracting an elastic extrapolation

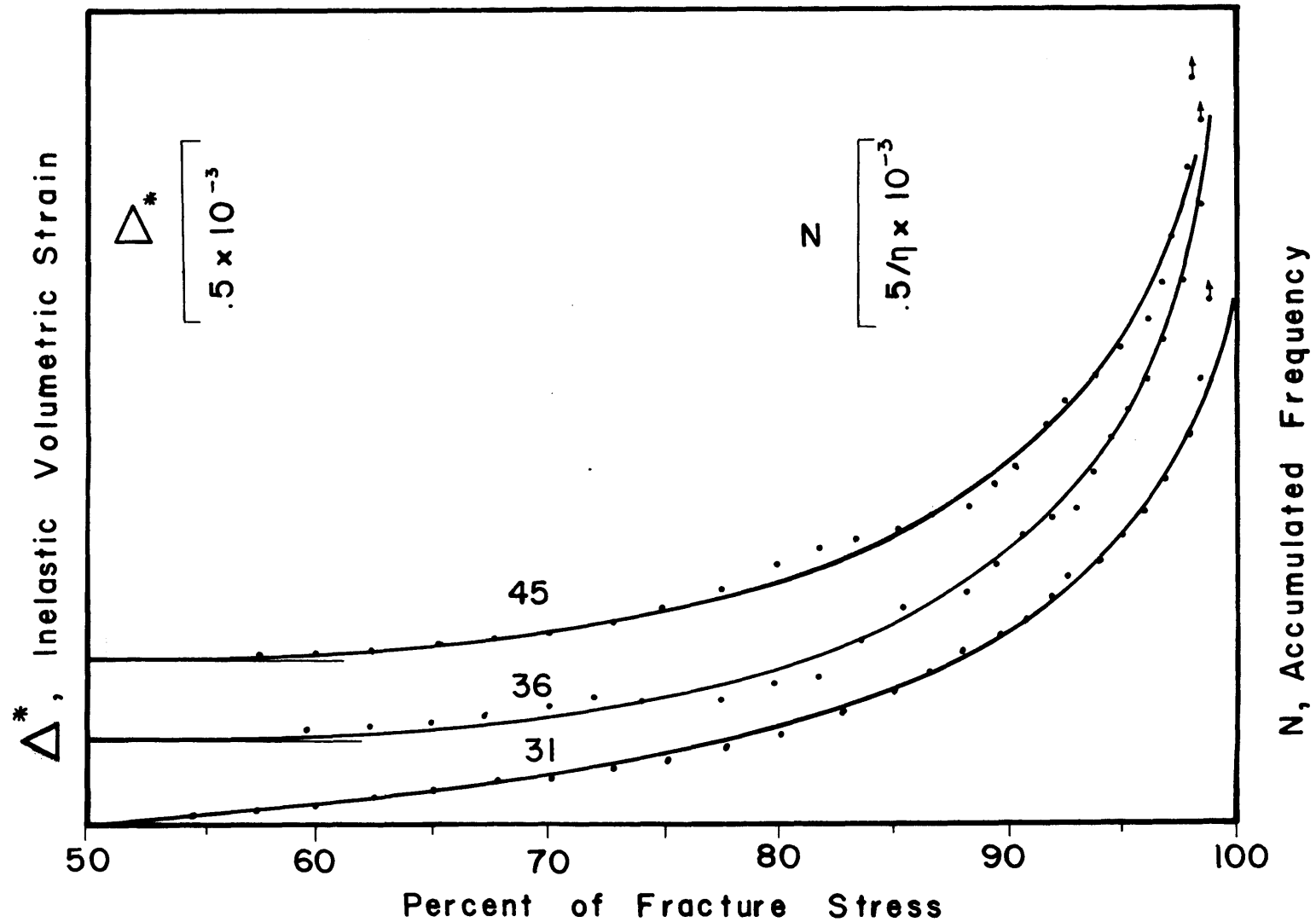


FIGURE 5. Accumulated frequency (data points) of microfracturing events fitted to the inelastic volumetric strain (smooth curve) in the dilatant region for three uniaxial compression tests on Westerly granite. The values of η are given in Table 2.

from the measured volumetric strain as outlined by Brace et al. [1966]. N, the accumulated frequency of microfracturing events detected in the dilatant region, is best-fitted to these curves and shown as data points. This was done by plotting N vs Δ^* over the entire range, and making a linear best fit. The correlation is very good -- well within experimental error. A noticeable exception is the region above 95% of the fracture strength, where microfracturing activity rapidly accelerates. It is also interesting to note that the behavior is remarkably reproducible; the difference between these three experiments in all respects, including strength, is within experimental error.

The proportionality of N and Δ^* also holds for the other rocks tested. Although their strengths vary from .5 to over 5 kb, the behavior of all the rocks, when normalized with respect to fracture stress, is quite similar. The results for these rocks are shown in Figure 6. The data points have been omitted here for clarity. Variation of the proportionality constant η , listed in Table 2, is considerable due to nonreproducibility of acoustical contact between experiments. The variation is particularly great for tests under confining pressure, when the gain was sometimes reduced to eliminate noise. Therefore η is simply a constant of proportionality and has no quantitative physical significance. Also given in Table 2 is the quantity F, which is Δ^* when the stress equals 95% of the stress difference C at fracture.

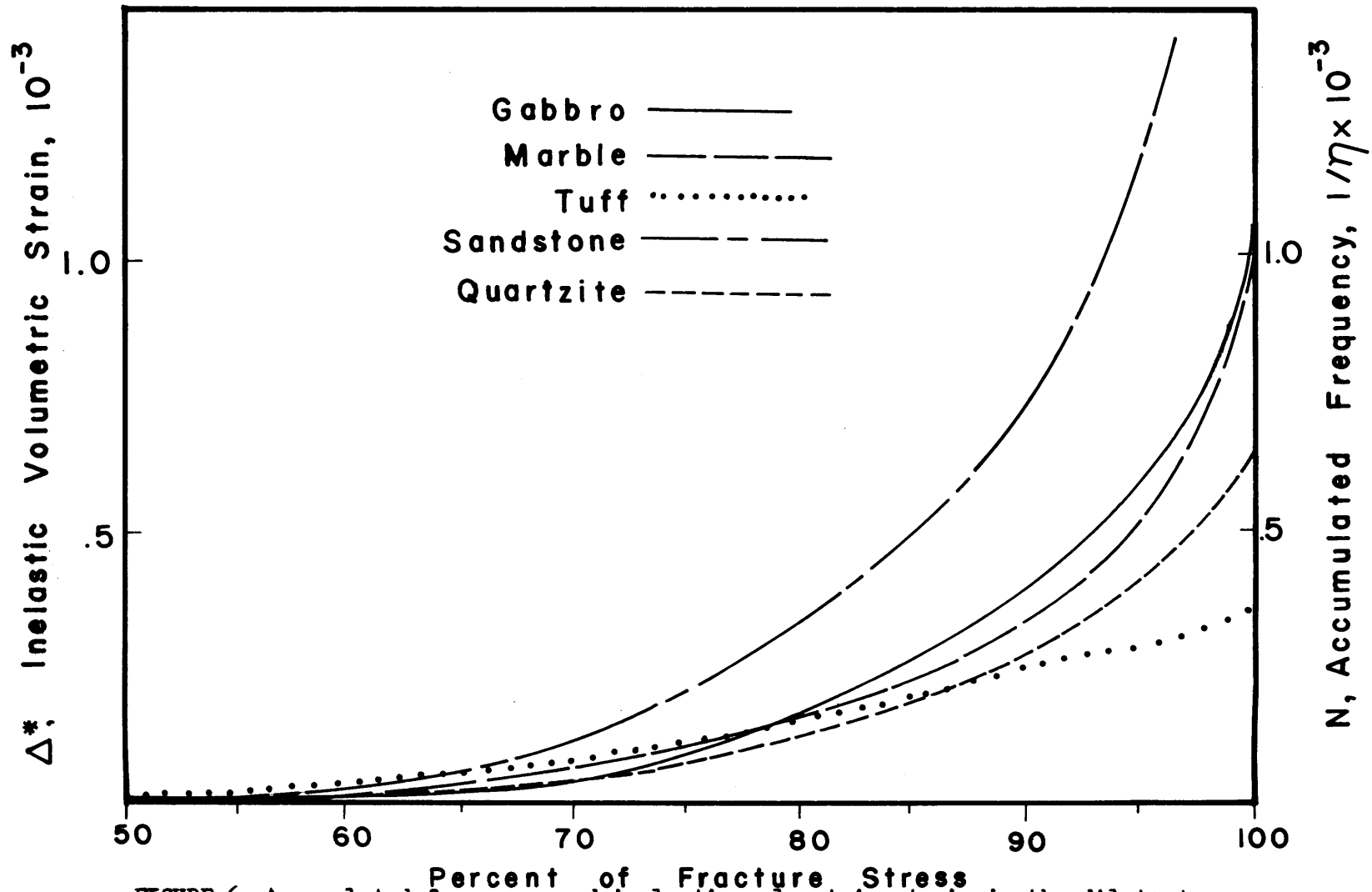


FIGURE 6. Accumulated frequency and inelastic volumetric strain in the dilatant region for five rocks in uniaxial compression. For values of η see Table 2.

TABLE 2. Results of Compression Tests

Rock	Exp. No.	Pressure, kb.	C, kb.	C', kb.	C'/C	F 10 ⁻³	η 10 ⁻⁶
Marble	30	0	0.50	0.28	.57	0.52	1.70
Colorado rhyolite tuff	27	0	0.91	0.43	.48	0.30	0.86
Pottsville sandstone	39	0	2.30	1.20	.52	1.15	5.20
Rutland quartzite	38	0	5.05	2.94	.58	0.40	4.15
San Marcos gabbro	43	0	2.15	1.16	.54	0.58	*
Westerly granite	31	0	2.81	1.44	.51	0.78	5.22
	36	0	2.82	1.50	.53	0.88	6.69
	45	0	2.84	1.56	.55	0.89	2.43
	61	1.00	7.90	4.34	.55	1.66	13.30
	71	2.00	11.40	5.00	.44	1.13	0.03
	63	3.00	13.60	5.16	.38	1.96	2.64
	60	4.00	15.80	5.70	.36	0.98	0.44
	62	5.00	16.80	7.40	.44	1.20	2.46

* Excessive noise occurred during experiment.

The quantity \underline{F} is used as a measure of dilatancy because strains at stresses greater than $0.95C$ are likely to be nonuniform and hence Δ^* would be nonreproducible and unreliable. \underline{C}' refers to the stress difference at which dilatancy is observed to begin, and \underline{C} fracture stress difference. The uncertainty in \underline{C} is a few percent, 10 to 15% in \underline{C}' , and in \underline{F} and η about 10%.

Triaxial experiments. Brace et al. [1966] concluded that confining pressure does not generally affect dilatancy. In order to see if the relation between microfracturing and dilatancy is affected by pressure, a series of experiments were conducted on Westerly granite at confining pressures up to 5 kb.

A typical result is given in Figure 7. Aside from the noticeable lack of activity at low stress differences, as we would expect from our above interpretation, the behavior is on the whole quite like that observed at atmospheric pressure. Comparisons of \underline{N} vs Δ^* were made with the result that dilatancy is found to be directly related to microfracturing as described above for the uniaxial experiments. The earlier conclusions that dilatancy is not appreciably affected by pressure are also confirmed.

Frictional sliding. Byerlee [1967] has recently suggested that friction in normally brittle materials is basically a brittle phenomenon. According to his model, frictional sliding takes place when the asperities on the sliding

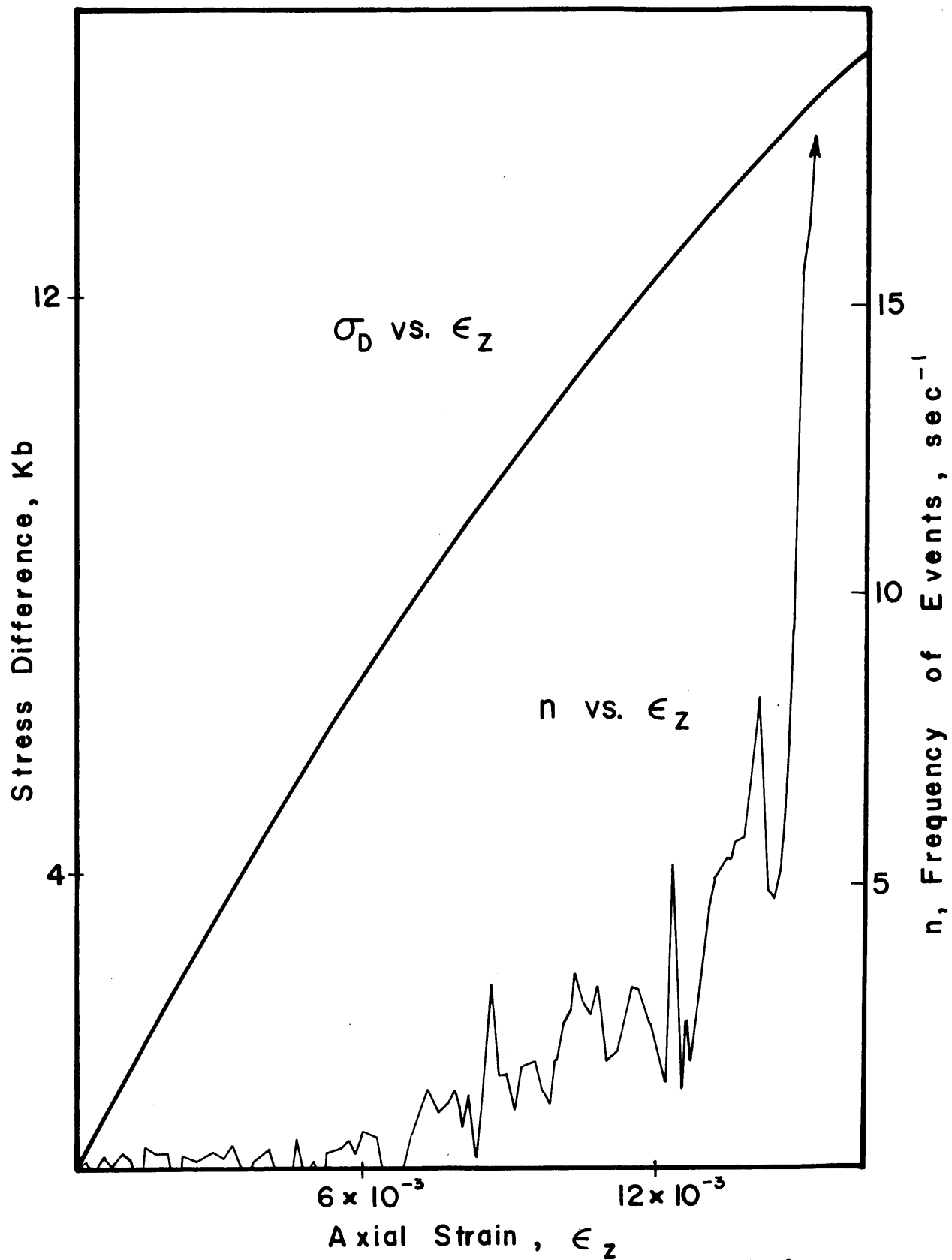
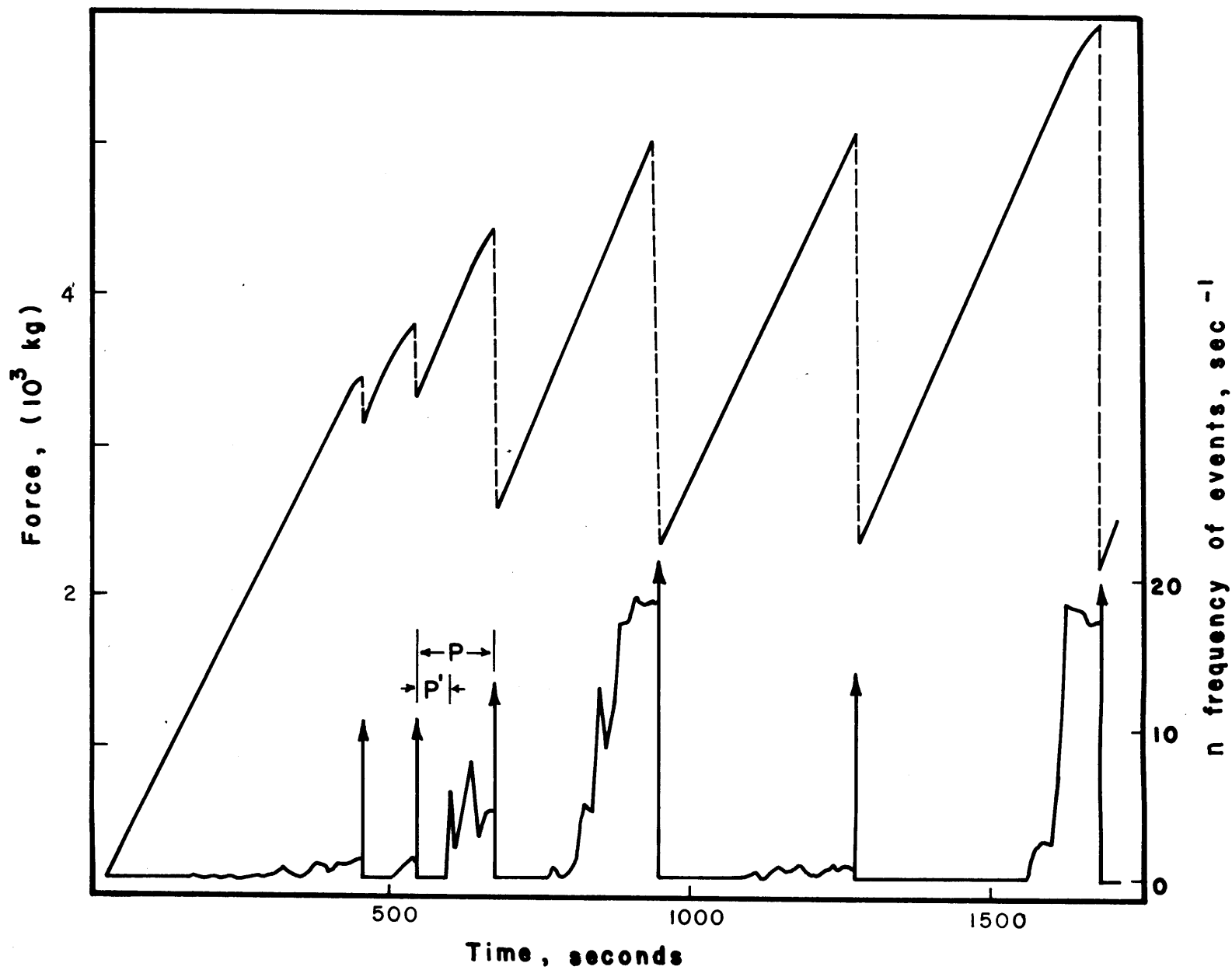


FIGURE 7. Microfracturing frequency and stress vs strain for Westerly granite in triaxial compression. Confining Pressure: 4 kb.

surfaces fail by brittle fracture. He suggested that two types of sliding take place: stick-slip, an inherently instable form of sliding which is accompanied by a large stress drop, and stable sliding, which does not lead to detectable stress drops. The latter often precedes the former. Because of the possible importance of friction in earthquakes [Brace and Byerlee, 1966], a study of the microfracturing that accompanies sliding was made to test this description of frictional sliding as a form of brittle fracture.

We show in Figure 8 the results of a typical experiment. The upper curve is a plot of force vs time. The solid portions of the curve are equivalent to force vs displacement because strain rate is constant. The dotted vertical portions are stick-slip events, and the curve as a whole is very similar to that described by Byerlee. Microfracturing, also given in Figure 8, shows a characteristic pattern during each stick-slip cycle. As force is increased, no events can at first be detected; apparently the surfaces are locked and no sliding is taking place. At some point prior to stick-slip, microfracturing abruptly begins to take place and continues at a roughly constant rate until stick-slip occurs. The arrows represent large numbers of events that were recorded during the stress drops. Immediately after the stick-slip, the level of activity falls again to a very low value, and on continued

FIGURE 8. Force vs time (upper curve) and microfracturing activity during frictional sliding of Westerly granite. Confining pressure: 1 kb.



loading the cycle is repeated. The region of activity preceding stick-slip corresponds fairly closely with the slightly nonlinear portions of the force-displacement curves which Byerlee [1966] attributed to stable sliding. If this interpretation is correct then these results imply that the sliding begins rather abruptly and proceeds at a nearly constant velocity. There seems to be little indication that any acceleration of activity occurs prior to stick-slip, which is in marked contrast with the behavior during the deformation of intact rock described above. Intact rock is typified by a continual acceleration of activity during deformation.

In Table 3 we list for the various experiments the mean frequency \bar{n} of occurrence of events in the regions of activity preceding each stick-slip and the fraction of the stick-slip cycle \bar{P}'/P at which this activity began. The behavior appears to be quite erratic. No pattern can be seen between successive stick-slip cycles during a given experiment or between different experiments. The level of activity may be high or low, be continuous throughout the cycle, or not occur at all. This lack of reproducibility was not observed in intact rock deformation and suggests that stable sliding is very structure sensitive, that is, it is affected by minor differences in the sliding surfaces.

Ductile deformation. It is generally assumed that at some temperature and pressure, most rock will become ductile,

TABLE 3. Results of Frictional Sliding Experiments

Exp. No.	Pressure kb.	1 st Stick, Slip		2 nd Stick, Slip		3 rd Stick, Slip	
		n	P'/P	n	P'/P	n	P'/P
72	2.0	99	.39	135	.51	60	.00
73	4.0	112	.90	0	1.00	83	.60
35	3.0	41	.36	*			
33	1.0	†		56	.50	4	.20

* Jacket leaked after first stick slip.

† First cycle interrupted by small stick slips. (see Figure 8).

that is, a large amount of inelastic strain can be supported without fracture [Griggs et al., 1960]. On the basis of microscopic examination, those workers have concluded that some plastic flow occurs during ductile deformation, but it has not been demonstrated that fully plastic flow, i.e. deformation produced entirely by dislocation motion, as in metals, is the mechanism of deformation.

The most detailed studies of rock ductility have been done on the carbonate rocks such as Yule marble. The primary reason is not because of their geologic importance but because carbonate rocks become ductile at relatively low temperature and pressure and hence are more readily amenable to experimental observation.

For the same reason, the rock we have chosen for a detailed examination of ductility is also a carbonate -- the marble which was described above in the section on uniaxial compression tests. In so doing, we lose some generality in the applicability of our results because silicate rocks will not behave identically, even at higher temperature and pressure, due to differences in the silicate and carbonate structures. In the light of the considerable experimental work that has been done on the carbonate rocks, however, it would be of interest to examine the role of microfracturing in the ductile deformation of these rocks.

It was shown above that the microfracturing of the

marble in uniaxial compression was, just like the brittle rocks, directly related to the dilatancy. Marble, however, deforms cataclastically at room pressure, and the similarity of dilatancy and microfracturing to brittle rock, seen in Figure 6, is misleading. Plotting event frequency vs strain, as in Figure 9a, brings out the fundamental difference between the behavior of marble from that of brittle rock. Comparing this with the stress-strain curve (Figure 9a), microfracturing in the marble begins at about the start of the region of high curvature (yielding region) of the stress-strain curve and proceeds at a nearly constant rate with no acceleration such as observed in brittle rock (compare Figure 4). Similarly, the curves of N and Δ^* vs strain are seen to be linear. The distortion of the linear relation in the plot of Δ^* and N vs stress was due simply to the highly nonlinear stress-strain curve.

The eventual weakening of this rock is not accompanied by the formation of a fault but rather by a gradual loosening of the grains. After testing, the sample resembles a rather loosely packed sand. This type of deformation, termed cataclasis, is normally thought to be produced by stable intragranular frictional sliding. This view is supported by the rather strong similarity of the accompanying microfracturing to that observed during stable frictional sliding. A steady rate of microfracturing is typical of both processes in contrast to the behavior of intact brittle rock. It was

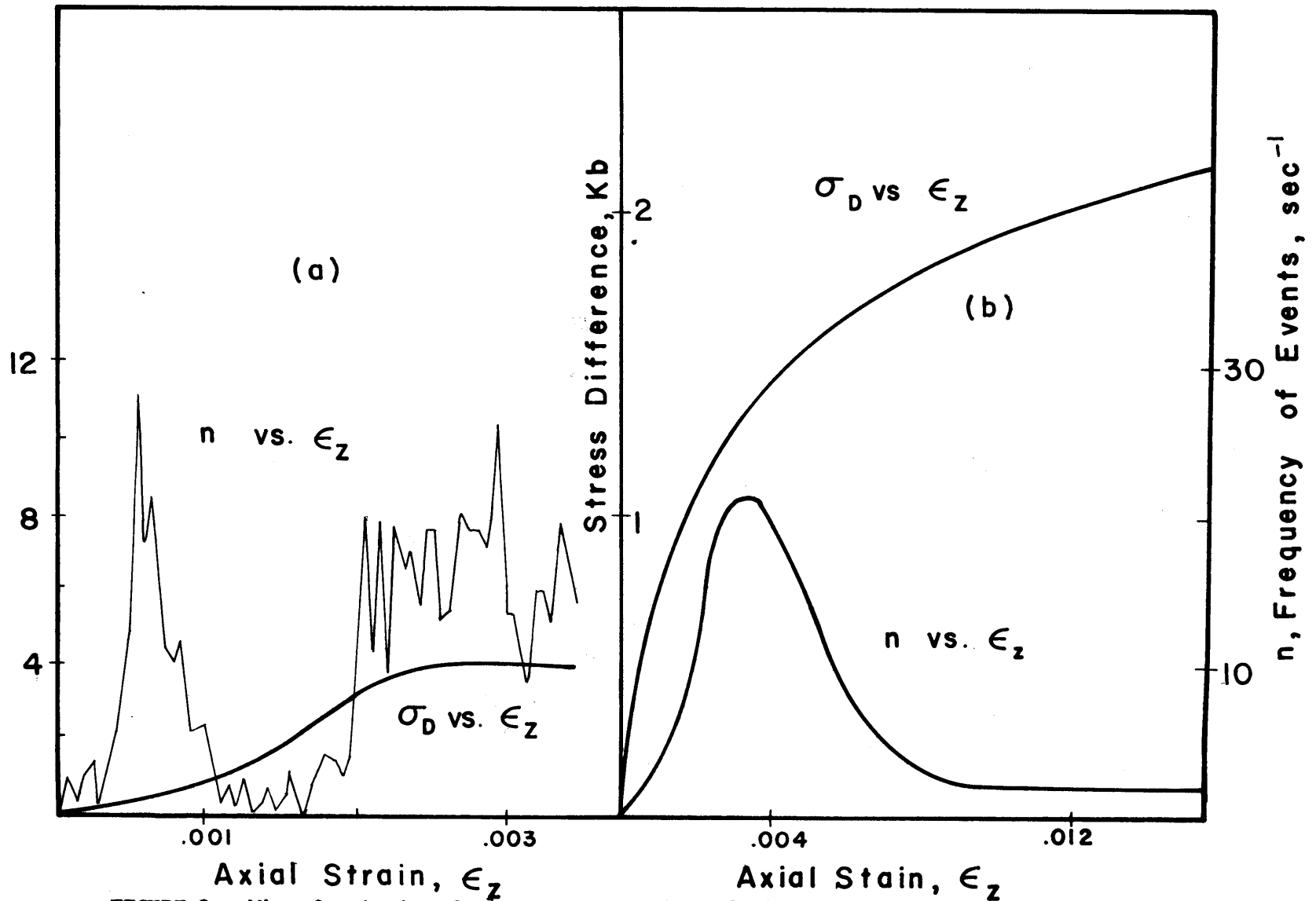


FIGURE 9. Microfracturing frequency vs strain and stress vs strain for marble.
 (a) Uniaxial Compression. (b) 1 kb confining pressure.

also found [see Chapt. 3] that the frequency-magnitude relation of microfracturing events also sharply distinguishes frictional sliding and cataclastic deformation from that of brittle intact rock.

The marble was deformed in compression under confining pressures of from 0.25 to 4 kilobars. Under all pressures, the rock was found to be ductile in stress-strain behavior, and examination of the specimens after testing revealed no trace of a fault. Microfracturing activity under confining pressure was found to be quite different from that described above. The level of activity was quite low, so the gain had to be increased in order to allow good detection. The result was that considerable noise was introduced. A count of background noise was made prior to each experiment with the specimen unloaded, and the final results were corrected for this ambient noise level. A smoothed curve of \dot{n} vs strain and the stress-strain curve for a typical experiment under confining pressure are shown in Figure 9b. Activity begins at a very low stress level, increases to a pronounced peak in the region of yielding, and decreases to a very low level in the nearly linear post-yield region. No definite change in this pattern was observed over the range of pressures at which tests were conducted, although the corrections for noise may have obscured small differences.

On the other hand, pressure had a pronounced effect on the stress-strain properties. The stress-axial strain curves

for the experiments at each confining pressure are shown in the upper part of Figure 10. We see that pressure both strengthens the rock and increases the degree of strain hardening in the post-yield region. These effects are very rapid at first but diminish rapidly with pressure. Compare, for example, the change in the first kilobar of pressure with that in the second, or third. At 3 kb the pressure effect becomes negligible -- at 3 and 4 kb confining pressure the stress-axial strain curves are identical.

Coupled with this behavior is a very systematic change in the strain-volumetric strain curves. These plots, in the lower half of Figure 10, are of total volumetric strain. The curves show the same general form, a small volume decrease occurs at low strains, the slope of the curve changes rapidly through the yield region, and finally the curve becomes linear after yielding. At low confining pressure, the large positive volumetric strain per unit axial strain reflects a large amount of dilatancy. The effect of pressure on the dilatancy is again quite similar to the effect of pressure on the stress-axial strain properties. The decrease in dilatancy resulting from an increase in pressure is large at low pressure and diminishes strikingly as the pressure is increased. At the highest pressure, 4 kb, there is no volumetric strain in the post-yield region.

Perhaps more diagnostic is Poisson's ratio in the linear post-yield region. Poisson's ratio ν^* , the strength

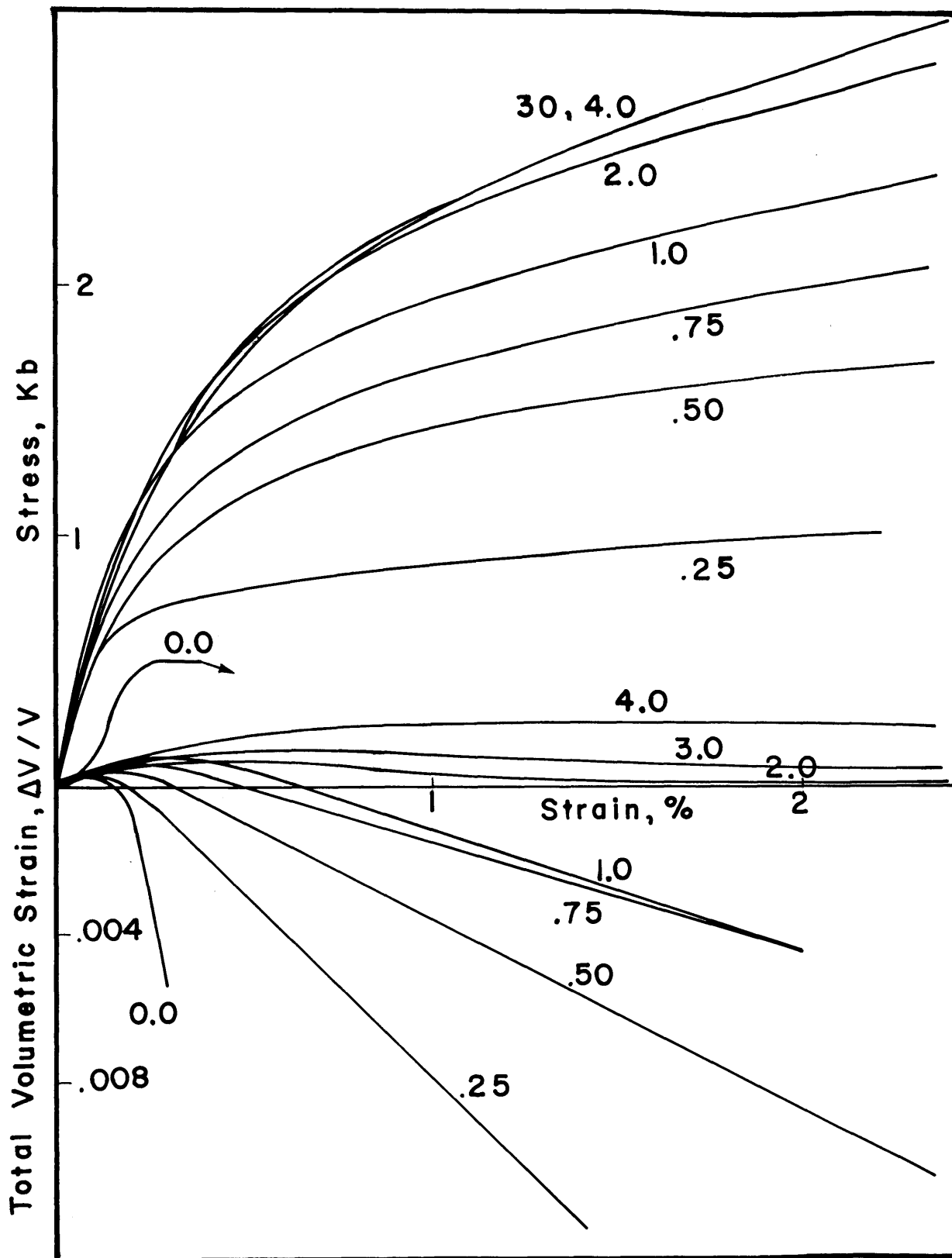


FIGURE 10. Stress vs axial strain and volumetric strain vs axial strain for marble deformed under several confining pressures.

TABLE 4. Compressive Tests on Marble

Exp. No.	Pressure kb.	Y kb.	$d\sigma/d\epsilon$ kb.	$d\Delta/d\epsilon$	ν^*
30	0	0.50	0.0	-4.70	2.85
65	0.25	0.87	11.9	-0.95	.97
66	0.50	1.46	17.4	-0.51	.75
76	0.75	1.76	28.8	-0.29	.65
67	1.00	1.95	34.2	-0.33	.66
70	2.00	2.24	43.5	-0.06	.53
77	3.00	2.28	51.0	-0.06	.53
68	4.00	2.28	50.5	0.00	.50

\bar{y} at 1% strain, the slope $d\sigma/d\epsilon$ of the stress-axial strain curve after yielding, and the slope $d\Delta/d\epsilon$ of the volumetric strain-axial strain curve in the same region are given in Table 4. These quantities are accurate to within 5%. Notice that \bar{v}^* decreases very rapidly as pressure is increased and appears to reach a limit of 0.5 at 4 kb. Almost all of the change occurs in the first 2 kb.

Fully plastic flow of a polycrystalline material inherently implies some very general properties (see, e.g., Hill [1950], Chapter II). Specifically, plastic deformation is unaffected by confining pressures, provides little or no sources for radiative elastic energy, and produces no volumetric strain. As shown above, all these conditions are very closely approached at confining pressures above 3 kb. The satisfaction of these criteria very strongly suggests that true fully plastic flow is the mode of deformation in this rock at high confining pressure. The mechanism of transition from cataclastic deformation to plastic flow is rather interesting. It is often said that the effect of pressure will be to inhibit cracking or frictional sliding whereas that of temperature will be to enhance plastic flow. Therefore an increase of either pressure or temperature, or both, will tend to produce plasticity. Just this effect of pressure is shown very graphically in the present experimental results. In the post-yield region, the linear relation between $\Delta v/v$ and ϵ_z shows that intragranular sliding

produces a constant contribution to strain. As pressure is increased, intragranular sliding rapidly decreases and the material begins to increasingly resemble a fully plastic solid in that its stress-strain behavior is affected by pressure to an increasingly smaller degree. The close link between the decrease in dilatancy and the rate of change of mechanical properties with pressure can be seen from Figure 11, in which v^* , the basic measure of dilatancy, is plotted vs pressure, as well as $\underline{\gamma}$ and $d\sigma/d\epsilon$. The change in v^* with pressure is very similar to that of $\underline{\gamma}$ and $d\sigma/d\epsilon$.

Some aspects of the microfracturing behavior need to be clarified with respect to this picture. Apparently some sort of reorganization takes place during the yield region which results in an equilibrium between plastic flow and cataclastic deformation. This is evidently accompanied by a brittle process, since a very distinct peak in activity is observed during yielding. Similar high rates of activity during yielding, followed by relative quiet, have been observed by Shoemaker [1961] in studies of the acoustic emission of steel and aluminum. His conclusions are that these emissions are due to plastic instabilities, such as the rapid release of dislocations from pileups. These cannot be entirely ruled out for marble, although at the same time brittle processes are not necessarily absent in metals. Twinning, in particular, may be a possible source of radiative energy in marble, although it should in general be accompanied by cracking.

The absence of microfracturing activity in the post-

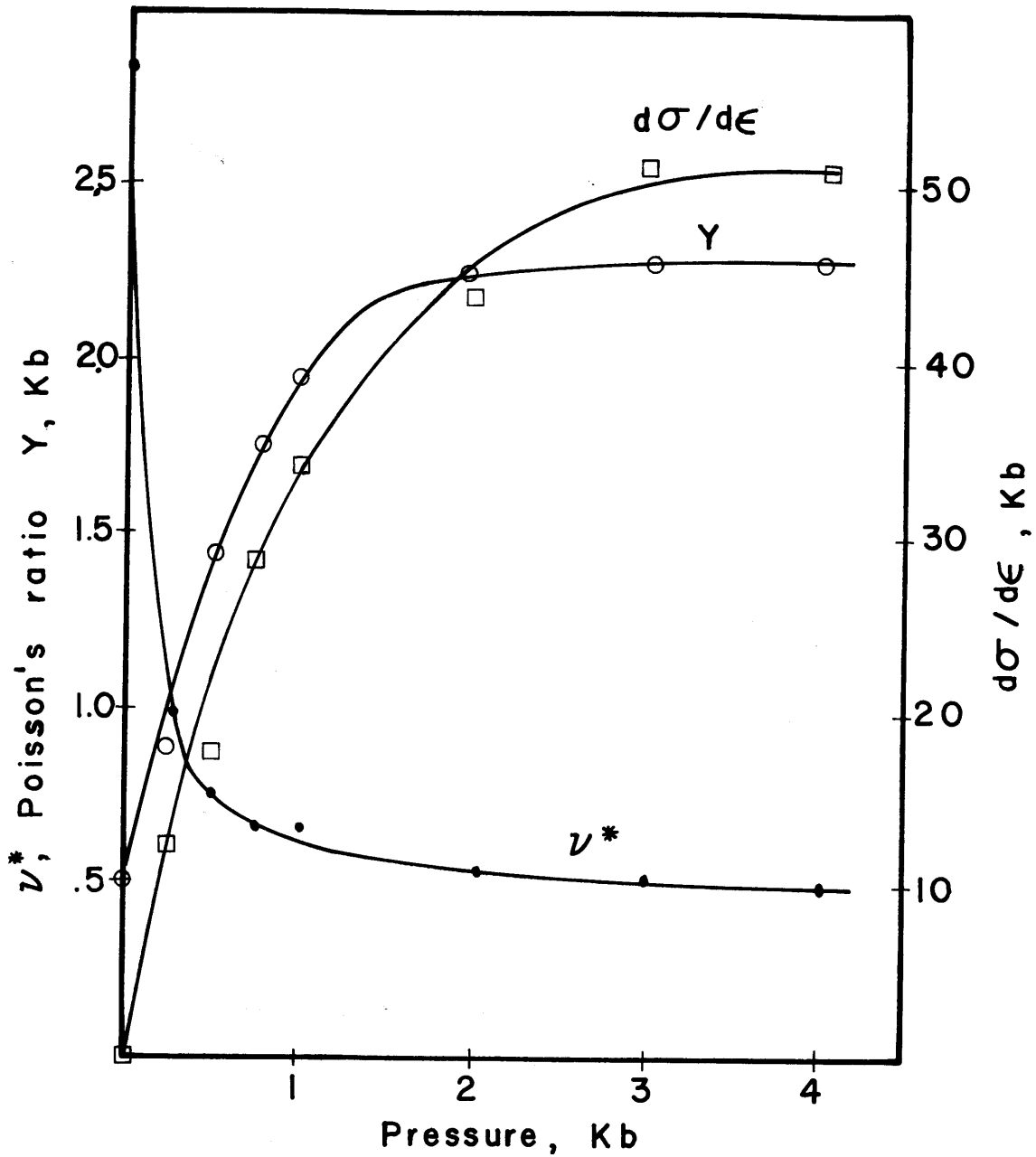


FIGURE 11. The pressure dependence of the parameters Y , $d\sigma/d\epsilon$, and ν^* for marble. Y is the strength at 1% strain, $d\sigma/d\epsilon$ the slope of the strain hardening curve, and ν^* Poisson's ratio in the post-yield region.

yield region, even when a large amount of dilatancy is observed, suggests that if intragranular frictional sliding is the mechanism responsible for producing dilatancy, the plastic rather than the brittle form of friction obtains in grain to grain interfaces. This is in agreement with recent observations (Byerlee, personal communication, 1967) that many ductile rocks, including carbonate rocks, under moderate confining pressure exhibit a plastic form of friction which is not accompanied by stick-slip.

A number of workers have studied the brittle to ductile transition in rock. The most systematic study is that of Heard [1960] who defined the transition on the basis of the form of the stress-axial strain curve and on the presence or absence of faulting evidence in the specimen after deformation. In this study we have seen that the transition is not sharply defined, but that even the transition from cataclastic deformation to plastic flow for marble takes place over a quite large range in pressure (Figure 11). Also, the form of the stress-axial ~~strain~~ curve and the appearance after testing yield little information as to the processes actually occurring.

Theory and Discussion

We have observed that microfracturing occurs in the deformation of brittle rock in compression and produces the characteristic inelastic properties of rock at high stresses

in a way analogous to that which closure of pre-existing cracks produces inelasticity at low stress. This process of microfracturing is a very well defined property, quite similar for a wide variety of different brittle rock types. It is distinctly different from the processes that occur during frictional sliding or ductile deformation. These observations disagree with some of our previous ideas about deformation and fracture of brittle materials and serve as a clue to a better understanding of these processes. In this section, some of these differences will be explored, and a few very simple concepts developed to explain some of the properties of brittle rock.

Brittle fracture occurs by the separation of the material into parts. Yet any direct calculation of the forces necessary to break atomic bonds in a crystalline solid gives strengths orders of magnitude greater than those observed.

In his classic work, Griffith [1921] resolved this problem by assuming that defects in the form of narrow cracks which produce stress concentrations exist in brittle materials. He proposed that fracture occurs when the stress at the tip of the crack with the highest stress concentration exceeds the stress necessary to break atomic bonds. This crack will then propagate unstably through the body, causing fracture. Using solutions for stress around an isolated crack in an elastic, homogeneous body, he then calculated a failure criterion based on this model.

According to Griffith's model, a brittle material should behave elastically until the most highly stressed crack propagates, and the sample fractures. This is clearly not what we observe for rocks in compression; cracks propagate at stresses much lower than the fracture stress, and many thousands of cracking events can be detected prior to fracture.

Brace and Bombolakis [1963] and Hoek and Bieniawski [1965] studied crack growth photoelastically in glass plates stressed in compression. They found that the initiation of crack growth under such conditions did not lead to failure, but that the cracks became stable after propagating some fraction of their initial length. It might be suggested that these observations resolve the contradiction presented above: Griffith's theory does not apply in compression because a crack in compression, unlike a crack in tension, cannot cause fracture by propagating unstably throughout the entire body.

If this argument is accepted, then we would expect that microfracturing does not occur in tension, where Griffith's theory would apply. However, Mogi [1962 a] demonstrated that in bending, which must involve tensile crack propagation, microfracturing was important. Indeed, the behavior he observed in bending is very similar in many respects to that observed in the present study in compression. The microfracturing behavior of rock in uniaxial tension [Brown,

1965] is also very similar to that observed in compression. The observed differences between the propagation of cracks in tension and compression therefore seems to have very little effect on microfracturing behavior. Cracks in tension as well as compression do not propagate through rock as Griffith's model predicts, although it has been conclusively shown that tensile cracks behave this way in other brittle materials such as glass. Why then, does rock behave differently than, say, glass?

The primary mechanical difference between these materials is that stress concentrations in rock do not arise solely from isolated cracks, as postulated by Griffith. Rock is a polycrystalline aggregate composed, in general, of several highly anisotropic phases. If a uniform stress is applied to such an inhomogeneous material, local stresses will fluctuate significantly from the applied value. The granular nature of rock complicates matters even further, since structural irregularities such as pores and cracks and interactions between them will produce additional fluctuations of the stress field within the body.

Consider how such an inhomogeneous body will react when subjected to a uniform increasing load. As the applied stress is raised, a point will be reached when in the small region in which stress concentration is highest, the strength will be exceeded, and a crack will propagate. This crack will rapidly be arrested, however, if it propagates into

adjacent regions in which the stress is lower. As the applied stress is increased still higher, the region with the next highest stress concentration will fail, and so on, until some sort of instability produces fracture of the entire body.

The formation of a macroscopic fracture in such an inhomogeneous medium, then, will be much more complex than the simple case given by Griffith. Since such a system is intractable by ordinary analytical techniques, we have chosen to describe the variation of stress within an inhomogeneous medium, such as rock, by a statistical model. Obviously such a model cannot describe the events that take place at a given point within the body, but will be sufficient to predict the gross mechanical properties, which are usually of more interest.

In order to introduce the model, we take the simple case of an inhomogeneous brittle material under a single component of uniform applied stress. Such a system is illustrated schematically in Figure 12, where we show an inhomogeneous body under a uniform applied stress $\bar{\sigma}$. Now consider that regions within the body, small enough such that the stress on them may be considered uniform, are subjected to a local stress σ , which varies in a random fashion throughout the body. Fracture will then occur within these small regions when σ exceeds \underline{S} , the strength. It might be argued that this strength will also fluctuate, so that we

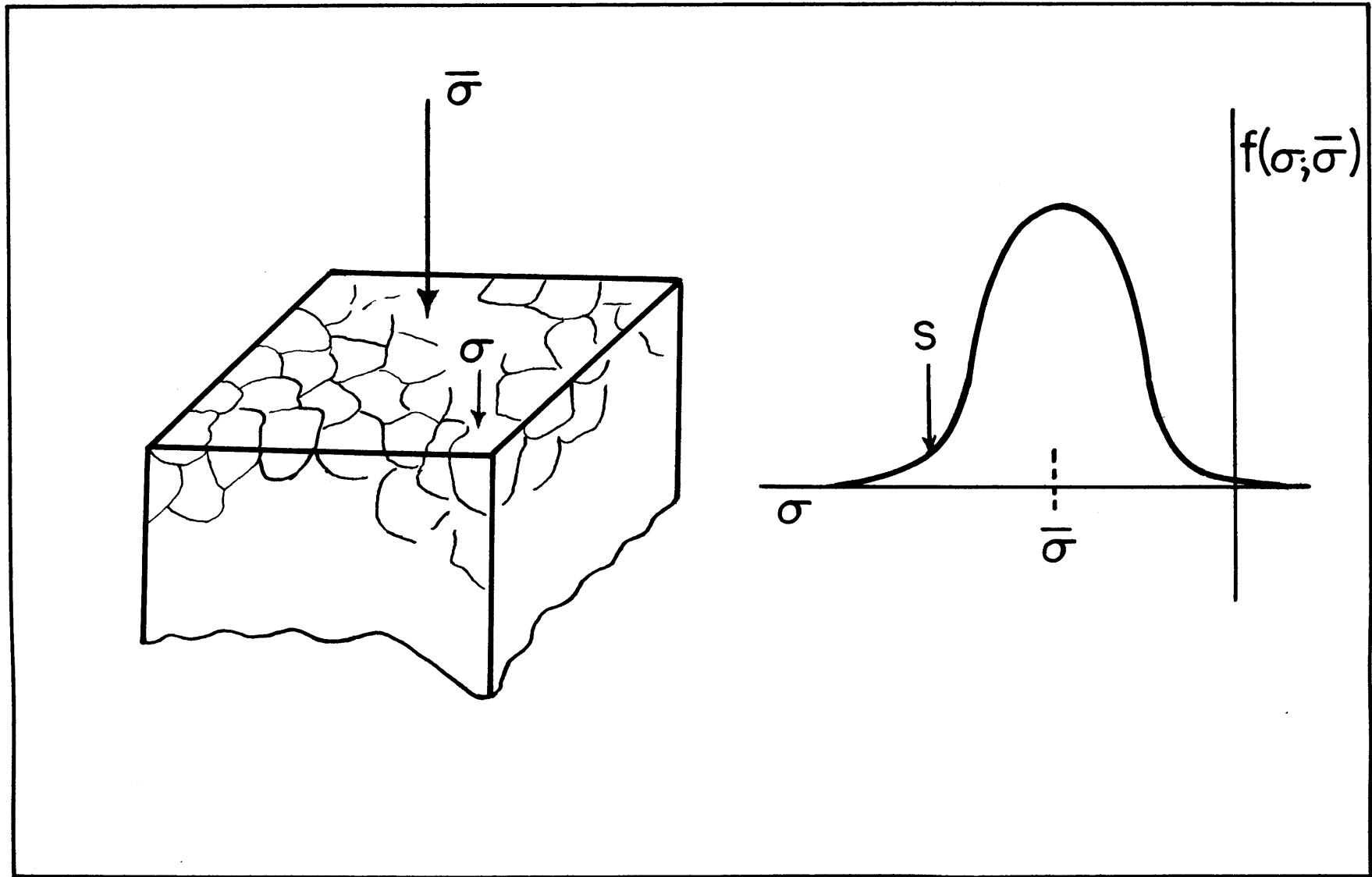


FIGURE 12. An illustration of the response of an inhomogeneous body to an applied stress $\bar{\sigma}$ is on the left. The local stress σ may vary significantly from point to point. On the right we show an arbitrary stress probability function $f(\sigma; \bar{\sigma})$ and the local strength S . For explanation see the text.

must consider these variations as well. However, in fracture mechanics it is not the stress or strength which is important but the difference between the two; so either of them or both of them can be considered as variable. Since strength is conventionally thought of as a constant, it will be simpler to retain this concept since the results will not be affected. The effect of cracks in producing stress concentrations will of course be much greater than that of other sources, so it is likely that fracture will take place in general only in regions in which cracks exist. We may think of \underline{S} , then, as defined on the presence of an average size and oriented crack. Variations of the size and orientation of cracks, as well as stress concentrations due to other sources, will be considered as variations of the local stress, σ , applied to such an average crack.

With such a model, σ can be considered to be a random variable. Therefore, the probability that the stress at a point is some value σ is given by a probability density function $f(\sigma; \bar{\sigma})$. Such an arbitrary function is shown in Figure 12. Also shown is our arbitrarily defined strength \underline{S} . From equilibrium, the mean of $f(\sigma; \bar{\sigma})$ is $\bar{\sigma}$. Consequently, as $\bar{\sigma}$ is increased, $f(\sigma; \bar{\sigma})$ will move to the left. Eventually, there will be a finite probability that the stress in a region will exceed \underline{S} , and microfracturing will begin. As $\bar{\sigma}$ is increased, the rate of microfracturing will steadily increase, since the frequency of microfracturing activity,

\underline{n} , during the increment $\bar{\sigma}$ to $\bar{\sigma} + d\bar{\sigma}$ will be given by

$$n(\bar{\sigma}) = K_1 f(s; \bar{\sigma}) d\bar{\sigma} \quad (1)$$

where K_1 is a constant. Accordingly, the accumulated frequency of events, \underline{N} , is given by

$$N(\bar{\sigma}) = K_1 F(s; \bar{\sigma}) = \int_{-\infty}^s K_1 f(\sigma, \bar{\sigma}) d\sigma \quad (2)$$

where $F(S; \bar{\sigma})$ is the probability distribution function of $\bar{\sigma}$. If we follow our previous assumption that such microfracturing events contribute an average increment η to the volumetric strain, then

$$\Delta^* = \eta K_1 F(s; \bar{\sigma}) \quad (3)$$

The statistical stress distribution, described by $f(\sigma; \bar{\sigma})$, is a fundamental property of a given rock and depends in detail upon its composition and microstructure. It should also be pointed out that the mean microscopic

strength \underline{S} , although defined somewhat arbitrarily, also represents a distinct property of any given rock. Therefore, the gross microfracturing process is well defined by equations 1 to 3 and should be fairly reproducible, as observed.

It is interesting to take the analysis a bit farther by suggesting a possible stress distribution that might occur in rock. When microfracturing activity is fairly low, for example, the events may be considered to be isolated in space. The local stress which produces each event will then be an independent random variable, and $F(S; \bar{\sigma})$ can be approximated by a normal distribution.

The mean of the distribution is $\bar{\sigma}$. The stresses, σ , must vanish everywhere when $\bar{\sigma}$ vanishes (we disregard residual stresses that may be present since they will be expected to be much smaller than applied stresses in the microfracturing region). A simple model satisfying this requirement is that the standard deviation, μ , is of the form

$$\mu = K_2 \bar{\sigma} \quad (4)$$

where K_2 is a constant. This implies that there exists a mean stress concentration factor ζ , where

$$\zeta = K_2 + 1 \quad (5)$$

In this model, the accumulated frequency of microfracturing is given by

$$N(\bar{\sigma}) = \frac{1}{2\pi K_2 \bar{\sigma}} \int_{-\infty}^S \exp \left[\frac{-(\sigma - \bar{\sigma})^2}{2(K_2 \bar{\sigma})^2} \right] d\sigma \quad (6)$$

In Figure 13, we show this function fitted to the experimental data for uniaxial compression of Westerly granite. The fit is very good for stresses between 50% and 95% of the fracture strength, but the data cannot be fitted in the region above 0.95C. This apparent change in mechanism of the process at approximately 0.95C appears to be real. This is the point at which rapid acceleration of microfracturing occurs. Above this stress it has been noted that the relationship between \underline{N} and Δ^* does not in general hold and that these quantities are also not reproducible. In associated studies [see Chapt. 4], we demon-

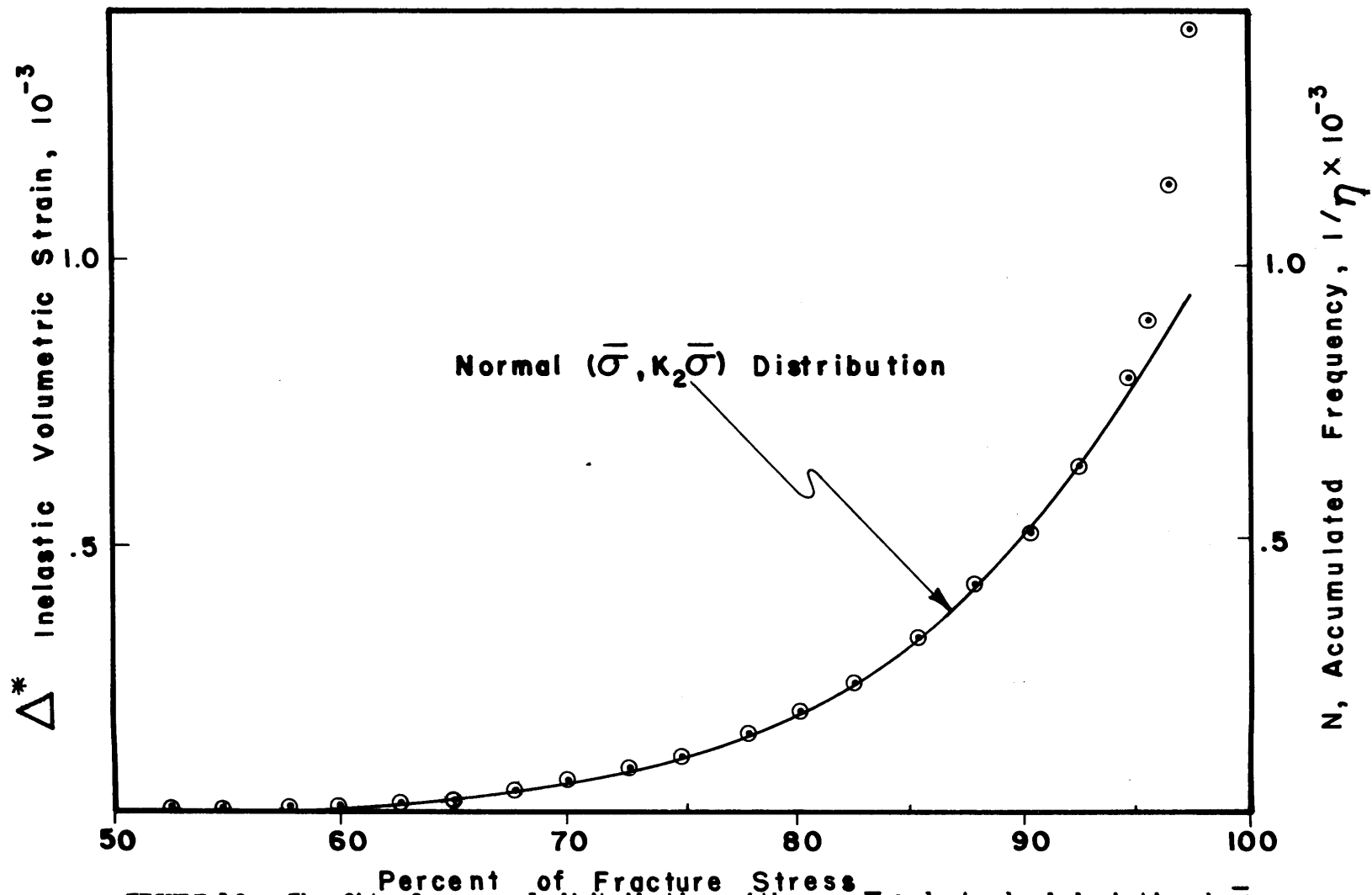


FIGURE 13. The fit of a normal distribution with mean $\bar{\sigma}$ and standard deviation $k_2\bar{\sigma}$ to the accumulated frequency and inelastic volumetric strain for Westerly granite²⁰¹ under uniaxial compression.

strated from more direct evidence the difference between this region and that at lower stress. By locating selected microfracturing events in space, I found that events at low stresses occur randomly throughout the specimen, whereas the events above $0.95C$ tend to cluster. These form the fault which leads to eventual fracture of the specimen. These observations agree with the results of the above statistical analysis, which suggests that events that occur in the region below this critical stress are randomly independent, whereas at greater stresses a larger number of events occur than predicted by the theory, suggesting the formation of an instability. These two regions can be described as zones of static and dynamic cracking, respectively. From the best fit to the experimental data in the static cracking region, the parameters ζ and S for Westerly granite under uniaxial compression are found to be 2 and $2.25C$, respectively.

For simplicity, the analysis has been carried out only for the special case of a single uniform component of mean (applied) stress. It can readily be shown that the results will be the same for deformation in a uniform general mean stress system. In the general case, however, S will be a function of all components of mean stress, and all components of local stress will be random variables defined on a joint probability space. In the case of nonuniform stresses, i.e. where the mean stresses vary in space, the analysis will

be somewhat more complicated since the probability distribution of σ will be a function of position.

Conclusions. The technique of detecting and analyzing microfracturing developed in this study has demonstrated that a great deal of information about the microscopic process accompanying deformation of rock can be obtained routinely. In particular, the conclusions of Brace et al. [1966] regarding the dilatancy of rock have been confirmed and expanded: for a very wide variety of brittle rocks of diverse structure and composition, and over a wide range of confining pressure, deformation is accompanied by small scale fracturing which begins at about half the fracture stress. As stress is increased, the cracking accelerates steadily until at a point a few percent below the fracture strength a rapid increase occurs, marking the formation of the fault. The inelastic stress-strain behavior of these rocks can be completely accounted for by the strains contributed by this cracking activity.

These results may improve our understanding of the strength of brittle rock. We have shown that Griffith's criterion of brittle fracture is not applicable to rock because the inhomogeneity inherent in rock will produce fluctuations in the stress field sufficient to arrest cracks shortly after they have been initiated. Proceeding from these concepts, a simple statistical model was introduced which predicts the observed microfracturing behavior. This theory, however, does not directly apply to rock fracture.

As yet, the process which leads to the formation of the fault and to eventual fracture of the rock is not understood, nor are the factors which govern the stress at which this occurs. Empirically, from the evidence of reproducibility of microfracturing, it is concluded that the fault begins forming when the crack density reaches some critical value. This is equivalent to the concepts of "critical dilatancy" or "critical void ratio" in the language of soil mechanics [Scott, 1963, p. 310]. The additional factor of the reproducibility of strength, coupled with the above observation, leads to the conclusion that, under identical conditions, the stress difference between fault initiation and fracture is constant.

These observations, of course, do not lead us very far toward an understanding of rock fracture, but they suggest an experimental approach. Our results have shown that for given conditions there is a "critical crack density," but it is not known how this depends on pressure and temperature, say, or time. The results reported for triaxial compression tests indicate that the pressure effect is slight but are inconclusive insofar as delineating the effect clearly. It is suggested that if further work was done to determine the influence on critical crack density of these various parameters an understanding of the process of fault formation and fracture might evolve.

CHAPTER 2

THE MECHANISM OF CREEP IN BRITTLE ROCK

Introduction

When rock is subjected to high deviatoric stress, time dependent strain occurs in a characteristic manner. This behavior, known as creep, occurs even in brittle rock at low temperature and pressure. Creep is usually studied in the laboratory by subjecting rock to a single component of stress which is held fixed while strains are measured as a function of time. Figure 14 shows a typical creep curve for such an experiment. Because of the nature of the curve, creep is usually described as occurring in three stages [Robertson, 1964]. Immediately after the load is applied, very rapid creep occurs which decays off swiftly. Creep strain at this stage is proportional to the log of time and the behavior is known as transient or primary creep. At fairly low stresses, transient creep may account for most of the time dependent strain of brittle rock. Transient creep is often followed, particularly at high stresses, by deformation at a constant strain rate which is termed secondary or steady-state creep. If secondary creep is allowed to continue, eventually creep begins to accelerate (tertiary creep) and fracture occurs. Such creep fracture in brittle rock appears similar in all

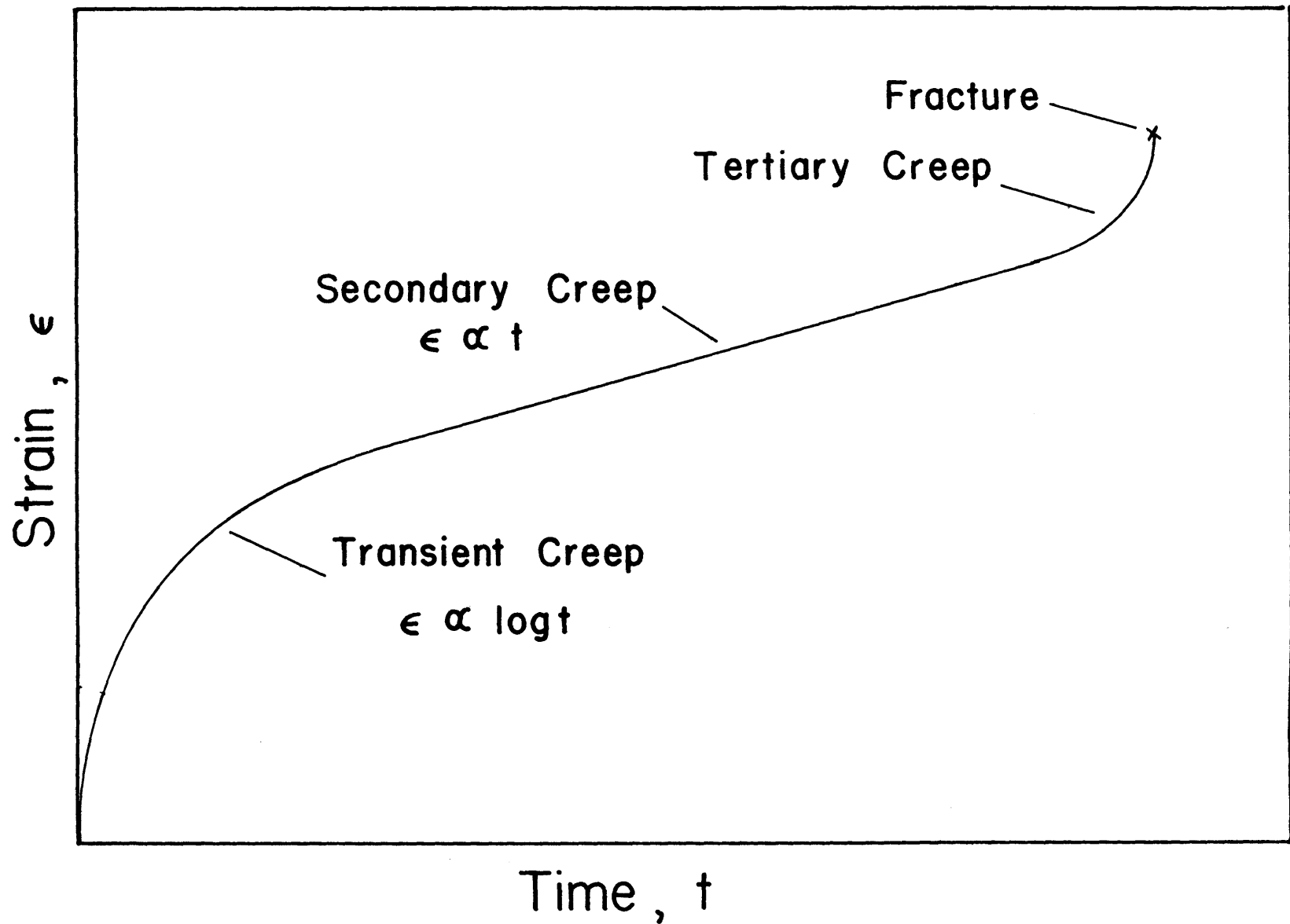


FIGURE 14. A typical creep curve for rock in compression.

respects to that observed in a conventional fracture test. In compression, for example, it occurs by catastrophic failure on a fault acutely inclined to the direction of maximum compression.

The creep behavior described above is very similar to that observed for metals, polymers, and many other plastic and viscoelastic materials. Because of this, creep of rock is often described in terms of viscoelastic rheological models, and interpreted with respect to mechanisms which are known to occur in metals.

Creep of rock, however, is typified by some unique characteristics which do not occur in metals and are not described by the usual rheological models. Matsushima [1960] found in creep tests on granite in compression that creep strain lateral to the direction of compression was larger than creep strain in the longitudinal direction. He also found that lateral creep rate increased much more rapidly with stress than did longitudinal creep rate. He concluded that the samples were cracking. Robertson [1960] also concluded that fracturing is an important mechanism of creep in rock. In experiments with Solenhofen limestone, he found that the density of the samples decreased significantly during testing.

Both of these results suggest that the volume of the rock increases during creep. The inelastic behavior in which volumetric strain increases relative to what would

be expected from elasticity is known as dilatancy and has been extensively studied in constant strain rate experiments on rock by Brace et al. [1966]. They also suggested that dilatancy was produced by small scale cracking. This idea was confirmed and expanded ~~above~~ (Chapter 3). In that study, the small cracking events, which we refer to as microfractures, were studied directly by detecting and analyzing the elastic waves which they radiate. By comparing the number of microfractures that were detected with observed macroscopic strains it was found that dilatancy can be entirely attributed to microfracturing. Watanabe [1963] did a similar study and found that creep strain was also directly proportional to microfracturing activity for granite under compression. Mogi [1962] obtained the same result in creep experiments in bending, as did Brown [1965] in uniaxial tension. Gold [1960] also found that cracking activity was directly proportional to creep strain in ice.

Experimental work therefore has demonstrated that creep in rock at low temperature and pressure is produced by microfracturing. Each microfracture contributes an increment of strain, resulting in time dependent dilatancy. In conjunction with the study in Chapter 1 we also developed a statistical theory of rock deformation in which rock was treated as an inhomogeneous brittle material. The theory was found to successfully predict the observed

microfracturing and dilatancy. The above observations that creep is also produced by microfracturing indicates that we did not take into consideration all aspects of microfracturing, however. The theory only considered microfracturing that is produced as stress is increased and ignored the time dependence of microfracturing. In that study the influence of time on the process could be neglected, because all experiments were done at the same constant strain rate. In order to obtain a complete theory of microfracturing, however, we must consider the effects of both stress and time on the process. In this study we shall extend the basic model into the time domain, and derive a creep equation for rock.

Analysis

Rock is a polycrystalline aggregate of in general several anisotropic phases. If a uniform stress is applied to such an inhomogeneous material the local stress at a point will not in general be the same as the applied stress, but will vary in some complex way throughout the body. The diverse cracks and pores which exist in rock will produce additional fluctuations of the stress field. This inhomogeneity is the basic factor which governs the microfracturing of rock. Without a precise knowledge of the irregularities producing the inhomogeneity, however, we cannot predict the state of stress throughout the body.

Instead, in the development of our basic model, we chose to define the probability that σ , the stress in a region (small enough such that the stress on it may be considered uniform) is some value in terms of a probability density function $f(\sigma; \bar{\sigma})$. The stress probability function $f(\sigma; \bar{\sigma})$ is in general a function of the applied stress $\bar{\sigma}$. We also proposed that each small region would fracture when the local stress σ exceeds \underline{S} , the local strength. Normally such fractures will not cause failure of the entire body because they will tend to propagate into adjacent regions where the stress is lower and be arrested. Each small fracture, however, contributes an increment of inelastic strain which in total produces the inelastic stress-strain behavior of the body. As the body is loaded, the stress in each small region tends to increase with the applied stress so that eventually there is a finite probability that σ exceeds \underline{S} , and microfracturing will begin to occur. If the stress is increased still further, microfracturing activity will accelerate until eventually the formation of some instability results in failure of the entire body.

In that model, we assumed that the local strength \underline{S} is constant in time. It is well known, however, that the strength of most brittle materials, including rocks, is time dependent. If such a material is subjected to a constant load it will, in general, fracture after some time interval. This weakening in time is known as static

fatigue. It has been shown for a wide variety of materials that static fatigue is due to stress corrosion, i.e. when a brittle material is stressed in a corrosive environment, the high tensile stresses at the tips of cracks accelerate the corrosion reaction there so that the cracks tend to lengthen. After a period of time at a sustained stress level, a crack will reach the critical Griffith length and propagate unstably. For a material to which the Griffith criterion applies, such as glass in tension, this will cause fracture of the specimen. In an inhomogeneous medium such propagating cracks will be arrested by fluctuations in the stress field exactly as described above, and many thousands may occur prior to fracture of the body as a whole. In an inhomogeneous medium, then, static fatigue will produce time dependent microfracturing.

The primary corrosive agent responsible for static fatigue of silicate materials is water [Charles, 1959; le Roux, 1965]. Although several different types of corrosive reactions have been proposed [le Roux, 1965; Stuart and Anderson, 1953], Charles has studied the static fatigue of a number of silicates and oxides and found them to be quite similar in behavior. On the basis of his results he argues that static fatigue of silicates is due to hydration of the silicon-oxygen bond. Because of the general nature of this reaction he suggests that all silicate materials should exhibit similar static fatigue behavior. In a more

detailed study, le Roux confirmed that this reaction is responsible for static fatigue in fused silica.

Although the detailed reaction mechanism is unknown for most materials and would be expected to depend on the environment and the composition of the stressed medium, the gross form of the time and temperature dependence of strength might be expected to be the same for a wide variety of materials due to the basic thermodynamic similarity of the stress corrosion process. A review of the published experimental data strongly supports this view. For many different materials, for which different reaction mechanisms have been proposed, the static fatigue behavior is very similar. Along the lines of this argument, in fact, Mould and Southwick [1959] attempted to define a "universal" static fatigue law.

Most of the static fatigue studies have been done on homogeneous materials, such as glasses. An inhomogeneous material will react differently. Each small region (which can be considered homogeneous) will undergo static fatigue, but the resulting behavior of the entire body will be time dependent microfracturing, resulting in creep. In the light of the basic empirical similarity of the static fatigue of brittle materials and Charles' conclusions regarding the silicates, we can approximate the static fatigue behavior of each region in an inhomogeneous body by the known behavior of homogeneous materials. Glass is such a

homogeneous system, and abundant data are available for it.

In static fatigue studies, the material is held at constant stress and data are generally reported as the mean fracture time, $\langle t \rangle$. For most of the materials which have been studied a good approximation for the stress dependence of $\langle t \rangle$ over five to seven orders of magnitude in time is given by

$$\langle t \rangle \Big|_T = a e^{b(S^* - \sigma)} \quad (1)$$

where S^* is the "no corrosion" strength, σ is stress, and a and b constants. This equation agrees well with the data for E glass [Schmitz and Metcalf, 1966], alkalie glass [Mould and Southwick, 1959], and pyrex and fused silica [Glathart and Preston, 1946]. Equation 1 is obviously not valid over all ranges. Since S^* is defined as the strength as $t \rightarrow 0$, (1) cannot hold for small t . It generally fits the data for $t > 10^{-2}$ sec and is quite good within the range of interest here. It is also important to note that (1) does not hold at low stresses, say below 0.2 to 0.4 S^* . This can be seen qualitatively, since at low stresses the normal crack blunting tendency of the chemical reaction should tend to counter the stress induced lengthening and inhibit the mechanism. The approximation which we shall assume

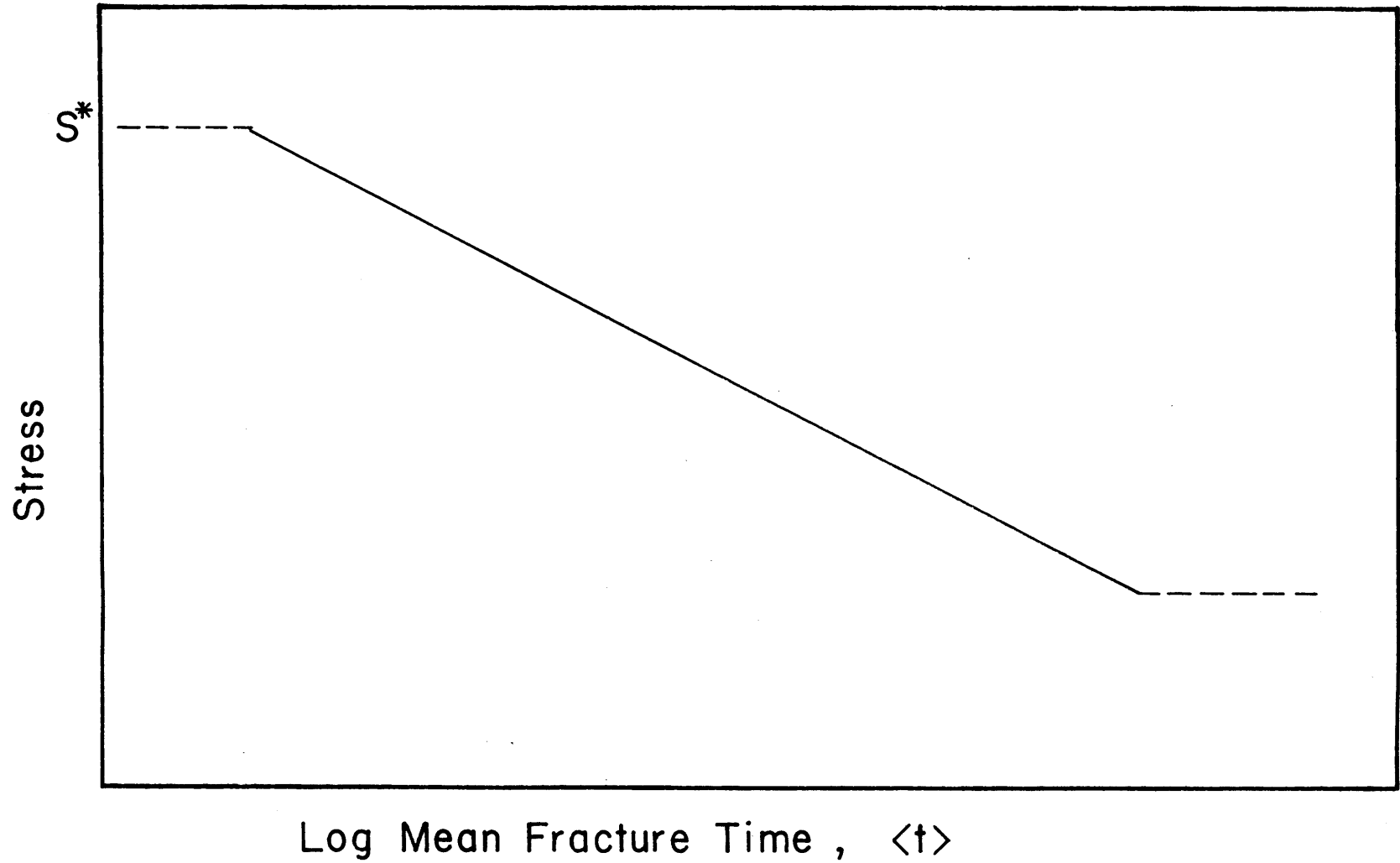


FIGURE 15. The static fatigue behavior assumed in the model. The solid curve agrees with the experimental data for a wide variety of brittle materials.

for the stress dependence of static fatigue is shown in Figure 15. The range of applicability of (1) is shown by the solid portion of the curve.

Charles [1959] and le Roux [1965] have studied the temperature dependence of static fatigue and found that over a considerable range of temperature the behavior could be given by

$$\langle t \rangle \Big|_{\sigma} = c e^{E/kT} \quad (2)$$

where E is the activation energy of the corrosion reaction, k is Boltzman's constant, T is the absolute temperature, and c depends upon the material and its environment.

Equations 1 and 2 agree well with all the available data on static fatigue within the range of interest which we are concerned with here. Accordingly we assume that static fatigue of small regions within an inhomogeneous silicate material follows the form, combining (1) and (2)

$$\langle t \rangle = (1/\beta) e^{bE(S^* - \sigma)/kT} \quad (3)$$

where σ is the local stress, and $1/\beta = ac$.

We will now incorporate the above behavior into the basic model and calculate the microfracturing behavior in time. This is characterized by considering that each of the small regions within the heterogeneous body have the following properties.

a) Each region undergoes static fatigue and follows the general empirical approximation, equation 3.

b) When a region fails, it contributes an average increment η to the volumetric strain. This has been demonstrated by the experimental observations of the proportionality of strain and cracking activity.

c) Each region acts independently.

d) Each region can only fail once.

Adopting these assumptions, let the probability that the stress in a region is from σ to $\sigma + d\sigma$ at time t be given by $f(\sigma; \bar{\sigma}, t)$, where $f(\sigma; \bar{\sigma}, t)$ is the probability density function of stress. In the case where $t=0$, this is the time independent function, $f(\sigma; \bar{\sigma})$. The probability $\mu(\sigma)dt$ that a region at stress σ will fracture during the following time interval dt is related to the mean fracture time by

$$\mu(\sigma)dt = dt / \langle t \rangle$$

and from (3), we have

$$\mu(\sigma)dt = \beta \exp[-bE(S^* - \sigma)/kT]dt \quad (4)$$

The volumetric creep rate $\dot{\Delta}$ is then given by

$$\dot{\Delta} = \eta \int_{S^*}^{\infty} f(\sigma; \bar{\sigma}, t) \mu(\sigma) d\sigma \quad (5)$$

We are treating the case of creep in compression. Compressive stress is taken as negative. For creep in tension, the limits of integration would be $-\infty$ and T^* , where T^* is the local tensile strength.

Since each region fails only once, the number of available regions in each stress range decreases at a rate

$$\frac{\partial}{\partial t} f(\sigma; \bar{\sigma}, t) = -f(\sigma; \bar{\sigma}, t) \mu(\sigma) \quad (6)$$

which integrates to give

$$f(\sigma; \bar{\sigma}, t) = f(\sigma; \bar{\sigma}, 0) \exp[-\mu(\sigma)t] \quad (7)$$

where $f(\sigma; \bar{\sigma}, 0)$, the initial density function, equals the time independent density function $f(\sigma; \bar{\sigma})$ defined earlier. Equation 4 allows us to write

$$d\mu(\sigma) = -(bE/kT)\mu(\sigma)d\sigma$$

Assuming that the initial distribution $f(\sigma; \bar{\sigma}, 0) = M$, a constant over $S^* \leq \sigma \leq 0$ and zero for $\sigma \geq 0$, the creep law is given by

$$\begin{aligned} \dot{\Delta} &= -\eta \frac{Mkt}{bE} \int_{S^*}^0 e^{-\mu(\sigma)t} d\mu(\sigma) \\ &= \eta \frac{MkT}{bEt} [e^{-t/\langle t \rangle_0} - e^{-t/\langle t \rangle_{S^*}}] \end{aligned} \quad (8)$$

where $\langle t \rangle_{S^*}^{-1} = \mu(S^*) = \beta$ and $\langle t \rangle_0^{-1} = \mu(0) = \beta \exp\left(\frac{-bS^*E}{kT}\right)$.

In the range of practical interest, $\langle t \rangle_{s^*} \ll t \ll \langle t \rangle_0$, the factor in brackets is essentially unity, and we have

$$\dot{\Delta} = \eta \frac{MkT}{bE\tau} \quad (9)$$

or

$$\Delta = \eta \frac{MkT}{bE} \log t \quad (10)$$

which gives the familiar form of transient creep in rock. η can also be considered to be the increment of axial or lateral strain produced by a crack, so (10) can apply alternatively to axial or lateral creep. The effect of the opening of cracks in an elastic body on the volumetric, axial and lateral strains have been given by Walsh [1965a, 1965b, 1965c].

It is interesting to note that although the mechanism is entirely different, the derivation of the creep law given above is formally identical to the exhaustion theory of Mott and Nabarro [1948], which was based on the diffusion of dislocation loops through barriers. The assumption that $f(\sigma; \bar{\sigma}, 0)$ is a constant does not seem reasonable. However,

unless $f(\sigma; \bar{\sigma}, 0)$ varies as steeply with σ as $\exp(-\mu(\sigma)t)$, it cannot significantly affect the creep law [Cottrell, 1953, p. 201]. Since the latter is nearly a step function, this condition is considered to be always true.

Stress dependence. It is widely known [Robertson, 1964] that creep in rocks is stress dependent. Generally creep rate has been found to be a power function of mean stress, and a table of the experimentally observed exponents is given in Robertson's paper. The factor M in (9) and (10) is an assumption of the form of $f(\sigma; \bar{\sigma}, 0)$. The form assumed is unimportant, from Cottrell's argument, and for analytic convenience it was assumed to be independent of σ . It is, however, a function of $\bar{\sigma}$ and this will affect the creep law. When a mean stress is initially applied to a sample in a creep test the probability function of stress, $f(\sigma; \bar{\sigma})$ will look something like the curve shown in Figure 16. The curve is truncated to the left of S^* since instantaneous fracture will occur in those regions in which the stress exceeds that value. Cottrell [Davis and Thompson, 1950] has shown that since $\exp(-\mu(\sigma)t)$ is approximately a step function, creep could be viewed as an advance of this step along the σ axis. The advance begins at S^* and proceeds to the right with time. This can be viewed as a decrease in the average local stress with time. After time t , strength has decreased from S^* to $S(t)$, sweeping out the shaded portion shown in the figure.

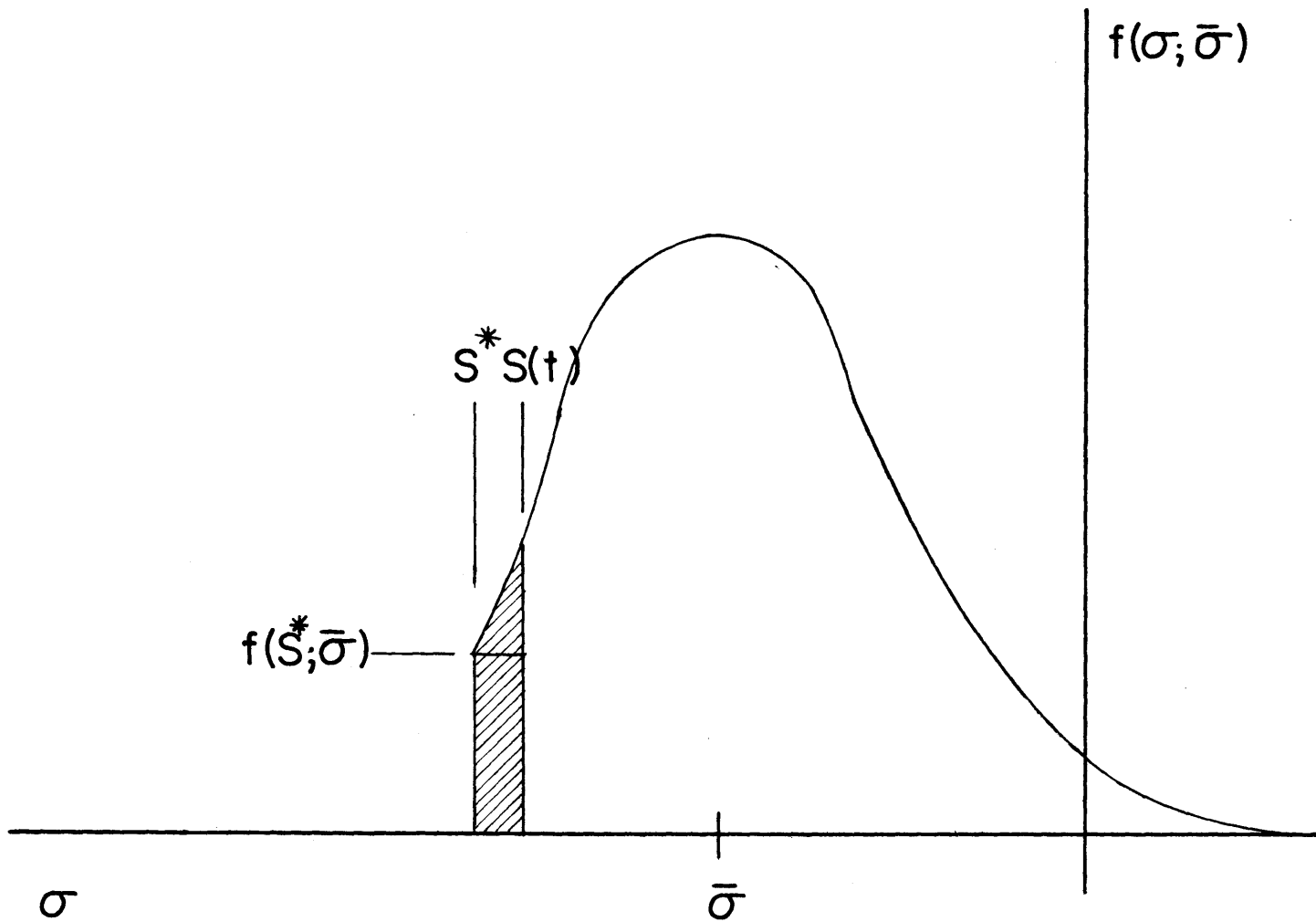


FIGURE 16. The creep model. The smooth curve $f(\sigma; \bar{\sigma})$ is the initial probability function of local stress σ when the applied stress is $\bar{\sigma}$. The regions in which σ is greater than S^* , the initial strength, fracture immediately. The strength at time t is given by $S(t)$. As the local strength is reduced in time, it sweeps through the shaded region, producing creep. The level of creep is approximated by $f(S^*; \bar{\sigma})$.

All regions in which their stress lies within the shaded region have failed. $f(\sigma; \bar{\sigma})$ refers to the initial stress distribution, described in the time independent model. $f(\sigma; \bar{\sigma}, 0)$ is equivalent to $f(\sigma; \bar{\sigma})$ and $f(\sigma; \bar{\sigma}, t)$ to the region of $f(\sigma; \bar{\sigma})$ excluding the shaded part. Within the range of interest for transient creep, the difference between $S(t)$ and S^* will be small compared to $\bar{\sigma}$, so that M can be approximated by

$$M \approx f(S^*; \bar{\sigma}, 0) = f(S^*; \bar{\sigma})$$

as shown in the diagram. Suppose next that creep tests are performed at several different levels of applied stress. A moderate change in $\bar{\sigma}$ will radically affect $f(S^*; \bar{\sigma})$ and hence the level of creep activity. To estimate this effect, we can use the results of constant strain rate experiments. $F(S(t); \bar{\sigma})$, the integral of $f(S(t); \bar{\sigma})$ was obtained in such experiments for a number of rocks in **Chapter 1**. The strain rate used in those experiments was fairly rapid (10^{-5} sec^{-1}) so that the derivatives of those curves will approximate $f(S^*; \bar{\sigma})$. In **Figure 17** we plot $f(S^*; \bar{\sigma})$ obtained in this way (the slope of the curve in **in Chapter 1, Figure 13**) versus mean stress for Westerly granite at room pressure. Clearly \underline{M} is a power function

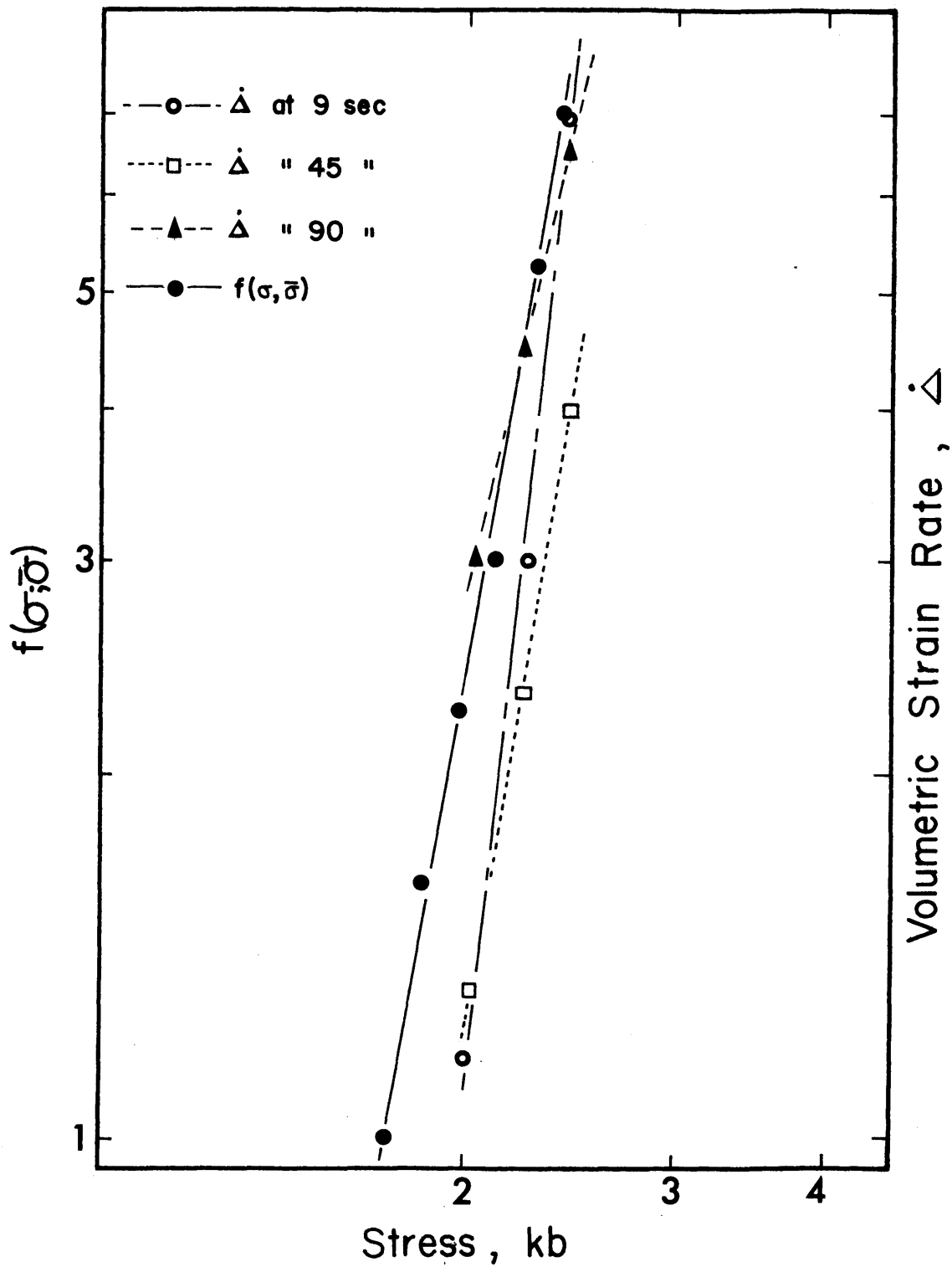


FIGURE 17. The predicted and observed stress dependence of volumetric creep rate for Westerly granite. The scales for $\dot{\Delta}$ are, at 9 sec: $0.5 \times 10^{-6} \text{sec}^{-1}$, at 45 sec: $0.25 \times 10^{-6} \text{sec}^{-1}$ and at 90sec: $0.1 \times 10^{-6} \text{sec}^{-1}$. $f(\sigma; \bar{\sigma})$ is in arbitrary units.

of stress. The exponent is 5.6. In the same figure is shown the relationship between volumetric strain rate and mean stress obtained in actual unconfined creep tests on a sample of Westerly granite taken from the same block Appendix IV. At three different times after application of the load, the plots of strain rate vs. stress indicate power function relationships with exponents 8.2, 6.1, and 4.5. These are all very close to the predicted value. In the constant strain-rate experiments we have shown that the form of $f(S^*: \bar{\sigma})$ is similar for many types of rocks. In general, this relation can be shown to fit a power function. Consequently, (10) can be expected to predict the correct stress dependence of creep, and may be rewritten in the form

$$\Delta = \eta \frac{\bar{\sigma}^n}{bE} \log t \quad (10a)$$

It should be pointed out that we have, for simplicity, dealt only with the response of the material to a single uniform component of mean stress. As was discussed with respect to the time independent theory, the stress distribution within a heterogeneous body will in general be a function of all components of applied stress. The influence of stress on the creep rate will not necessarily be

the same for different types of creep tests, such as torsion and tension. Experimentally, however, it appears that (10a) applies to a wide range of different types of tests [Robertson, 1964] where m and n depend on the type of test.

Discussion

Following the experimental evidence suggesting that creep in rock at low temperature and pressure is due to time dependent cracking, we have assumed that the mechanism is microscopic static fatigue and derived an equation for transient creep in rock. The results predict behavior which agrees closely with that observed experimentally. There are several additional implications of (10a) which can be discussed briefly. Equation 10a implies that creep should be linearly dependent on absolute temperature. It is known qualitatively that an increase of temperature does tend to increase the creep rate in most rocks, but it will be difficult to determine the exact form of the influence, since it is difficult to maintain constant environmental conditions in tests at different temperatures. The parameters b and E in (10a) are environment dependent and their effect is likely to be as great or greater than that of temperature. Very little is known about the effect of environment on the mechanical properties of rock. Charles [1959] and Colback and Wiid [1965] have found that strength

is dependent on environment, particularly on the amount of water present. The present theoretical results suggest that the influence of temperature and environment on creep will be topics of interest for future experimental work.

The present results deal only with transient creep. Are then secondary and tertiary creep produced by different mechanisms? Probably not -- the experimental evidence that cracking is the mechanism responsible for creep in rock applies to the latter stages of creep as well as the transient stage. It is more likely that some of the assumptions that we have made in the theoretical development do not hold under the conditions where the latter stages of creep are important, at large t and high $\bar{\sigma}$.

The primary assumption made concerns the assumed form of static fatigue behavior. It was mentioned earlier that this relation may not hold at large t , where the rate of static fatigue has been observed experimentally to diminish. This however does not explain the behavior of creep at large t . If the limits of static fatigue were approached, the effect on creep would be the reverse; creep would come to a standstill. We then made three additional assumptions: that each region fails only once, that each region contributes a constant average increment to strain, and that the regions act independently.

The assumption that each region fails only once may not apply at large t . A more plausible model is that the

stress drops to a lower value in a region when it fails. In that case, it will be available for fracture at some later time when $S(t)$ has decreased to the new value of stress. Such a process of reactivation of regions may lead to secondary creep if at some point the number of reactivated regions is just sufficient to offset those which are fracturing.

There is some experimental evidence that the second assumption, that each microfracturing event contributes a constant amount to strain, may not be a good approximation at large t . We have studied the size distribution of microfracturing events during constant strain rate experiments and found that the events tend to become statistically larger with increasing stress (see Chapter 3). In some senses, a creep test can be considered to be one limit of constant strain rate experiments. For example, in our model, a constant strain rate experiment (at an infinitely high strain rate) is visualized as the curve of $f(\sigma; \bar{\sigma})$ sweeping to the left (Figure 16) with $\bar{\sigma}$ and intercepting S^* . In a creep experiment, on the other hand, the curve $f(\sigma; \bar{\sigma})$ is considered stationary and $S(t)$ sweeps to the right. An experiment at a finite strain rate can be considered a combination of the two extremes. Physically, then, the response of rock should be similar for either an increase of $\bar{\sigma}$ in a constant strain rate experiment or an increase of t in a creep test. By this argument, we might expect

that microfractures become larger with increasing t in creep. If this is true, then η may be approximated by

$$\eta = \xi + \zeta t$$

in which case the creep law will be given by

$$\Delta = \frac{\bar{\sigma}^n}{bE} kT [\xi \log t + \zeta t] \quad (11)$$

The creep law given in (11) predicts both transient and secondary creep. In this view they are both produced by the same mechanism.

The process of tertiary creep may also be understandable from our knowledge of the behavior of rock in conventional fracture experiments. Tertiary creep is characterized by a rapid acceleration of activity followed by fracture of the specimen. Rock deformed at a constant strain rate is also typified by a rapid acceleration of microfracturing activity (and strain) prior to fracture. In Chapter 4 we studied this behavior and found that this acceleration of activity was associated with a clustering of microfracturing events leading to the formation of the fault

which eventually caused fracture. By analogy, we might expect tertiary creep to be due to the same phenomenon. In other words, regions do not fracture independently during tertiary creep.

The above remarks regarding the possible mechanisms of secondary and tertiary creep are of course speculative. They serve mostly to delineate the limitations of the present theoretical analysis, and, by suggesting some possibilities, to point out some of the problems which should be attacked in future experimental studies. Although a great deal is presently known of the mechanical properties of rock, the time dependence of these properties has unfortunately to a large extent been neglected. A knowledge of these effects will be very important toward obtaining a better understanding of geologic processes.

CHAPTER 3

THE FREQUENCY-MAGNITUDE RELATION OF MICROFRACTURING
IN ROCK AND ITS RELATION TO EARTHQUAKES

Introduction

The deformation of brittle rock in laboratory experiments is accompanied by very small scale cracking. Such microscopic cracking, referred to as microfracturing, can be studied directly by the detection and analysis of the elastic radiation produced by each event in a manner analogous to that used in studying earthquakes. In contrast to seismic waves, however, microfracturing radiation is typified by very high frequencies. The main part of the power spectrum of such events has been found to lie approximately from 100 khz to 1 Mhz (see Chapter 4).

Using an experimental system capable of operating with signals in such a frequency range, we have shown (see Chapter 1) that the pattern of microfracturing activity observed in rock deformed at a constant strain rate in compression can be directly related to the inelastic stress-strain behavior typical of rock. This pattern was found to be similar for a variety of rock types over a wide range of confining pressure. The observed microfracturing behavior was found to be adequately described by a statistical model of rock deformation in which rock was treated as an inhomoge-

neous elastic medium.

In the statistical analysis of a process such as microfracturing, a rather important relation, and one which is fairly simple to study experimentally, is the frequency of occurrence of events as a function of amplitude. This functional dependence, which is known in seismology as the frequency-magnitude or recurrence relation, is a fundamental property of the stochastic process.

Mogi (1962a) and Vinogradov (1959, 1962) studied experimentally the frequency-magnitude relation of microfracturing events in rock. A surprising result was that this relationship was found to be the same as that for earthquakes, i.e., frequency was a power function of maximum trace amplitude. In terms of magnitude, this is given by the Gutenberg and Richter relation

$$\log N = a + bM \quad (1)$$

where N is the frequency of events that occur at a given magnitude M, and a and b are constants.

Mogi's (1962a, 1962b, 1962c, 1963a, 1963b, 1963c) observations were part of a study of the general microfracturing behavior of rock subjected to bending stresses. He demonstrated that in many ways the statistical behavior of

microfracturing activity observed in laboratory experiments is similar to that which has been observed for earthquakes. In addition to his observation of the similarity of the frequency-magnitude relations, he showed that the buildup of activity preceeding fracture in laboratory tests is similar to earthquake foreshock sequences. In later work, he reproduced foreshock and aftershock sequences in models. By treating microfracturing as a stochastic process, he was able to describe some of the properties of the phenomenon and to relate these qualitatively to the degree of heterogeneity of the model material.

A serious drawback to Mogi's experimental observations and those of other previous microfracturing investigators was that they were limited to the audio frequency range. Because the frequency content of microfracturing events is primarily much higher than this, his conclusions are open to question. In the related investigation (see Chapter 1) a system was used which has a bandwidth which extends well into the microfracturing frequency range. It was found that the increased frequency response of this system resulted in a sensitivity of detection which was higher by several orders of magnitude than that of the previous workers. Therefore, it was decided to extend Mogi's study of the frequency-magnitude relation using this system. In addition, it was of interest to see if this relation could also be observed under the more geologically realistic conditions

of compressive stress and high confining pressure.

Although the mechanism of shallow earthquakes is apparently some sort of fracture process, Mogi's contention that microfracturing observed in the laboratory is simply a scale model of seismicity is not immediately obvious. If the basis of the similarity can be clearly understood, however, then we shall have in experimental studies of rock deformation a tool for understanding the physical processes responsible for earthquake phenomena. In this study, by observing the dependence of the parameters of the frequency-magnitude relation on several physical variables and by extending the basic model of microfracturing, as outlined in Chapter 1, to explain these observations, we shall attempt to clarify some of the problems raised by Mogi's work. What, for example, is the physical significance of the observed frequency-magnitude relation, and what determines the values of the parameters a and b in equation (1)?

Experimental Technique

The experimental method used in this study is similar to that reported above (Chapter 1). The rocks tested have also been described there. Briefly, the procedure consisted of stressing a rock sample to fracture as in a conventional uniaxial or triaxial compression test. Microfracturing activity occurring within the sample was detected with an

attached barium titanate piezoelectric transducer. The signal was amplified, shaped, and admitted to a 100 channel pulse height analyzer. The amplification system had a flat frequency response from 100 hz to 1 Mhz. The major change in technique in the present experiments was that the analyzer was operated in pulse height analyzer mode. In this mode, each channel corresponds to a successively higher increment in amplitude, so that as the rock is stressed, each event occurring within a predetermined period of time (live time) is counted in the channel corresponding to its maximum trace amplitude. The signals are typically of the form of decaying sinusoids with periods of a few microseconds (see Chapter 4). The analyzer measures the amplitude of each event 1 μ sec after the initial rise. Consequently, in order to insure that the amplitudes measured were nearly the maximum for the events, and to prohibit an event from triggering the analyzer more than once, the signals had to be shaped. This was done with a circuit (Appendix III) which has as its output the envelope of the negative half of the wave train. This was found to give very satisfactory results.

Each channel was adjusted so that it covered a width of 1 mv in amplitude. The upper and lower limits of analysis were set at 100 mv and 1 mv, respectively, referred to input at the analyzer, so that two orders of magnitude in amplitude were analyzed. The number of events that occurred at

each amplitude level in the live time was printed out digitally and the frequency-magnitude relation determined simply by plotting this data in logarithmic coordinates.

Previous workers determined the frequency-magnitude relation of microfracturing during fracture experiments by analyzing all the events which were detected over the entire duration of the experiment. Due to the greatly increased sensitivity of the present system, the frequency-magnitude relation could be determined much more accurately, and the change in this behavior during the course of an experiment could be followed in considerable detail. The frequency-magnitude relation was determined as a function of stress, rock type, and confining pressure in uniaxial and triaxial compression tests.

Experimental Observations

Typical results are given in Figure 18, which shows frequency versus maximum trace amplitude in logarithmic coordinates at two different stress levels in a uniaxial compression test on San Marcos gabbro. The data represented by each curve was collected as the rock was stressed over an interval of several hundred bars. The stresses indicated are the simple midpoints of the intervals. Notable is the strong linearity of the curves; as with earthquakes, the data very closely fits a power function. The most convenient way of analyzing this data is to refer it to the

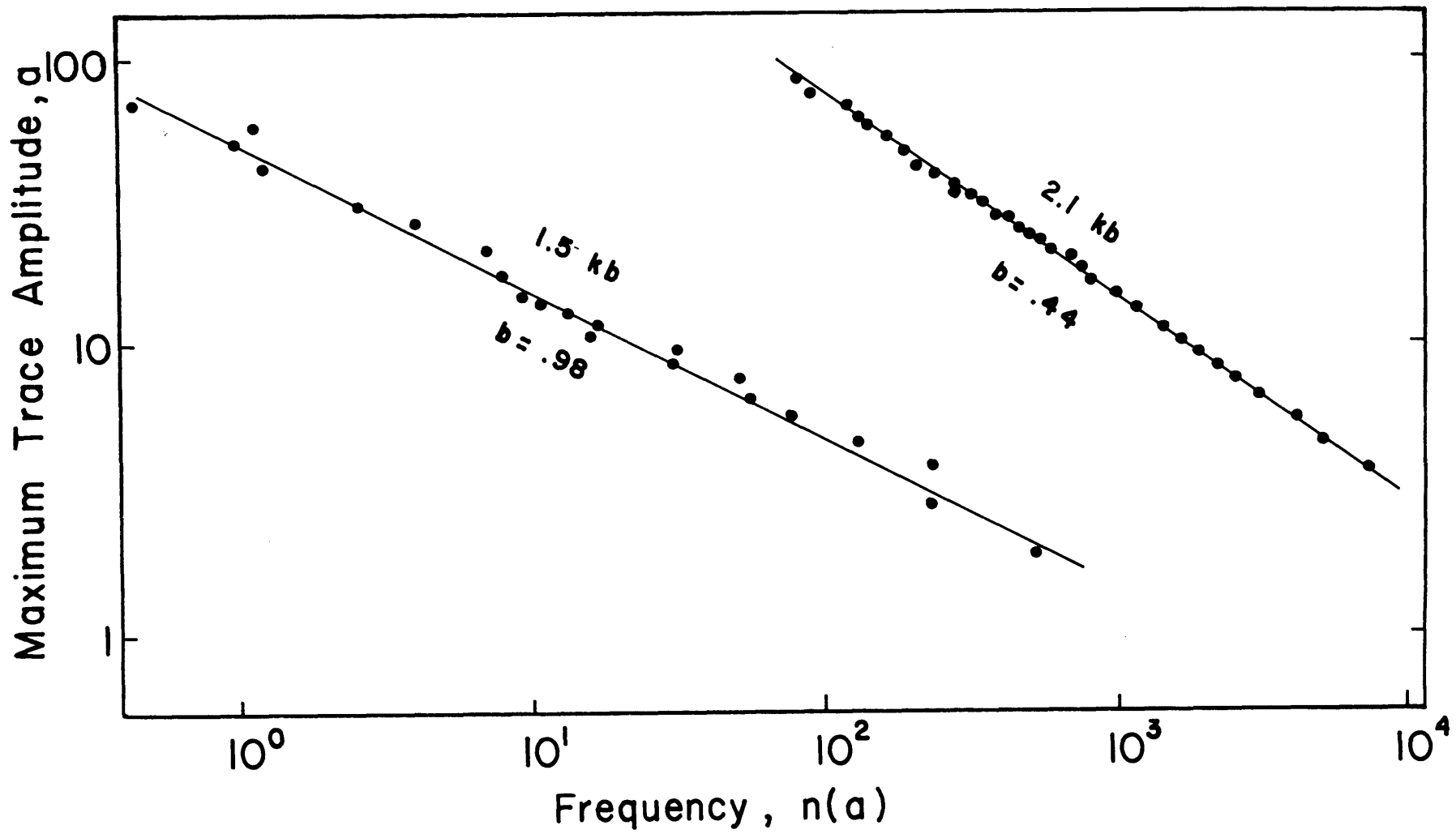


FIGURE 18. Amplitude frequency vs maximum trace amplitude for microfracturing events that occurred at two stress levels during the uniaxial compression of San Marcos gabbro.

Ishimoto-Iida statistical relation

$$n(a)da = ka^{-m}da \quad (2)$$

where $n(a)$, the amplitude frequency, is the rate that events of amplitude a to $a + da$ occur, a is the maximum trace amplitude, and k and m constants. The most important parameter, m , is simply the slope of the line fitting a plot such as shown in Figure 18. However, the above relation is equivalent to the Gutenberg and Richter instrumental magnitude form, and Suzuki (1959) has shown that the constant b in the latter form is related to m by

$$b = m - 1 \quad (3)$$

We therefore shall use the more familiar parameter b in the discussion of our results. Notice in Figure 18 that b is not constant throughout the experiment but decreases markedly with an increase in stress.

Some of the rocks tested, however, do not behave in such a simple way. Figure 19 shows the characteristic behavior of Westerly granite at several stresses. At low and

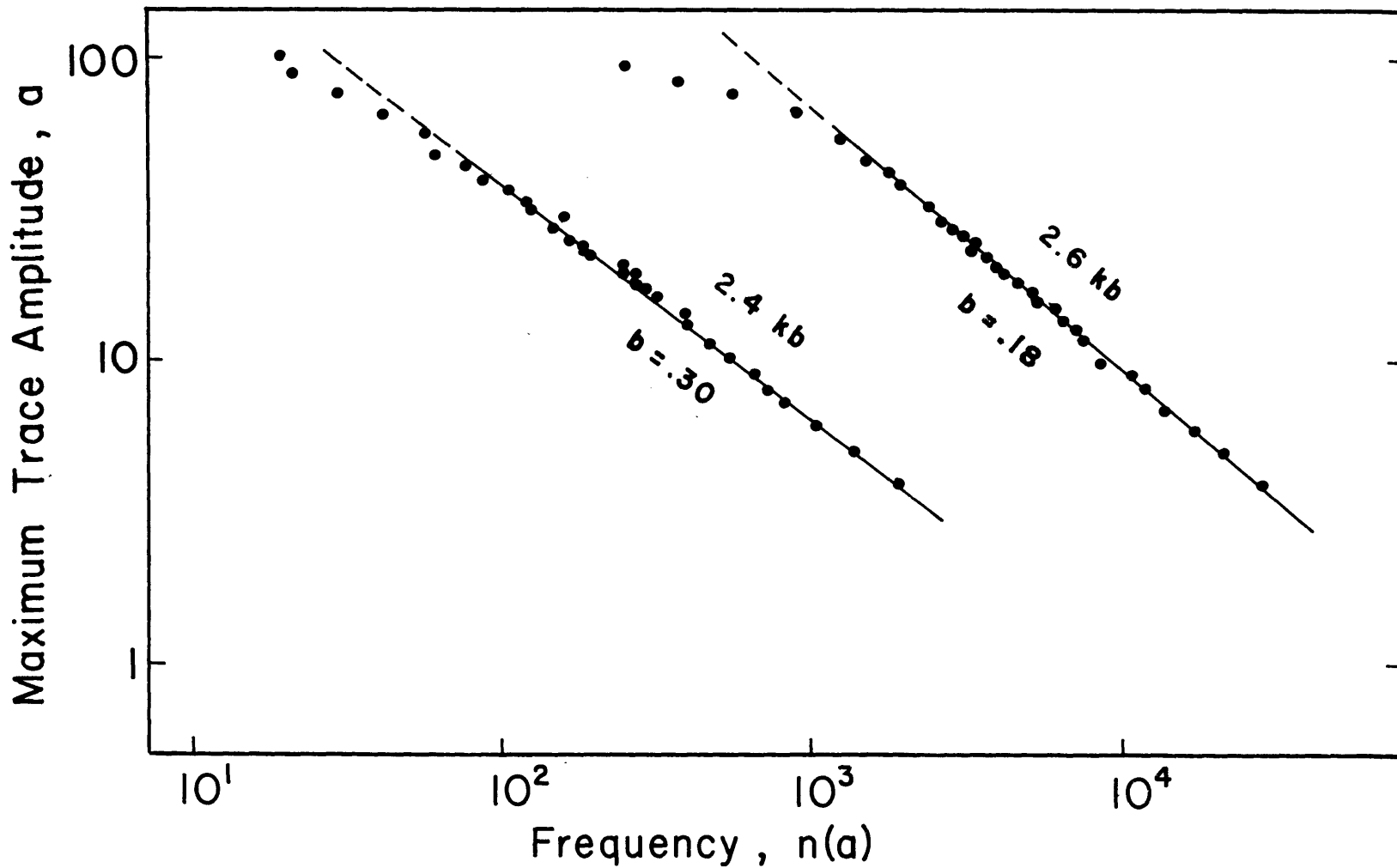


FIGURE 19. Amplitude frequency vs maximum trace amplitude for microfracturing events that occurred at two stress levels during the uniaxial compression of Westerly granite. Note the deviation from linearity at high amplitude.

moderate amplitudes, the frequency-magnitude relation is very similar to the more typical case shown in Figure 18, but fewer large amplitude events have occurred than would have been expected from a linear extrapolation of the data. This deviation is very much like that observed for earthquakes of magnitude 8 and above (cf. Gutenberg and Richter, 1949). It will be mentioned below in the discussion of the theoretical results that this deficiency of large events may be a result of the finite dimensions of the sample.

The observation that the parameter \underline{b} is a function of stress prompted a more detailed examination of this behavior. A group of rocks with widely differing physical properties were fractured in uniaxial compression, and magnitude-frequency curves such as those shown in Figure 18 were determined for a number of stress intervals during loading. A single rock, Westerly granite, was chosen to examine the effect of confining pressure. In these experiments, the frequency-magnitude relation was determined as a function of stress at several confining pressures.

The rocks were stressed at a constant rate of about 10^{-5} sec^{-1} . Events which occurred over successive stress intervals of several hundred bars were sampled and the values of \underline{b} were computed from curves such as shown in Figure 18. The data obtained for the uniaxial experiments, given in Table 5, is summarized as a plot of \underline{b} versus normalized stress for the various rocks in Figure 20. The

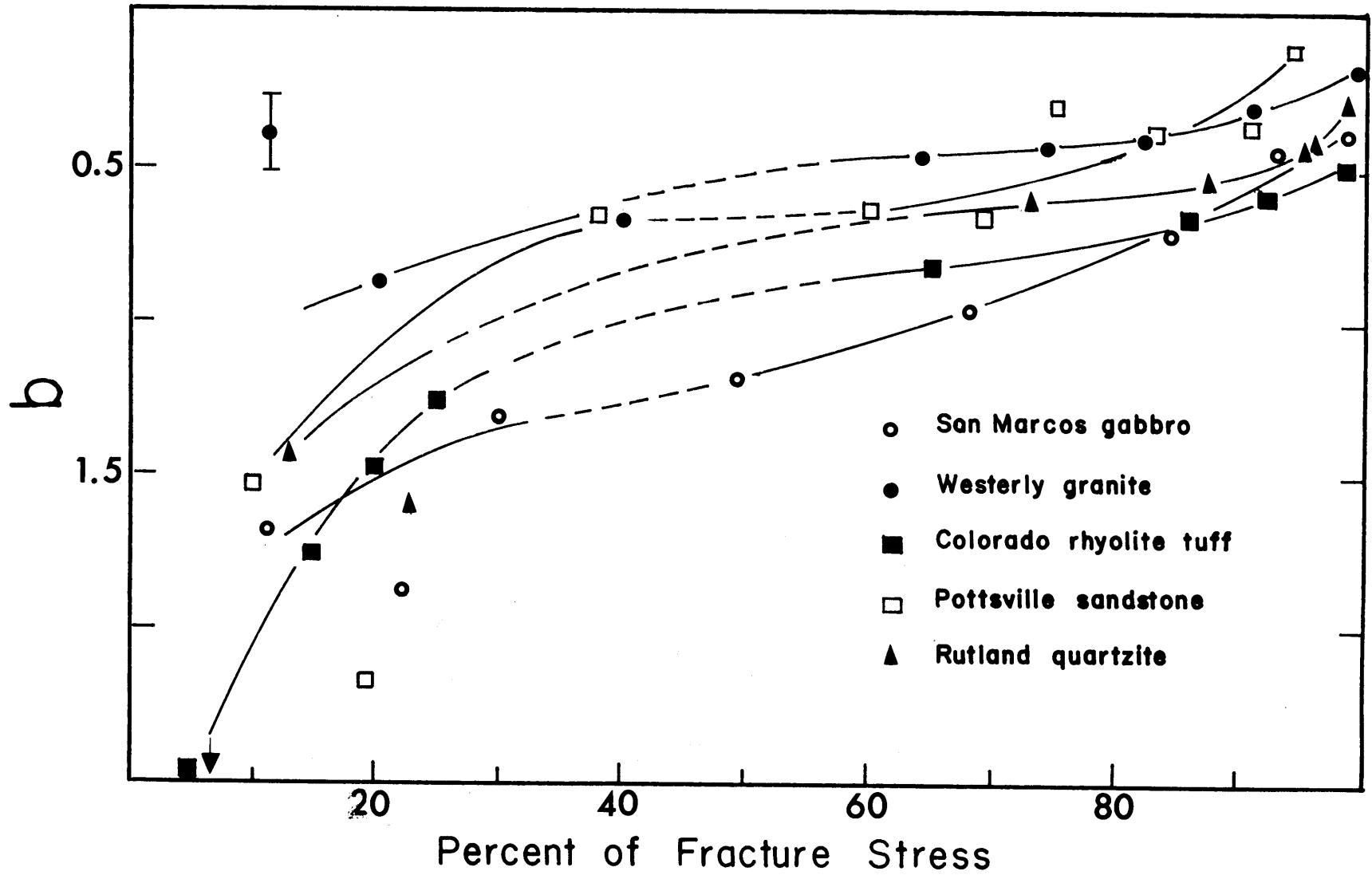


FIGURE 20. The Gutenberg and Richter parameter b plotted as a function of normalized stress for five rocks deformed in uniaxial compression. Each data point was found from a curve such as shown in Figures 18 and 19.

TABLE 5. b Values for Various Rocks Stressed in Uniaxial
Compression

Rock	σ , kb.	σ/c^*	b
Westerly granite	.30	.12	1.32
	.40	.25	.68
	1.70	.64	.47
	2.00	.74	.44
	2.20	.82	.41
	2.40	.91	.30
	2.60	.98	.18
San Marcos gabbro	.25	.11	1.70
	.50	.22	1.90
	1.10	.49	1.20
	1.50	.68	.98
	1.90	.84	.72
	2.10	.93	.44
	2.20	.97	.40
Colorado rhyolite tuff	.05	.05	2.58
	.15	.16	1.78
	.20	.21	1.50
	.25	.26	1.28
	.65	.65	.84
	.85	.86	.67

TABLE 5. cont.

Rock	σ , kb.	σ/C	b
Colorado rhyolite tuff (cont.)	.90	.92	.60
	.92	.97	.50
Marble	.05	.08	1.48
	.15	.25	1.52
	.25	.41	1.91
	.40	.66	2.50
	.52	.86	1.95
	.57	.95	1.90
Pottsville sandstone	.25	.10	1.55
	.50	.19	2.20
	1.00	.38	.66
	1.60	.60	.64
	1.85	.69	.66
	2.00	.75	.30
	2.20	.83	.38
	2.40	.91	.37
2.50	.94	.11	

TABLE 5. cont.

Rock	σ , kb.	σ/C	b
Rutland quartzite	.75	.13	.95
	1.25	.23	1.62
	4.00	.73	.60
	4.75	.87	.53
	5.20	.95	.42
	5.25	.96	.41
	5.30	.97	.29

* C refers to stress at fracture.

error bar given in the diagram is an average value; the error is larger at lower stresses, where a smaller amount of events were detectable, and smaller at higher stresses.

Perhaps the most striking thing about this data is that the curves for the various rocks are very similar although they are shifted relative to one another.

In order to discuss these results, the general nature of microfracturing activity in brittle rock, which was described above (Chapter 1), must be reviewed briefly. Activity was divided into three successive stages. At low stress in unconfined experiments, microfracturing activity was attributed to frictional sliding on pre-existing cracks and the crushing of pores. In the second stage, at stresses from about 30 to 50% of the fracture strength, rock was nearly linearly elastic and few events could be detected. In the third state, microfracturing resumes and steadily increases until fracture. In this latter region, the rock becomes dilatant, *i.e.*, if we disregard elastic compression, the rock increases in volume. In this stage, microfracturing radiation was shown to be due to the propagation of new cracks. Therefore, we can consider the behavior shown in Figure 20 in two parts, separated by a central region in which little or no activity was observed. In the region below about 30% of the fracture stress, where the events analyzed are probably due mainly to sliding on pre-existing cracks, the \underline{b} values are very high, indicating a preponderance of small events. Above about 60% of the strength, where the signals are radiated from propagating cracks, the \underline{b} values fall

between 1 and 0, with a consistent tendency for \underline{b} to decrease as stress is raised. This indicates that as stress is increased, the events become statistically larger. Note that the \underline{b} values in this latter region are in the range usually observed for earthquakes. The significance of this will be brought out later when it is suggested that the statistics of the process in this region should be the same as that of earthquakes.

A marble was also studied, with quite different results. This rock, which deforms cataclastically at atmospheric pressure, exhibits a frequency-magnitude relation that is similar in form to that found for the brittle rocks but is characterized by very high \underline{b} values over the entire range of stress (see Table 5). The similarity of these \underline{b} values to those found in the low stress region of the brittle rocks re-emphasizes the conclusions (see Chapter 1) that cataclastic deformation is indeed due to stable intragranular sliding.

Under confining pressure, much the same behavior is observed. Microfracturing in triaxial compression of Westerly granite at confining pressures up to 5 kb has the same frequency-magnitude relation as that described in the case of uniaxial compression. Figure 21 shows \underline{b} as a function of stress difference normalized with respect to fracture stress difference at five different confining pressures. Stress difference is defined in the usual way as $(\sigma_1 - \sigma_3)$, where σ_1 and σ_3 are the major and minor compressive stresses respectively. This data is also listed in Table 6.

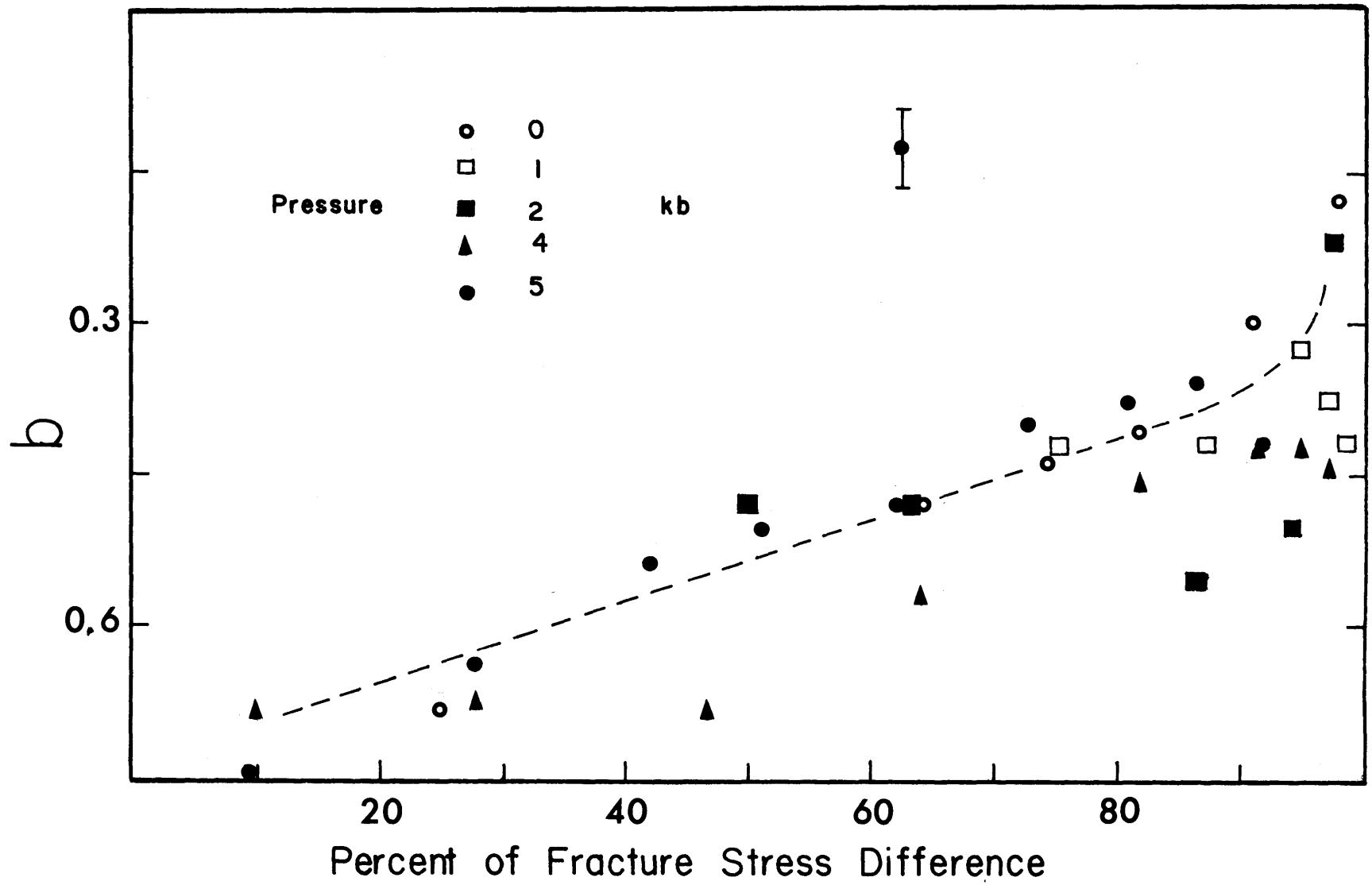


FIGURE 21. The parameter b plotted as a function of normalized stress difference for Westerly granite deformed in triaxial compression at five confining pressures.

TABLE 6. b Values for Microfracturing in Westerly Granite
at Various Confining Pressures

Pressure, kb.	$(\sigma_3 - \sigma_1)$, kb.	$(\sigma_3 - \sigma_1) / (\sigma_3 - q)_f^*$	b
1.0	6.50	.76	.42
	7.50	.88	.42
	8.10	.95	.32
	8.25	.97	.38
	8.40	.99	.43
2.0	5.90	.50	.48
	8.40	.71	.48
	10.20	.87	.56
	11.20	.94	.50
	11.60	.98	.22
4.0	1.58	.10	.69
	4.50	.28	.68
	7.40	.47	.69
	10.10	.64	.58
	12.80	.82	.46
	14.20	.91	.43
	14.90	.95	.43
15.30	.97	.45	

TABLE 6. cont.

Pressure, kb.	$(\sigma_3 - \sigma_1)_{kb.}$	$(\sigma_3 - \sigma_1) / (\sigma_3 - \sigma_1)_f$	b
5.0	1.60	.09	.75
	5.00	.28	.64
	7.60	.42	.54
	9.10	.51	.50
	11.10	.62	.48
	13.00	.73	.41
	14.40	.81	.38
	15.40	.86	.36
	16.40	.92	.42

* $(\sigma_3 - \sigma_1)_f$ refers to stress difference at fracture.

The stress dependence of \underline{b} at each pressure has the same general characteristics observed in the uniaxial experiments. Again, \underline{b} falls between 1 and 0 and shows a steady decrease with stress. The high \underline{b} values in the low stress region are not observed in the triaxial experiments. This behavior is expected because confining pressure keeps cracks tightly closed and restricts sliding. The most interesting feature of Figure 21 is that within experimental error, pressure seems to have no effect on the stress dependence of \underline{b} if it is normalized with respect to the fracture stress. For brittle rocks such as Westerly granite, strength increases rapidly with pressure so that at a higher pressure the same value of \underline{b} will occur at a much higher absolute stress.

As described above (Chapter 1) the microfracturing activity that accompanied frictional sliding of brittle rock was quite different from that which occurred during deformation of brittle rock but similar to that during cataclastic deformation of marble. Since we have observed above that the frequency-magnitude relation of events detected during cataclastic deformation of marble is quite distinct from that of microfracturing which occurs in the high stress region of brittle rock, it would be interesting to see if the same holds for frictional sliding. We have also noted above that the \underline{b} values typical of microfracturing which occurs in the low stress region during uniaxial

tests are similar to those typical of cataclastic deformation. In the light of our interpretation of the mechanism involved in that region, the b values observed in frictional sliding experiments should be, as in those cases, characteristically high.

Frictional sliding of brittle rock under high confining pressure is punctuated by jerky stick-slip events (Brace and Byerlee, 1966) which produce large sudden stress drops. Preceding each stick-slip, however, there is usually some stable sliding, during which microfracturing activity is detectable.

Several experiments were done in a manner similar to those of Brace and Byerlee. In these tests, Westerly granite samples with pre-existing ground sliding surfaces were stressed under high confining pressure. In each test, microfracturing was observed prior to several stick-slips (for a more detailed description of the experimental method, refer to Chapter 1). As stress was raised during each stick-slip cycle, events were sampled in three regions: the lower, middle, and upper third of the stress cycle prior to stick-slip. A frequency-magnitude relation was determined for the microfracturing events that were detected in each of these regions.

It was found that this data also fit the Gutenberg and Richter formula. The b values are given in Table 7, where the values in the lower, middle, and upper regions are

TABLE 7. b values for frictional sliding of Westerly granite

Confining Pressure, kb.	Stick-slip	b		
		1	2	3
2.0	1 st	1.60	1.60	1.24
	2 nd	2.30	1.17	1.56
1.0	1 st	*	0.80	2.70
	2 nd	*	1.34	1.30
	3 rd	*	1.32	1.15

* Insufficient events were observed.

referred to as 1, 2, and 3, respectively. The results show that \underline{b} values for frictional sliding are consistently high. This reinforces the earlier view that the microfracturing that occurs during cataclastic deformation and in the low stress region in uniaxial experiments is due to frictional sliding.

The results of this examination show that the frequency-magnitude relation of microfracturing events is a well defined property of brittle rocks with several distinct characteristics. Firstly, although the relation is in general very well approximated by the Gutenberg and Richter equation, the primary statistical parameter \underline{b} depends strongly on the state of stress, and only to a lesser extent on the physical properties of the rock. The earlier work of Mogi (1962a) and Vinogradov (1959, 1962) was restricted to averaging this behavior over all stresses. Mogi's conclusions that the degree of heterogeneity of the rock is the primary factor determining the value of \underline{b} is probably a result of this averaging process. He found that more heterogeneous rocks are characterized by much higher \underline{b} values. The qualitative criterion of heterogeneity which he used, however, was in general related closely to porosity; thus he found that a very porous rock such as pumice has a higher \underline{b} value than a compact rock, which he considered less heterogeneous, such as granite. As was shown in the related work (~~Chapter~~, **ter 1**) the more porous the rock the larger the proportion

of microfracturing events occur in the low stress region relative to the high stress region. Consequently, if the frequency-magnitude relation is determined by analyzing events over the entire stress range, the average \underline{b} values obtained for the more porous rocks will be shifted toward the high values characteristic of low stresses.

The second point to be made is that the frequency-magnitude relation sharply distinguishes between the two processes that occur. At low stress, where crack closing and sliding are important, high values of \underline{b} are observed. Above about 50% of the fracture strength, where new fractures are propagating, \underline{b} is lower, in the range usually found for earthquakes, and decreases as stress increases. This behavior is similar at all pressures and for all brittle rock types tested.

Theory

Mogi (1962a), as well as Suzuki (1959), have given derivations of the Ishimoto-Iida statistical formulation of the frequency-magnitude relation. In this section we shall extend a basic physical model of microfracturing in a very simple way, and following Mogi's statistical approach, obtain a more complete expression of this relation. The analysis that follows, however, will only deal with the behavior in the region in which new fractures are forming, at high stresses.

In Chapter 1 we introduced a statistical model of rock deformation in which rock was treated as an inhomogeneous elastic medium. This model was found to successfully predict the pattern of microfracturing activity observed in compression tests in the laboratory. If rock under crustal conditions in the laboratory can be considered to be similar to rock on a geological scale, as Mogi suggests, a consideration of the properties of a general inhomogeneous brittle material should reveal the similarities (and dissimilarities) between rock and crustal deformation. The model outlined earlier attempted to describe such a general material, although in that case it was applied to rock behavior observed in the laboratory.

In this study we have shown that the frequency-magnitude relation of microfracturing events in the laboratory is indeed quite similar to that observed for earthquakes. Since in the laboratory we have the advantage of being able to determine the conditions under which our observations are made, we have been able to define the physical parameters which affect this relation. It is still not known, however, if we can directly apply our observations, such as the stress dependence of \underline{b} , directly to earthquakes. This again depends on how far the similarity can be taken. In order to gain some insight into the basis for the similarity of microfracturing and earthquakes, we shall extend the model to consider the frequency-magnitude relation. To clarify the

analysis, however, we shall first briefly review the basic model and discuss its applicability to crustal deformation.

Suppose that a rock in the laboratory, or on a much larger scale a portion of the earth's crust, is subjected to a uniform applied stress, $\bar{\sigma}$, as shown in Figure 12. Due to the presence of elastic and structural inhomogeneities, however, the local stress at a point, σ , will not in general be equal to $\bar{\sigma}$ but will vary in some complex way from this mean value. For such an inhomogeneous medium the local stress σ cannot, in theory, be predicted without a detailed knowledge of the configuration of inhomogeneities in the body. At the present state of our knowledge, the stress distribution within such a body cannot be treated with conventional elasticity theory. Therefore we take a heuristic approach and, assuming that the inhomogeneities will be small relative to the body itself, consider σ as a random variable. Consequently, we can define the probability that the stress within a region (small enough such that the stress on it can be considered uniform) is some given value σ in terms of probability density function $f(\sigma; \bar{\sigma})$. This notation implies that the probability function of σ will depend on $\bar{\sigma}$. For example, the mean of $f(\sigma; \bar{\sigma})$ can be shown from equilibrium to be $\bar{\sigma}$. Each small region is also characterized by a strength, S , that is, fracture will occur within the region if the local stress exceeds S . The presence of some sort of weakness, e.g. "Griffith" cracks, is included in

this definition of \underline{S} . Variations in \underline{S} are equivalent to variations in σ .

How will this material react when it is stressed? In Figure 12 we show this situation, with an arbitrary density function. As the applied stress is increased, $f(\sigma; \bar{\sigma})$ will gradually change, since it is a function of $\bar{\sigma}$, and move to the left, intercepting \underline{S} so that the probability of local fracture steadily increases. Fracture will occur in regions where the local stress exceeds \underline{S} , and we will assume that these fractures will be arrested if they propagate into adjacent regions of lower stress. In order to describe a frequency-magnitude relation for these events, we need to consider how such fracture propagation takes place.

Suppose we have a fracture of area A , such as shown in Figure 22, growing in a heterogeneous stress field. It follows from the properties of our model that a fracture can only propagate through regions where σ exceeds S . In the case of uniform stresses, *i.e.*, the mean stresses are not functions of position, the probability that the local stress exceeds the strength is uniform in space and is given by $F(S; \bar{\sigma})$, the distribution function over \underline{S} ($F(S; \bar{\sigma})$ is the integral of $f(\sigma; \bar{\sigma})$ to the left of S . See *e.g.* Parzen, 1962; Volkov, 1962). Therefore the probability that a crack will be arrested somewhere within an arbitrary area is constant and is given by $[1 - F(S; \bar{\sigma})]$. It then follows that $g(A)d(a)$, the probability that a fracture will stop as it grows from size

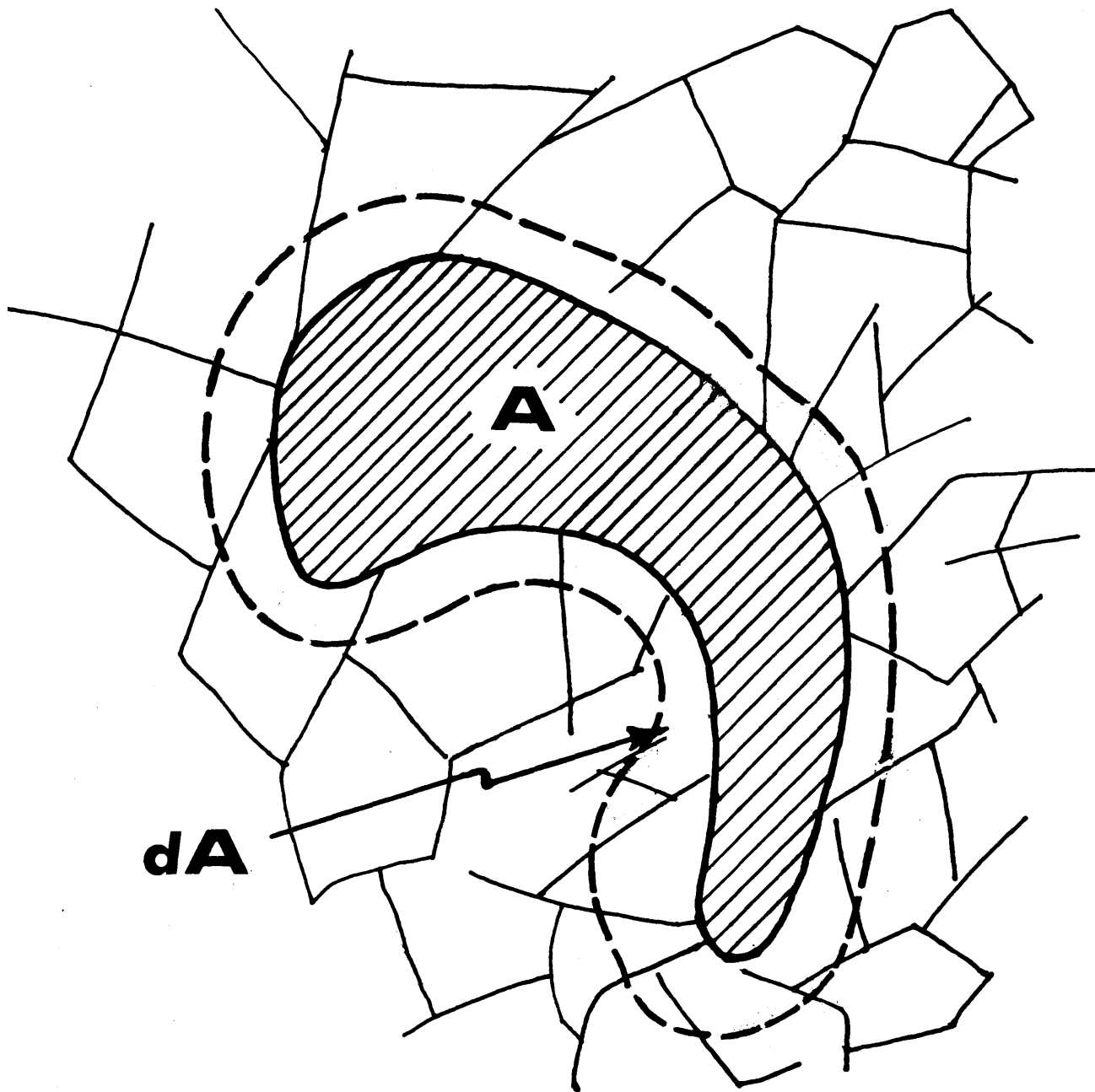


FIGURE 22. Top view of a fracture propagating through an inhomogeneous medium. We treat the case of a fracture of area A (crosshatched region) that is arrested as it propagates an additional increment dA (bounded by the dashed line).

A to A + dA, is given by

$$g(A)dA = \frac{[1-F(S;\bar{\sigma})]}{A}dA \quad (4)$$

Physically, this says simply that this probability varies directly with the probability that the stress at a point is less than S, and inversely to the area swept out by the fracture. This model takes into account two basic properties of fracture propagation. Firstly, since the definition of $F(S;\bar{\sigma})$ requires the presence of a fracture, we imply that a fracture weakens the region it penetrates (i.e., the stress concentration due to the fracture augments the stress in the region into which the fracture is growing). Secondly, (4) shows that the probability of a fracture growing an additional increment increases as the fracture becomes larger since it is sampling a larger number of regions.

Due to the conditional nature of $g(A)dA$,

$$g(A)dA = \frac{-dN(A)}{N(A)} \quad (5)$$

where $N(A)$, the accumulated frequency of fractures larger than A, is given by

$$N(A) = \int_A^{\infty} n(A) dA \quad (6)$$

and $n(A)dA$ is the frequency of fractures that occur within the range A to $A + dA$. Rearranging the right sides of (4) and (5) and setting them equal, we have

$$[1-F(S;\bar{\sigma})]d(\log A) = -d[\log N(A)] \quad (7)$$

which upon integration yields

$$A^{-[1-F(S;\bar{\sigma})]} = N(A) \quad (8)$$

Differentiating (8) with respect to A , we obtain

$$n(A)dA = [1-F(S;\bar{\sigma})]A^{-[1-F(S;\bar{\sigma})]-1} dA \quad (9)$$

So far we have made only the most basic assumptions regarding the mechanism of fracture propagation. On this basis we have deduced, in equation (9), the size distribution of fractures that will occur in an inhomogeneous medium. This result should apply equally to extension or shear fractures, for example, and to both earthquakes and microfracturing. The scale of the body does not enter into the model. In order to calculate from equation (9) the distribution of the maximum trace amplitude, the quantity we actually measure, however, we must introduce a specific fracture mechanism.

With the assumption that the fractures are in the form of narrow, penny-shaped cracks, and that cracks of different size are similar, we can approximate the stress-relieved volume, V , by a sphere enclosing the fracture and

$$A = \alpha V^{2/3} \quad (10a)$$

where α is a constant. Also, we have the relation

$$V = \tau \bar{\sigma}^{-2} E \quad (10b)$$

where E is the strain energy released. The constant τ includes the elastic constants and the relative stress drop coefficient. From the general relation of seismology, we also have

$$E = \gamma a^{\nu} \quad (10c)$$

where a is the maximum trace amplitude of the elastic radiations, γ and ν constants. This relation is known empirically for earthquakes, and can also be demonstrated theoretically (K. Aki, personal communication, 1967).

From (10a), (10b), and (10c), a relation between the fractures size A and the maximum trace amplitude a can be obtained. Substituting this into equation (9), it can be shown that $n(a)da$, the frequency of events that occur within the amplitude range a to $a + da$, is given by

$$n(a)da = Ka^{-m}da \quad (11)$$

where

$$K = (2/3)[1-F(S;\bar{\sigma})] \alpha^{1-F(S;\bar{\sigma})} (\gamma_T)^{-(2/3)[1-F(S;\bar{\sigma})]} (\bar{\sigma})^{(4/3)[1-F(S;\bar{\sigma})]-1} \quad (12)$$

and

$$m = (2/3)v[1-F(S;\bar{\sigma})] + 1 \quad (13)$$

Equation (11) is the Ishimoto-Iida relation, expressed in terms of the physical parameters of our model. The Gutenberg and Richter parameter \underline{b} is given from equations (3) and (13) by

$$b = (2/3)v[1-F(S;\bar{\sigma})] \quad (14)$$

Several definite things can be said about \underline{b} from this expression. First, since $F(S;\bar{\sigma})$ increases with increasing stress, \underline{b} must decrease as stress is increased, as our experimental data indicates (cf. Figures 20 and 21). Secondly,

because $F(S; \bar{\sigma})$ is a distribution function, \underline{b} is limited between $2\nu/3$ and 0. For earthquakes, from the well known empirical relation between energy and magnitude (Richter, 1958)

$$\log E = 11.4 + 1.5M$$

we know that $\nu = 1.5$ and accordingly the limits of \underline{b} for earthquakes are 1.0 and 0. This agrees very well with observation, since we know that all earthquakes except possibly some of volcanic origin are characterized by \underline{b} values between .5 and 1.

For simplicity, the above calculations have been made for the special case of a single uniform component of mean stress. The theory will of course also hold for general uniform stresses, except that a joint distribution function defined in terms of all components of mean stress must be used. For nonuniform stresses, however, the situation is quite different. Qualitatively, since fracture will tend to occur where the stresses are highest, $\bar{\sigma}$, and hence $F(S; \bar{\sigma})$, will always tend to decrease away from the origin of a fracture. Therefore the fractures will always tend to be smaller, and \underline{b} will be larger, than if the stresses were uniform. This is partially confirmed by comparing the data of Mogi

(1962a, 1962b), who studied the magnitude-frequency relation of microfracturing of rock in bending, with the present data for uniform compression. His \underline{b} values, for similar rocks, are consistently higher.

It is also interesting to note that volcanic earthquakes, which often are typified by anomalously high \underline{b} values of 2 to 3, must have occurred in a nonuniform stress field according to this theory.

Conclusions

Mogi (1962a, 1962b, 1962c, 1963a, 1963b, 1963c) demonstrated the striking similarities between the statistics of microfracturing events observed in the laboratory and the statistics of earthquakes. In the light of this observation, he suggested that rock deformation is a scale model of crustal deformation and interpreted his results accordingly. His conclusion was at once very profound and very puzzling. What possible physical similarities exist between the two processes to account for the strong similarity in behavior?

In this study we have begun to understand the importance of physical parameters such as stress and confining pressure in determining the frequency-magnitude relation in microfracturing. We have yet to decide how far these results can be extended to earthquakes. Can we, for example, use observed \underline{b} values to determine, say, the stress level during an earthquake sequence?

In order to understand such problems, we have developed a general model which is applicable to rock deformation on both a laboratory and crustal scale. In the present analysis, we have found, from equation (9), that the size distribution of fractures in an inhomogeneous medium is a power function of fracture size, and that the exponent of this relation must vary inversely with stress. At that stage, we had introduced only two basic assumptions: first, stress varies significantly from the mean value within the body, and second, fracture occurs when the local stress exceeds some critical value. These conditions seem reasonable both for rocks in the laboratory and for portions of the earth's crust. The only fundamental difference between the two is in the scale of the inhomogeneities. Therefore equation (9), which should be applicable to both cases, implies that the stress dependence of \underline{b} for earthquakes will be similar to that observed in the laboratory.

On the other hand, the values of the parameters \underline{a} and \underline{b} in equation (1) under given conditions depend on the fracture mechanism, transmission properties of the medium, and instrumental characteristics. We have assumed in the analysis that these are independent of fracture size (eqs. 10a, b, and c). Mogi (1962a) suggested that the frequency-magnitude may hold over the entire spectrum of fracture size from earthquakes to microfracturing. Certainly it seems to hold over several orders of magnitude for earth-

quakes and for microfracturing. Recently, however, Smith et al. (1967) noted that microearthquakes and earthquakes which occurred in the same region of California are not similar. Fault lengths for the microearthquakes were found to be much larger than would have been predicted by extrapolation from data on larger shocks. Also, stress drops for the microearthquakes were unusually low. Therefore, the parameters in equations (10a), (10b), and (10c) will not be the same for both microearthquakes and earthquakes in that region. In this light, it is not surprising that they found that the \underline{b} value for microearthquakes was not the same as that for the larger earthquakes. If similarity does not hold over all sizes, then the form of the frequency-magnitude relation given here only approximates the relation over a limited range of interest. In order to predict the behavior over the entire range, we must know how equations (10a), (10b), and (10c) change with source dimensions.

Aside from these problems, Mogi's suggestion of the similarity of microfracturing and earthquakes is largely upheld in the present work. It was found, however, that the state of stress, rather than the heterogeneity of the material, plays the most important role in determining the value of \underline{b} . The \underline{b} value for earthquakes has been extensively studied and has been found to be characteristic of the seismicity within a given region. Consequently, regional variations of \underline{b} may reflect variations of the state of stress.

For example, McEvilly and Casaday (1967) noted that after-shock sequences of magnitude 5 earthquakes in different regions of northern California are two distinct types, characterized by widely disparate b values. This may reflect a difference in the mean stresses or in the stress gradients.

In concluding this discussion, a general limitation of the model should be set forth. We have assumed an infinite medium, but in an actual case in which we study a sample of finite dimensions, or in the case of the earth a finite stressed region, the behavior should be limited at large amplitudes. We might expect that as a fracture approaches these limiting dimensions it will begin to significantly reduce the strain energy stored in the system. If this occurs, large fractures will tend to attain a shorter terminal length than predicted by the model, and consequently the frequency of very large events reduced. This may be the effect that we have observed earlier, illustrated in Figure 19, in which there is a deficiency of large events in a manner analogous to that observed for great earthquakes. Certainly the large earthquakes which have been well studied, such as the Alaskan earthquake of 1964, tend to encompass nearly the entire tectonic region in which they lie.

An alternate explanation of this phenomenon is also possible. Brace and Bombolakis (1963) and Hoek and Bieniawski (1965) have shown in two dimensional photoelastic studies that cracks in compression do not propagate in an

instable manner indefinitely, but become stable and stop after propagating some fraction of their original length. This self-stablizing property of cracks in compression may produce a limitation at large amplitude. That is, if a fracture is not stopped by inhomogeneities, it may eventually stop of its own accord.

CHAPTER 4

AN EXPERIMENTAL STUDY OF THE FRACTURING PROCESS IN
BRITTLE ROCK

Introduction

One of the most interesting properties of brittle rock is the extensive small scale cracking which accompanies the deformation in compression. We refer to such cracking events as microfractures to distinguish them from fracture of the rock as a whole. Many thousands of microfractures have been observed to occur prior to fracture in laboratory experiments.

Microfractures radiate elastic energy in a manner analogous to earthquakes [~~see~~ Chapt. 1] and, consequently, it is possible to study them directly by using techniques akin to those of seismology. Elsewhere [~~see~~ Chapt. 1] we reported certain statistical characteristics of microfractures, which were detected with a piezoelectric transducer during compression tests. By comparing the pattern of microfracturing directly with observed macroscopic behavior, it was shown that several features of the inelastic stress-strain behavior of brittle rock, such as dilatancy, could be attributed to microfracturing. This observation was found to hold for a wide variety of rock types and over a considerable range in confining pressure.

Statistical characteristics, however, can only delineate the gross properties of the microfracture process. This is usually adequate for studying the influence of microfracturing on the macroscopic properties of rock, since such properties are essentially statistical averages of the properties of the grains, cracks, pores, and pore fluid. A notable exception, in brittle rock, is strength. Brittle fracture of rock in compression generally occurs by faulting at an angle acute to the direction of maximum compression. The formation of the fault is apparently the basic instability inherent in rock fracture, but it is not a uniquely defined property. Although the angle of inclination of the fault to the direction of maximum compression is fairly reproducible, the exact location and azimuth of the fault cannot be predicted. Therefore, it is likely that this is a structure dependent process; that is, it depends on the detailed microscopic configuration of the rock. Strength, then, unlike other properties, may not be an average of the strength of the component parts. Because of this, indirect studies such as the statistical analysis of microfractures can probably yield only a superficial understanding of the fracture process.

Observations of microfracturing activity during compression tests demonstrated that microfracturing began at approximately half the fracture stress (see Chapter 1). As stress was increased above this, the rate of occurrence

of microfracturing events steadily increased until just before fracture, where a very rapid acceleration of activity was observed. Very likely the formation of the fault was connected somehow with microfracturing, but it was not at all clear how this might occur. One possibility is that a single large microfracture becomes instable and propagates through the entire body. On the other hand, a number of small cracks could coalesce to form the fault. Unfortunately present methods of observation are insufficient to indicate which alternative is more nearly correct. What is needed is a technique whereby the step-by-step development of the fault can be traced. In this study we describe such a technique; it applies certain of the methods of seismology to a sequence of selected large microfractures which were recorded during compression of Westerly granite.

A further stimulus for this investigation was the work of Mogi [1962a, 1962b, 1963]. Mogi studied the microfracturing behavior of rock in bending and compared his laboratory results with earthquakes. He concluded that the statistical behavior of microfractures is very similar to that observed of earthquakes and suggested that laboratory fracture experiments may be a scale model of crustal deformation. Of particular interest in the present context is Mogi's observation that the buildup of microfracturing prior to fracture is similar to foreshock sequences, and that fracture may correspond to the main shock. According

to this interpretation, a knowledge of the process of rock fracture may also lead to an understanding of the mechanism of large earthquakes.

Experimental Technique

Prior to the development of any of the experimental apparatus used in this series of investigations, preliminary studies of microfracturing were made to determine the main frequency content of the signals. This was done by simply observing the signals which were emitted from rock deformed to fracture in compression. The signals were detected with a barium titanate transducer attached to the specimen, amplified with a wide band system, and observed with an oscilloscope. It was found that the main frequency spectrum of microfracturing was between 100 khz and 1 Mhz.

As was discussed in a related **section (Chapter 1)**, this led to the development of a new experimental system for the statistical study of microfracturing events. For our present purposes, i.e. locating selected events within the sample, we require a different system however. The primary information required here is the relative arrival times of signals detected at several locations. Although some signal distortion could be tolerated, the frequency response of a system for such a study must be high enough so that arrival times could be measured to a fraction of a microsecond.

The sample used in this study, shown in Figure 23, is of the form designed by Mogi [1966] to eliminate end effects. It consists of a right cylinder of rock 2.5 cm in diameter and 10 cm long attached to hardened steel end-caps with 1.25 cm radius fillets of steel-filled epoxy. The detector array was composed of six piezoelectric transducers located as shown on the central 5 cm section of the specimen. Each detector was a barium titanate compressional mode disc 6 mm in diameter and 2.5 mm thick, which was firmly attached to the specimen with Tracon 2902 conductive epoxy. Attachment with the epoxy significantly increased the signal to noise ratio over that obtained with the simpler contact used in the statistical studies. In order to prevent bending, the specimen was very carefully ground parallel and square to within 0.002 mm per cm. In addition, a small piece of cellophane tape, as shown in the diagram, was attached to the top of the specimen to center the load. The rock tested, Westerly granite, has been described in ~~the~~ **Chapter 1**, 1966.

The sample was stressed, as in a conventional uniaxial compression test, at a constant strain rate of 10^{-5} sec^{-1} , with the standard loading system [see Chapt. 1]. Signals from the six transducers were recorded during the experiment with a Precision Instrument model 214 magnetic tape recorder. This recorder, which has 14 channels, has a flat frequency response from 200 hz to 200 khz at 60 ips, which was used

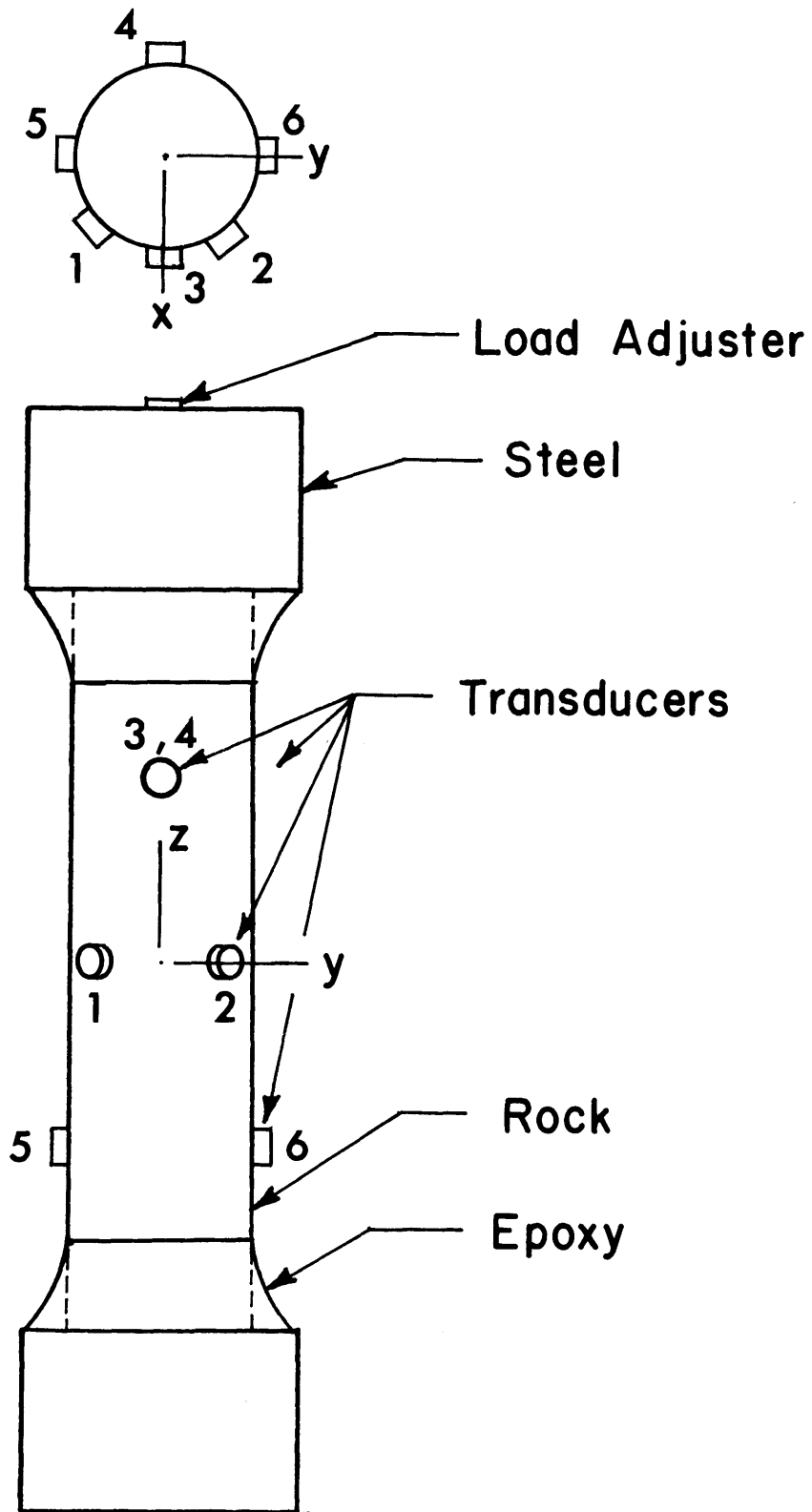


FIGURE 23. Diagram of the sample and transducer array used in locating microfracture events. Sample design is after Mogi (1966).

throughout. Amplification was achieved with Ithaco model 253AM42 post-amplifiers which produced 80 db gain. Ithaco model 123M47 piezoelectric transducer preamplifiers, which have unity gain and 1000 megohm input impedance, were installed only a few inches from the specimen in order to eliminate cable effects. The amplifiers and preamplifiers have frequency responses equal to that of the recorder.

Since thousands of events were recorded during the experiment, it was necessary to select only a few of the largest events for study. In order to locate the largest events, during the experiment a time mark was placed on a seventh channel of the recorder a few microseconds after the occurrence of each large event. This was done by using the output from one of the amplifiers to actuate a Schmitt trigger, which in turn triggered two one-shot multivibrators in series. The output of the first one-shot was used as a delay, that of the second for the time mark. These devices were standard Digital Equipment logic cards.

After the experiment, the tape was reversed and played back two channels at a time through a Tektronix 545B oscilloscope with a type 1A1 dual trace plug-in. The oscilloscope was triggered with the time marks, and the first arrival of each selected event at the two transducers photographed. This procedure was repeated for all six channels, taken two at a time, and the relative arrival times for each event measured from the photographs. The precision

of measurement was $0.5 \mu\text{sec}$.

When the tape is reversed, small misalignments between the magnetic heads will produce apparent time differences between different channels. In order to correct for such errors, all channels were synchronized. This was done in the following way. Square pulses from a pulse generator, at a repetition rate of 500 pps, were recorded for 20 seconds on one channel on an unused part of the tape prior to reversal. Simultaneously, these pulses generated a series of identical delayed pulses, using the time mark system described above, which were recorded on an adjacent channel. For symmetry, the process was then repeated, with the direct and delayed pulses recorded on reversed channels. This procedure was done for all six channels, pairwise. When the tape was then reversed, the (now) leading pulses on a given channel were used to trigger the oscilloscope, on which photographs were taken of the (now) delayed pulses on the adjacent channel. Then, in a similar manner, the leading pulses from the second channel were used to trigger the oscilloscope for photographing the delayed pulses on the first channel. From the delay time differences observed in this way, the apparent time shifts between channels were calculated and applied as corrections to the arrival time data.

Experimental Observations

Signals observed. An examination of the contents of the tape was made after the experiment in order to study the waveforms of the microfracturing signals that had been recorded. This study demonstrated what had been tentatively suggested by the preliminary investigations with the wide band system: two distinct types of signals were detected during the experiment. Typical waveforms of the two types of signals are shown in Figure 24; notice the difference in time scales. The higher frequency signals, referred to as Type I, are decaying sinusoids of period approximately 10 μ sec, and are the same as those observed earlier in the preliminary investigations, except that frequencies higher than 200 khz were not recorded with the present system because of its extremely sharp high frequency cutoff. On the other hand, the lower frequency Type II signals were only tentatively observed in the preliminary investigations due to their rare occurrence. An estimated 10^5 Type I events were recorded during the experiment, compared to only approximately 10^2 of the Type II.

Consider next the possible mechanisms that might be responsible for these signals. It has been shown in ~~Chapter 1~~ that microfracturing, as the name implies, is a process involving the formation of small cracks in rock under stress. The length of such cracks would be expected to be

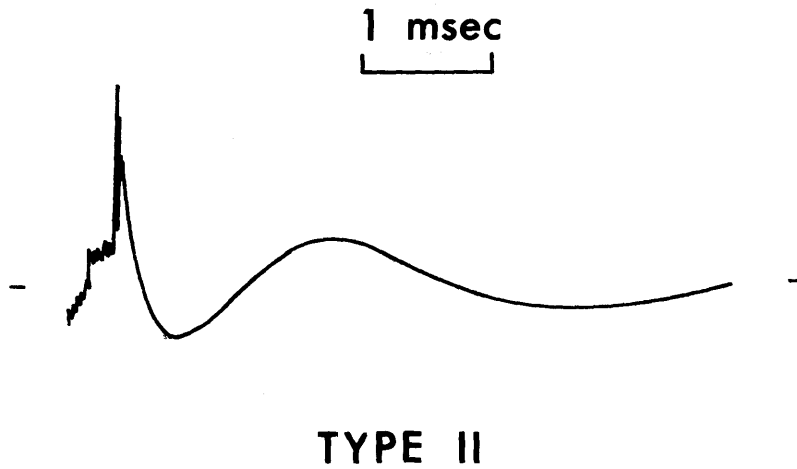
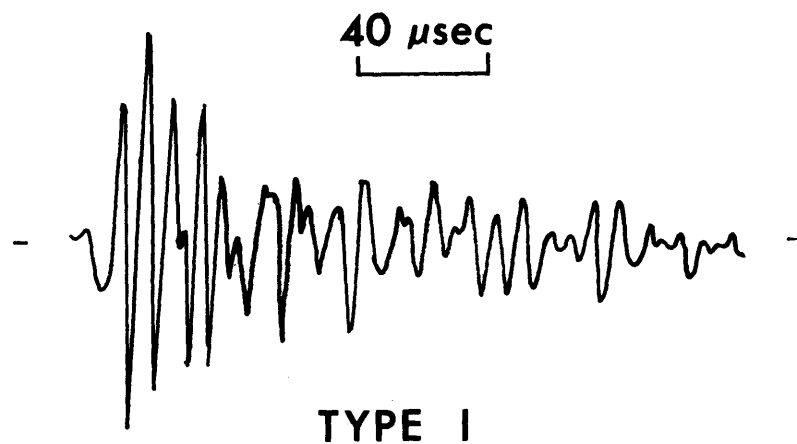


FIGURE 24. The two types of signals observed in microfracturing studies. The figures are tracings from oscilloscope photographs.

in the order of a grain diameter, say 1 mm. An estimate of the propagation time of a crack of these dimensions in a brittle material, making the approximation that it travels at an average of about half the Rayleigh wave velocity, is only a few microseconds. The main energy radiated by such a short-lived disturbance will be at quite high frequencies. In seismic modeling experiments, for example, Savage and Mansinha [1963] studied the elastic radiation from cracks of this size produced in glass plates. They found that most of the energy received from these sources was at about 100 khz. In the light of these observations, it is suggested that microfracture propagation is the mechanism responsible for the high frequency Type I events. This is verified below, when on the basis of this assumption, solutions for source locations were made which were well behaved and yielded wave velocities which agree with known values.

There remains the question of the origin of the Type II signals. The waveform of these events (see Figure 24) is characterized by a very fast initial rise, followed by a decaying sinusoid of low frequency. Superimposed on the initial rise are often oscillations of much higher frequencies, in the range typical of Type I events. In the related study [Chapter 1] we demonstrated that each microfracturing event (i.e. Type I) produces a small increment of strain which in total is responsible for the inelastic macroscopic stress-strain properties of rock. If examined in suf-

ficient detail, then, a stress-strain curve for rock would not be continuous, but would be punctuated by a series of strain jumps, each corresponding to a microfracturing event. The resulting signal produced by an event which occurs close to a transducer may then be a superposition of the response of the transducer to the elastic waves radiated by the propagating crack and to a displacement jump at the free surface. The Type II waveform is in fact what would be expected as the response of an accelerometer with poor low frequency response to a displacement step function (A. Gangi, personal communication, 1967). It represents primarily a "ringing" of the transducer below its resonant frequency. Unlike Type I events, the Type II signals are usually only recorded at one transducer.

A considerable amount of work has been done by previous investigators on elastic radiations emitted from rock during deformation. The detection systems used in previous work, however, were all limited to the audio frequency range or less [e.g. Mogi, 1962a]. Consequently, in the light of the above observations, the previous work was probably limited to studies of the Type II events. The previous workers, for example Watanabe [1963], reported that approximately 10^2 events were detectable during a compression test, which agrees with our observations for Type II events. In our statistical studies we used a system with a much higher frequency response, and 10^5 to 10^6 events could be detected and

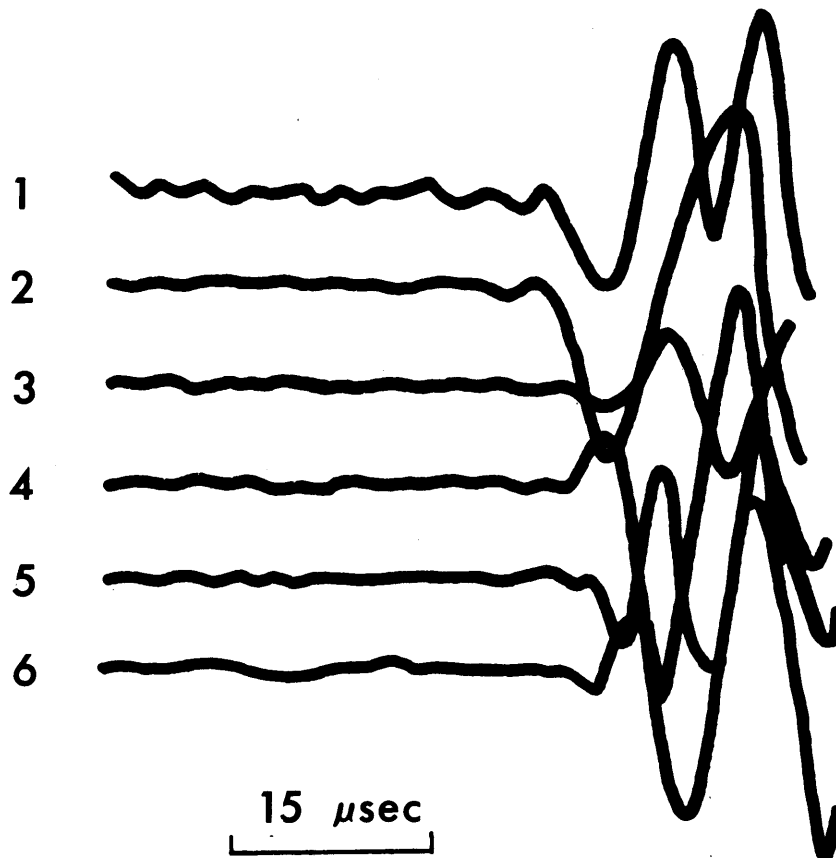


FIGURE 25. Tracings from oscilloscope photographs of the first arrivals at the six transducers. Arrival time corrections have been included. The numbers to the left refer to the transducer numbers shown in figure 23.

analyzed during the course of an experiment. In those investigations, we were detecting nearly all the events, rather than simply those which occurred near a transducer.

Source locations. Using the method described above, relative arrival times at each transducer were determined for a number of the larger events. Source locations were calculated with a least squares technique, using a uniform velocity model. The method of solution is described more fully in Appendix III. P wave arrivals were found to be indistinct and often absent in the records, so S wave arrivals were used for the solutions. An example of the first arrivals is shown in Figure 25.

A total of 22 events were located with this procedure. The results are given in Table 8 in order of decreasing stress. The absolute and normalized stresses at which the events occurred are known only to within a few percent, but the stress differences between successive events are quite accurate. The latter were obtained by dividing the stress interval over which recording was done by the length of tape used, and locating each event on tape. The locations reported are referred to a set of Cartesian coordinates with its origin at the center of the specimen, as shown in Figure 23. The locations are accurate to within 3 mm, and have been checked by calculating station errors from the difference between the calculated and observed arrival times at each transducer. The solutions yielded velocities between

TABLE 8. Source Locations for Selected Microfracturing
Events

Tape Code	Stress, σ , kb.	σ/C	x cm.	y cm.	z cm.
83	2.67	.998	-.49	.16	-.01
86	2.65	.990	.32	.56	1.35
88	2.62	.978	-.25	.08	1.24
92	2.59	.968	-.00	.00	.14
93	2.58	.965	.00	.00	.93
94	2.57	.963	.20	-.31	.64
95	2.56	.960	-.71	.00	-1.86
99	2.52	.945	.20	.54	.53
100	2.51	.940	-.12	1.08	1.66
103	2.48	.925	-.36	-.28	-2.47
104	2.47	.920	.27	.63	.51
114	2.35	.880	.08	.57	1.46
116	2.33	.870	.13	.52	2.02
117	2.32	.866	.00	.00	.38
120	2.28	.852	.27	-.82	1.86
126	2.21	.830	-.31	1.04	1.69
128	2.19	.816	.66	-.69	-1.30
129	2.18	.812	-.31	.08	-1.24
136	2.09	.780	-.45	.00	-1.12

TABLE 8. cont.

Tape Code	Stress, σ , kb.	σ / C	x cm.	y cm.	z cm.
143	2.00	.748	.32	1.43	5.30
146	1.97	.738	-.63	.33	1.48
147	1.95	.730	1.17	.91	-1.41

about 3.0 and 3.5 km/sec, which agrees with the measured S wave velocities of Simmons [1964] for this rock.

The results show that the events are concentrated within the central section of the specimen, rather than near the ends as would be expected if stress concentrations due to end effects were important. Only one event, no. 143, originated at the rock-steel interface at the end of the specimen.

It has been found in Chapter 10 that microfracturing due to the propagation of cracks typically begins at about half the breaking strength, \underline{C} , and accelerates steadily until about 0.9 to 0.95 \underline{C} , when a very rapid increase in activity occurs. In conjunction with that work, a statistical model of rock deformation was introduced and found to adequately predict the observed behavior. A hypothesis of random independence of the microfracturing events was tested against the experimental results, and it was concluded that the events that occur below the point of rapid acceleration of activity could be considered independent, whereas those above it could not. The processes that occur in these two regions of stress were termed static and dynamic cracking, respectively. In order to clarify this view, the located events were divided into two groups, approximately according to in which of these regions they occurred.

The locations of events that occurred in the static and dynamic regions, respectively, are shown in Figures 26

and 27. The diagrams show the central 7.5 cm section of the specimen in front, top, and side views with respect to the fault which eventually led to fracture. The fault trace is shown as a dashed line. The group that occurred in the static cracking region, events 114 through 147, appear to be scattered throughout the body. There is some clustering evident, however. A region about a third the way up from the center of the specimen and a region about halfway down from the center are marked by a number of closely spaced events. The events in either of these clusters, however, were not related closely in time and the regions did not seem to correspond to areas of pronounced deformation which could be distinguished in visual examination of the specimen. Certainly, they show little relation to the fault. The strongest clustering, in the upper region, may indicate a bias in the sampling procedure. Sampling was done from the output of transducer 3 on an amplitude basis. Therefore the events sampled for study may be biased toward those which occurred near this transducer. At any rate, in view of the small number of events located, little significance can probably be placed on this clustering.

In any event the distribution in Figure 26 differs markedly from that in the dynamic cracking region (Figure 27). The events in the dynamic region group tightly on a plane which corresponds closely with the observed fault. This clustering is tightest in the section of the fault on the positive y

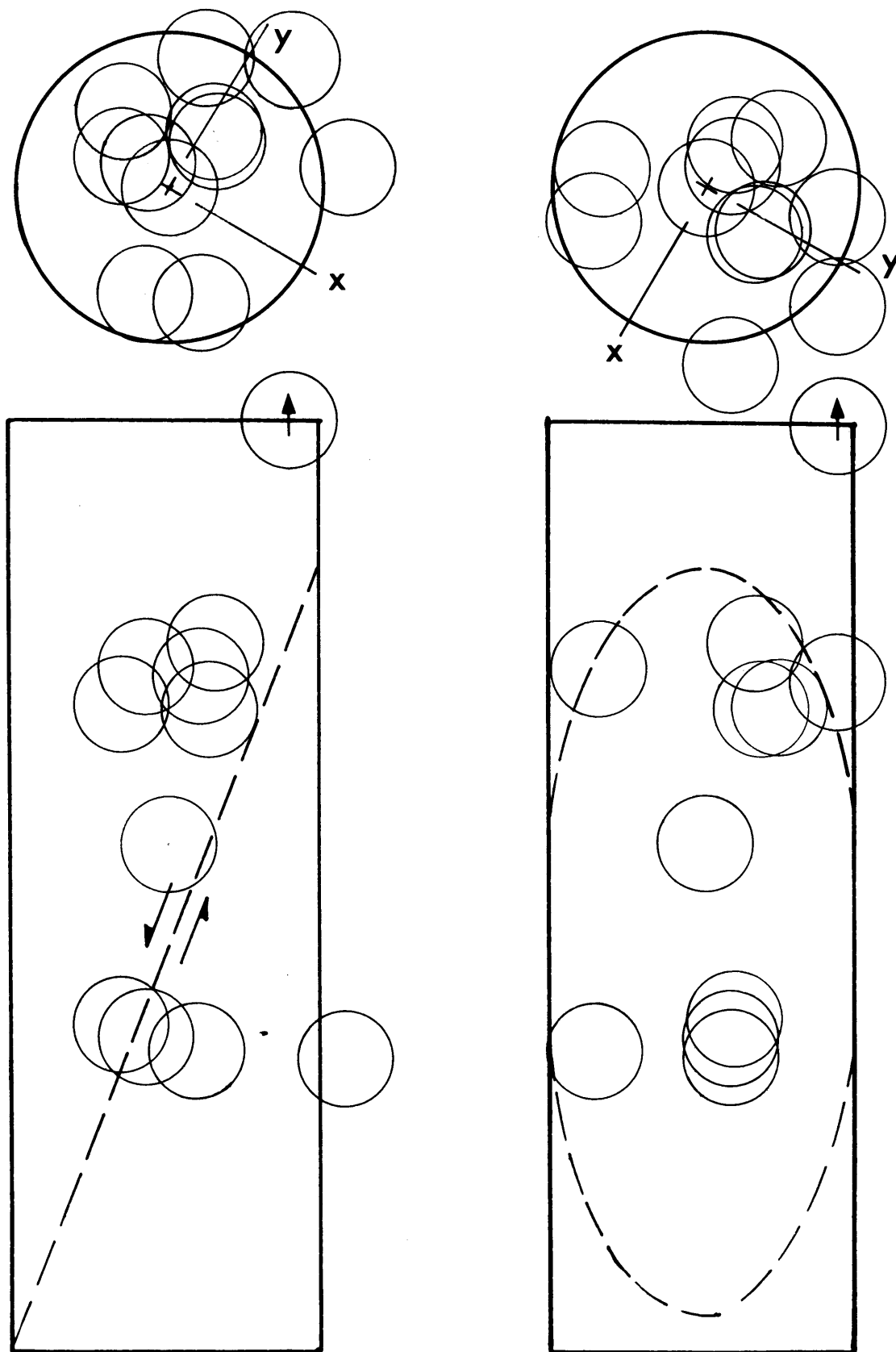


FIGURE 26. Front, top, and side views of the central section of the sample showing locations of the events which occurred in the static cracking region. The fault trace is given by the dashed line.

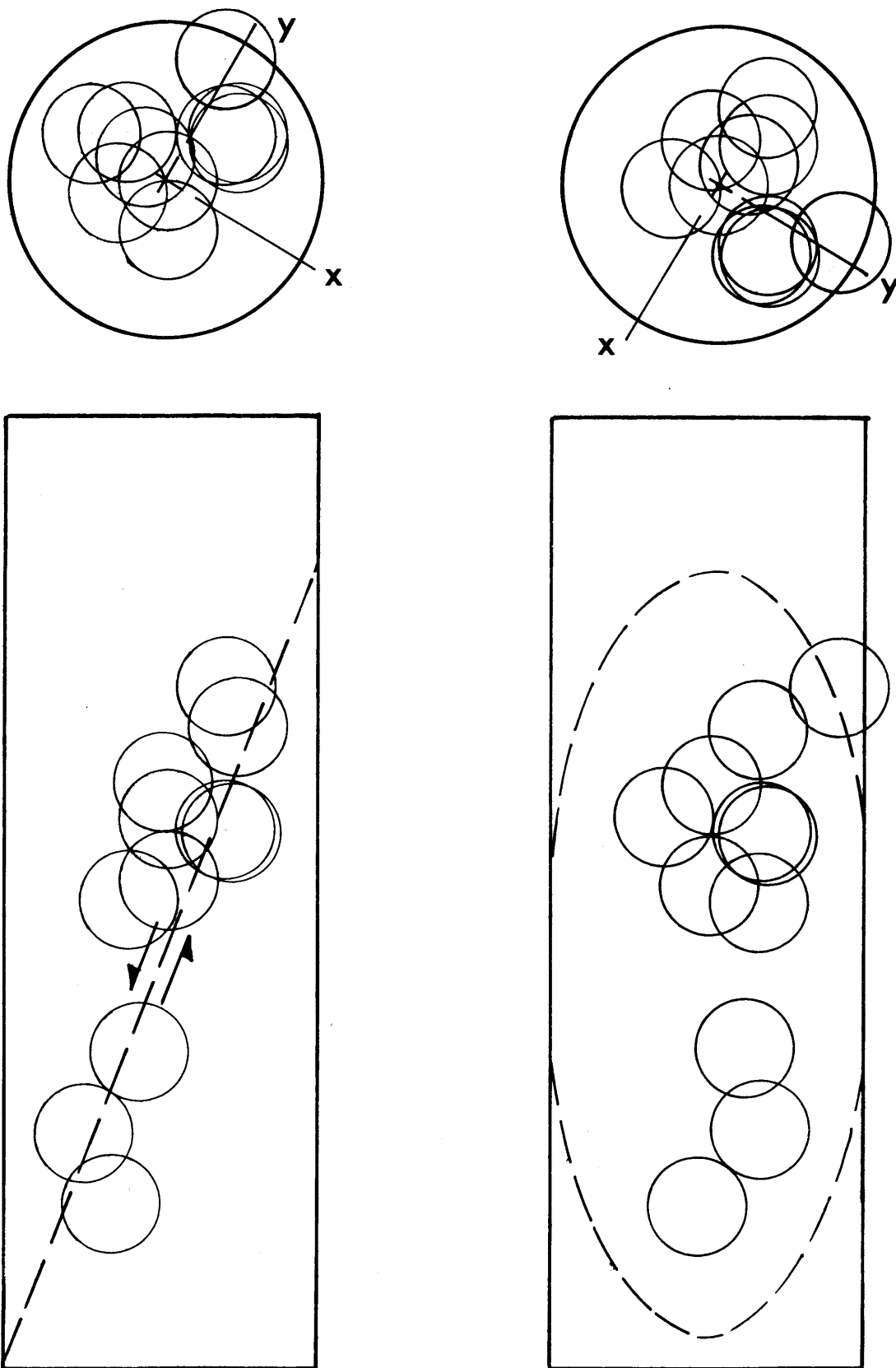


FIGURE 27. The same figure as Figure 26 showing the location of events which occurred in the dynamic cracking region.

side of the xz plane from z equals 0 to 2 cm. This may be again due to biased sampling. The strong correlation of the events with the fault plane, in contrast to the events in the static crack region, suggests that these events are related to the formation of the fault.

Discussion

The marked clustering of events in the dynamic cracking region on the plane on which faulting eventually takes place provides some insight into the brittle fracture process. It suggests that microfractures in that region are not independent, but as stress approaches the fracture strength they begin to coalesce in some way to form the fault. Evidently there is a critical stress above which cracks interact in some way to partially fault the specimen, but this fault does not become unstable immediately. There is no apparent progression in time of events from one end of the fault to the other, but they tend to cluster more strongly in one region. This region may be the point of weakness which concentrated microfracturing on the fault plane.

In contrast, the locations found in the static cracking region show only a weak clustering. With the present evidence it is not possible to confirm the statistical evidence that they are independent. Certainly they appear to be unrelated to the fault.

From the present observations, it would appear that if

it were possible to continuously monitor and locate microfracturing events during a fracture experiment, we would be able to predict the approximate time and place that faulting of the sample would take place. If we extend the concepts of Mogi regarding the similarity of microfracturing events observed in the laboratory and earthquakes, it might be expected that the seismic activity preceding large earthquakes is similar to that observed prior to rock fracture. Foreshocks often occur from a few hours to a few days prior to major earthquakes. They are usually spatially related to the main shock, and recent studies [Stauder and Bollinger, 1966; Stauder, 1967] have shown that they may have the same mechanism as the main shock. Usually only a few foreshocks are of sufficient magnitude to be detected, so they cannot be established as foreshocks until after the main shock. If foreshocks occur prior to the main shock in a similar way that microfractures occur prior to fracture as we have observed, a method of earthquake prediction is suggested by our results.

Oliver et. al. [1966] and Brune and Allen [1967] have found that microearthquake activity may possibly be used to indicate the gross seismicity of a region. The present results suggest that if continuous microearthquake monitoring is done in a seismically active region, the occurrence of (1), a marked increase in activity, and (2), spacial clustering of shocks, may indicate an impending major earthquake.

The present results are not totally conclusive, particularly with respect to the activity in the static cracking region. In order to clarify the processes occurring there, a larger number of events must be studied and their locations determined more precisely. An original purpose of this study was to determine the mechanism of individual events. Due to the poor P wave data, however, it was not possible to determine P wave radiation patterns. It would be interesting to know, for example, if the mechanisms of the events which line up on the fault in the dynamic cracking region are the same as that for the main fracture. The answers to such questions are of great importance both to earthquake prediction and to our knowledge of rock fracture.

CONCLUSIONS

Since we have made in each chapter detailed conclusions with regard to the subject matter of that chapter, we shall in this section simply make a brief summary of the results of the study.

The experimental results have shown that microfracturing is a very basic and well defined property of brittle rock. The inelastic properties of brittle rock at high stress difference are almost entirely attributable to microfracturing. The microfracturing that occurs during deformation results in an inelastic increase of volumetric strain. The effect of microfracturing on all components of macroscopic strain is analogous to that produced by the closing of cracks at low stresses. The closing of cracks also produces elastic radiations which can be detected. This activity disappears at moderate stress and actual microfracturing due to the propagation of cracks begins at about half the fracture stress difference and steadily accelerates as stress is raised. Just prior to fracture, however, a rapid acceleration of activity occurs which has been traced to the coalescence of microfractures to form the fault.

Microfracturing that accompanies frictional sliding and the deformation of ductile rock is distinctly different from that observed in brittle rock. Cataclastic deforma-

tion and frictional sliding were shown to be quite similar with respect to the microfracturing which accompanies them. A ductile rock, as pressure was raised, was found to undergo a gradual transition from cataclastic to fully plastic flow.

Although an entirely new experimental technique was used which allowed a study to be made of microfracturing in a much greater depth of detail than had been done previously, the results of earlier workers were by and large verified. In particular, the observations of Mogi and Vinogradov on the frequency-magnitude relation of microfractures were verified and expanded. Partly to clarify Mogi's ideas on the similarity of microfractures and earthquakes, theoretical studies of the microfracturing process were made. The approach was to attempt to define the basic properties of an inhomogeneous brittle medium by the methods of statistical strength theory. Because both rock in the laboratory and on the scale of the earth's crust can be considered to be described by such a model, the theoretical results were applied in turn to both the experimental results and to observations which have been made on the statistics of earthquake occurrence. This work clarified the degree of similarity which could be expected between microfracturing and earthquakes and delineated the extent to which the experimental results may be carried over to explain earthquake behavior. The model also served to

clarify the extent to which the Griffith fracture theory is applicable to rocks.

In the light of earlier experimental evidence that creep in brittle rock at low temperature is a process of time dependent microfracturing, the theory was extended in the time domain by assuming that simple static fatigue is the mechanism of creep. The behavior predicted by this model was found to agree quite well with that observed experimentally.

This study was intended to outline the general characteristics of the microfracturing process on a fairly broad scope. Some topics, such as the frequency-magnitude relation, have been treated in detail whereas others, perhaps just as important, have merely been touched upon. Many of these latter aspects of microfracturing will require considerable further work before they will be completely understood. Numerous suggestions for such future studies have been included in the text.

ACKNOWLEDGEMENTS

This research was supported by NSF grant GA - 6B and by the Air Force Cambridge Research Laboratories, Office of Aerospace Research, United States Air Force, Bedford, Mass. through contract 19

I am especially indebted to W. F. Brace, who's constant interest provided continual stimulation during the course of this study. In addition, J. B. Walsh, Frank Press, M. Nafi Toksoz, K. Aki, A. Gangi, and John Fairborn made important suggestions. I would like to thank R. Reiker and K. Thompson of Air Force Cambridge Research laboratories for kindly allowing me the use of the tape recorder and amplification system which was employed in the location of events. The location solutions were made at the Massachusetts Institute of Technology Computation Center.

I would like to thank my wife, Paula, and son, Erich, for the forbearance and patience they showed during the more trying times of my graduate career.

BIBLIOGRAPHY

- Brace, W. F., and J. D. Byerlee, Stick-slip as a mechanism for earthquakes, Science, 153 (3739), 990-992, 1966.
- Brace, W. F., B. W. Paulding, and C. Scholz, Dilatancy in the fracture of crystalline rocks, J. Geophys. Res., 71 (16), 3939-3953, 1966.
- Brace, W. F., and E. G. Bombolakis, A note on brittle crack growth in compression, J. Geophys. Res., 68 (12), 3709-3713, 1963.
- Brace, W. F., and A. S. Orange, Electrical resistivity changes in saturated rock under stress, Science, 153 (3743), 1525-1526, 1966.
- Brune, J. N., and G. Allen, A microearthquake survey of the San Andreas fault system in Southern California, Bull. Seis. Soc. Am., 57 (2), 277-296, 1967.
- Brown, J. W., An investigation of Microseismic activity in rock under tension, M. S. Thesis, 84 pp. Pennsylvania State Univ., 1965.
- Byerlee, J. D., The frictional characteristics of Westerly granite, Ph. D. Thesis, 179 pp. Massachusetts Inst. of Technology, June, 1966.
- Byerlee, J. D., Frictional characteristics of granite under high confining pressure, J. Geophys. Res., 72 (4), 3639-3648, 1967.

- Charles, R. J., The strength of silicate glasses and some crystalline oxides, pp. 225-250, Fracture, Proc. Int. Conf. on Fracture, M.I.T. Press, Cambridge, 1959.
- Cottrell, A. H., Dislocation and plastic flow in crystals, Oxford, Clarendon Press, 223 pp., 1953.
- Davis, M., and N. Thompson, Creep in a precipitation-hardened alloy, Proc. Phys. Soc., B 63, 847-860, 1950.
- Franklin, J. A., The influence of the testing machine on the generation of acoustic emission, M. Sc. Thesis, 104 pp. Univ. of London, 1965.
- Glathart, J. L., and F. W. Preston, Fatigue modulus in glass, J. Appl. Phys., 17 (3), 189-195, 1946.
- Gold, L. W., The cracking activity in ice during creep, Canad. J. Physics, 38 (9), 1137-1148, 1960.
- Goodman, Richard E., Subaudible noise during compression of rocks, Geol. Soc. Amer. Bull., 74, 487-490, 1963.
- Griffith, A. A., Theory of rupture, First Int. Cong. Appl. Mech., Delft, 55-63, 1924.
- Griggs, D. T., F. J. Turner, and H. C. Heard, Deformation of rocks at 500° to 800°C, Geol. Soc. Amer. Mem. 79, pp. 39-104, 1960.
- Gutenberg, B., and C. F. Richter, Seismicity of the Earth, Princeton Univ. Press, 273 pp., 1949.
- Heard, H. C., Transition from brittle to ductile flow in Solenhofen limestone as a function of temperature, confining pressure, and interstitial fluid pressure, Geol.

- Soc. Amer. Mem. 79, pp. 193-227, 1960.
- Hill, R., Mathematical Theory of Plasticity, Oxford, Clarendon Press, 356 pp., 1950.
- Hoek, E., and Z. T. Bieniawski, Brittle fracture propagation in rock under compression, Intl. J. Fracture Mech., 1 (3), 137-155, 1965.
- Konstantinova, A. G., The shape of elastic pulses accompanying rock breaking, Bull (Izv) Acad. Sci. U.S.S.R. Geophys. Ser. (4), 604-610. (Engl. Trans. AGU 421-426), 1959b.
- Konstantinova, A. G., Time distribution of elastic pulse energy during destruction of rocks, Bull (Izv) Acad. Sci. U.S.S.R. Geophys. Ser. (11), 1580-1592 (Engl. Trans. AGU 1056-1061), 1960.
- Konstantinova, A. G., The connection between the energy of elastic pulses generated in the destruction of solids and the stress and dimensions of the ruptures, Bull (Izv) Acad. Sci. U.S.S.R. Geophys. Ser. (1), 194-198 (Engl. Trans. AGU 135-137), 1962.
- Konstantinova, A. G., Use of the seismoacoustic method to study the heterogeneity of specimens, Bull. (Izv) Acad. Sci. U.S.S.R., Earth Phys. (1), 63-67 (Engl. Trans. AGU 37-40), 1966.
- Lanczos, G., Linear Differential Operators, Prentice Hall, Engelwood Cliffs, N.J., 492 pp., 1962.

- Malone, A. W., An experimental system for the laboratory study of acoustic emission from stressed rock, M. Sc. Thesis, 96 pp., Univ. of London, 1965.
- Matsushima, S., Variation of the elastic wave velocities of deformation and fracture under high pressure, Disaster Prevention Res. Inst., Kyoto Univ., Bull. 32, 1-8, 1960a.
- Matsushima, S., On the flow and fracture of igneous rocks, Disaster Prevention Res. Inst., Kyoto Univ., Bull. 36, 2-9, 1960b.
- McEvilly, T. V., and K. B. Casaday, The earthquake sequence of September, 1965 near Antioch, California, Bull. Seis. Soc. Am., 57 (1), 113-124, 1967.
- Mogi, K., Some precise measurements of fracture strength of rocks under uniform compressive stress, Felsmech. Ingenieurgeol., IV (1), 41-55, 1966.
- Mogi, K., Study of the elastic shocks caused by the fracture of heterogeneous materials and its relation to earthquake phenomena, Bull. Earthquake Res. Inst., 40, 125-173, 1962a.
- Mogi, K., Magnitude frequency relation for elastic shocks accompanying fractures of various materials and some related problems in earthquakes, Bull. Earthquake Res. Inst., 40, 831-853, 1962b.
- Mogi, K., The fracture of a semi-infinite body caused by an inner stress origin and its relation to earthquake phenomena, 1st paper, Bull. Earthquake Res. Inst., 40, 815-829, 1962c.

- Mogi, I., The fracture of a semi-infinite body caused by an inner stress origin and its relation to earthquake phenomena, 2nd paper, Bull. Earthquake Res. Inst., 41, 595-614, 1963a.
- Mogi, K., Some discussion of aftershocks, foreshocks, and earthquake swarms -- the fracture of a semi-infinite body caused by an inner stress origin and its relation to earthquake phenomena, 3rd paper, Bull. Earthquake Res. Inst., 41, 615-618, 1963b.
- Mogi, K., Some discussions on earthquake phenomena from the standpoint of fracture theory, in geophysical papers dedicated to Prof. Kenso Sassa, Tokyo, pp. 315-321, 1963c.
- Mott, N. F., and F. R. N. Nabarro, Dislocation Theory and transient creep, Report on strength of solids, Phys. Soc., London, 1-19, 1948.
- Mould, R. E., and R. D. Southwick, Strength and static fatigue of abraded glass under controlled ambient conditions, II Effect of various abrasions and the universal fatigue curve, J. Am. Cer. Soc., 42 (12), 582-592, 1959.
- Obert, L., Use of subaudible noise for prediction of rockbursts, U. S. Bur. Mines Rept. Inv. 3555, 10 pp. 1941.
- Obert, L., and W. Duvall, Use of subaudible noise for prediction of rockbursts, U. S. Bur. Mines Rept. Inv. 3634, 13 pp., 1942.
- Obert, L., and W. Duvall, Microseismic method of predicting rock failure in underground mining, Pt. 1, general method, U. S. Bur. Mines Rept. Inv. 3796, 26 pp., 1945a.

- Obert, L., and W. Duvall, The microseismic method of predicting rock failure in underground mining, Pt. 2, laboratory experiments, U. S. Bur Mines Rept. Inv. 3803, 14 pp. 1945b.
- Obert, L., and W. Duvall, Microseismic method of determining the stability of underground openings, U. S. Bur. Mines Rept. Inv. 5731, 17 pp., 1957.
- Obert, L., and W. Duvall, Seismic methods of detecting and delineating subsurface subsidence, U. S. Bur. Mines Rept. Inv. 5882, 12 pp., 1961.
- Oliver, J., A. Ryall, J. N. Brune, and D. B. Slemmons, Microearthquake activity recorded by portable seismographs of high sensitivity, Bull. Seis. Soc. Am., 56 (4), 899-924, 1966.
- Parzen, E., Stochastic Processes, Holden-Day, San Francisco, 324 pp., 1962.
- Richter, C. F., Elementary Seismology, Freeman and Co., San Francisco, 520 pp., 1958.
- Robertson, E.C., Creep in Solenhofen limestone, Geol. Soc. Am. Mem. 79, pp. 227-244.
- Robertson, E. C., Viscoelasticity of rocks in state of stress of the earth's crust, W. R. Judd ed., American Elsevier Publishing Company, New York, pp. 181-234, 1964.
- le Roux, Haydee, The strength of fused quartz in water vapour, Roy. Soc. Lon. Proc. Ser. A 286, pp. 390-401, 1965.
- Savage, J. C., and L. Mansinha, Radiation from a tensile fracture, J. Geophys. Res., 68 (23), 6345-6350, 1963.

- Schmitz, G. K., and A. G. Metcalfe, Stress corrosion in E glass fibers, Ind. Eng. Chem. Prod. Res. and Dev., 5 (1), 1-8, 1966.
- Scott, Ronald F., Principles of Soil Mechanics, Addison Wesley, Reading, Mass., 550 pp., 1963.
- Shoemaker, P.S., Acoustic emission, an experimental method, M.S. Thesis, 122 pp., Michigan State Univ., 1961.
- Simmons, Gene, Velocity of shear waves in rocks to 10 kilobars, 1, J. Geophys. Res., 19 (6), 1123-1130, 1964.
- Smith, S., G. Sammis, and W. Jackson, Microearthquake source dimensions and energy release, Trans. AGU, 48 (1), 201, (abstract), 1967.
- Stauder, W., and G. A. Bollinger, The focal mechanism of the Alaska earthquake of March 28, 1964 and of its aftershock sequence, J. Geophys. Res., 71 (22), 5283-5296, 1966.
- Stauder, W., Seismic evidence of present deformation in island arc structures, Trans. AGU, 48 (1), p. 218, 1967.
- Stuart, D. A., and O. L. Anderson, Dependence of ultimate strength of glass under constant load on temperature, ambient atmosphere, and time, J. Am. Cer. Soc., 36 (12), 416-424, 1953.
- Suzuki, Z., A statistical study on the occurrence of small earthquakes, Sci. Rept. Tohoko Univ. Geophys. Ser., 11 (1), 10-54, 1959.

- Vinogradov, S. D., Acoustic observations in collieries of the Kizelsk coal basin, Bull. (IZV) Acad. Sci. U.S.S.R. Geophys. Ser. No. 4, 1957.
- Vinogradov, S. D., On the distribution of the number of fractures in dependence on the energy liberated by the destruction of rocks, Bull. (IZV) Acad. Sci. U.S.S.R. Geophys. Ser. (12), 1850-1852, (Engl. Trans. AGU 1292-1293), 1959a.
- Vinogradov, S. D., Elastic impulses originating in a massif under pressure, Bull. (IZV) Acad. Sci. U.S.S.R. No. 2, 1959b.
- Vinogradov, S. D., Experimental study of the distribution of the number of fractures in respect to the energy liberated by the distruction of rocks, Bull. (IZV) Acad. Sci. U.S.S.R. Geophys. Ser., 171-180, (Engl. Trans. AGU 119-125), 1962.
- Vinogradov, S. D., Acoustic observations of rock bursts in the Anna Lead Mine, Czechoslovakia, Bull. (IZV) Acad. Sci. U.S.S.R. Geophys. Ser. No. 4, 1963.
- Volkov, S. D., Statistical Strength Theory, Gordon and Breach, New York, 267 pp., 1962.
- Walsh, J. B., The effect of cracks on the uniaxial elastic compression of rocks, J. Geophys. Res., 70 (2), 399-411, 1965a.
- Walsh, J. B., The effect of cracks on the compressibility of rock, J. Geophys. Res., 70 (2), 381-389, 1965b.

Walsh, J. B., The effect of cracks in rocks on Poisson's ratio, J. Geophys. Res., 70 (20), 5249-5258, 1965c.

Walsh, J. B., and W. F. Brace, Elasticity of rock: a review of some recent theoretical studies, Felsmech. Ingenieurgeol. IV (4), 283-297, 1966.

Watanabe, H., The occurrence of elastic shocks during destruction of rocks and its relation to the sequence of earthquakes in geophysical papers dedicated to Prof. Kenzo Sassa, Tokyo, pp. 653-658, 1963.

APPENDIX I

END EFFECTS

One of the topics of interest prior to beginning the main study was the influence of end conditions on microfracturing behavior. In a conventional compression test, the elastic mismatch between the piston and the end of the rock specimen produces shear tractions which alter the strength of the specimen [Mogi, 1966]. Depending on the sign of the traction, strength may be increased by clamping or decreased by splitting at the ends. In either case the end effects are likely to strongly influence microfracturing. An extensive study of end effects was recently made by Mogi [1966]. He found that end effects could be substantially reduced by use of specimens of a new design. It was partly to see if this type specimen was required for microfracturing studies that an investigation of end effects was made.

Two uniaxial compression tests were done on Westerly granite, one using the dogbone shaped specimen of Mogi, the other a conventional straight cylinder. Microfracturing was monitored during the experiments (Figure 28) and found to be quite different for the two specimens. The most striking difference is at low stresses, where an extremely high level of activity was observed in the straight cylinder test which was absent in the other. This activity was probably due to

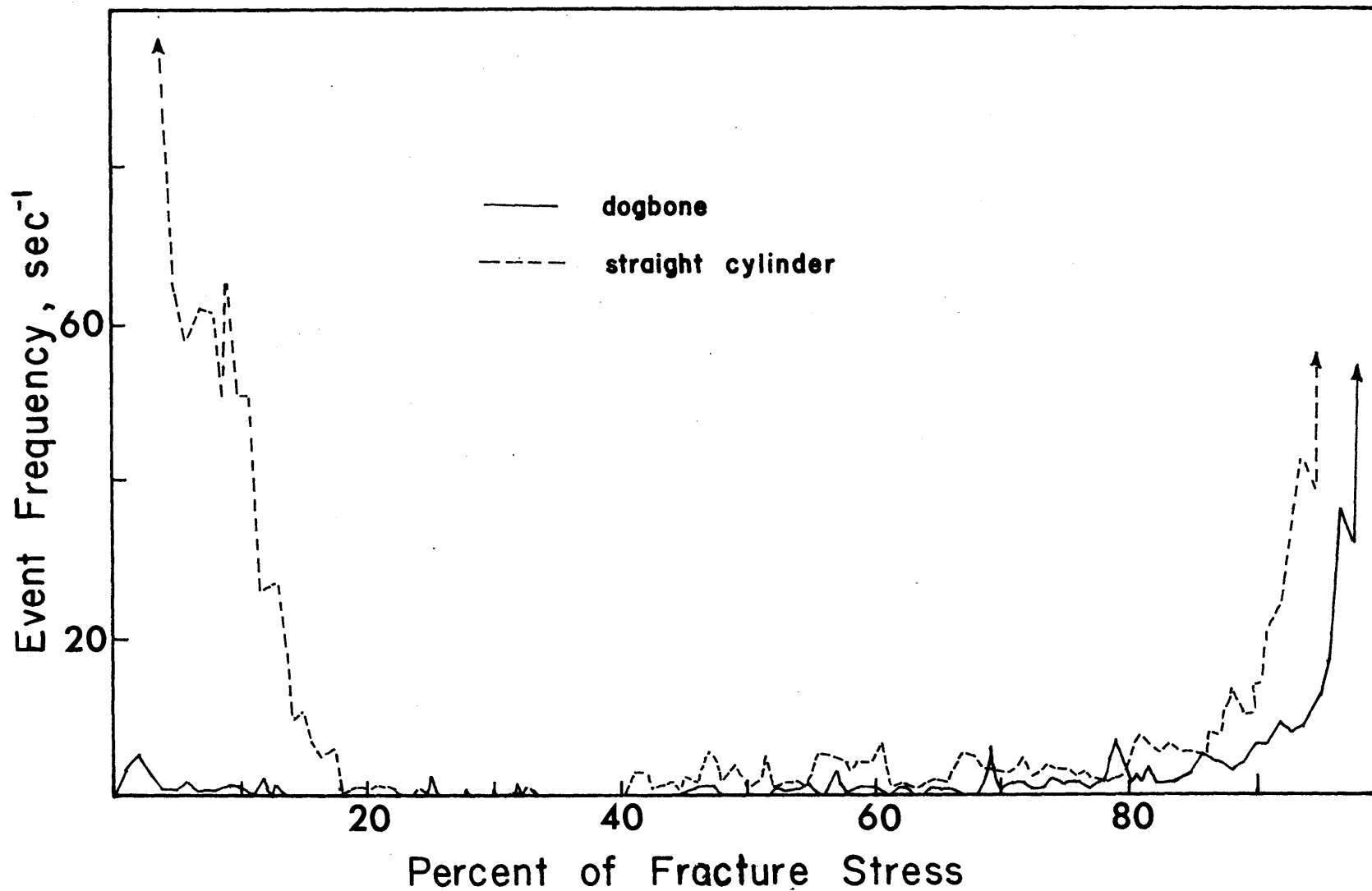


FIGURE 28. Microfracturing frequency vs normalized stress for the dogbone shaped specimen and for a conventional straight cylinder of Westerly granite fractured in uniaxial compression.

cracking and splitting at the corners of the ends of the specimen, which was also observed visually. These observations explain the anomalous results of Franklin [1965]. He studied microfracturing during uniaxial compression tests using conventional specimens and found that most of the activity occurred at low stresses.

Mogi also found that end effects in triaxial compression tests were absent. Since jacketing of the dogbone shaped specimens is difficult, it was of interest to see if conventional specimens were suitable for use in tests under confining pressure. Several triaxial tests were made using copper jacketed straight cylinders. Little or no microfracturing was observed in the low stress region during these experiments. The conclusions of Mogi regarding the influence of end effects on strength thus also are correct with respect to the microscopic fracture process. Therefore, the Mogi dogbone was adopted for uniaxial experiments whereas tests under confining pressure were made using conventional specimens.

APPENDIX II

PULSE SHAPER

In preliminary investigations it was determined that for the amplification and detection system used in the statistical studies that microfracturing signals are typically decaying sinusoids of period 2 to 3 μ sec and trainlength 10 to 100 μ sec. For input to the pulse height analyzer it was required that signals be negative pulses in the millivolt range with rise times from 0.1 to 1.0 μ sec and width at least 1 μ sec. Dead time (time after the arrival of a signal during which the analyzer will not count) is 20 μ sec for multiscaling and $40 + 0.2N$ μ sec, where N is the channel address, for pulse height analysis. Since the length of the pulse trains to be analyzed are often longer than the dead time, several counts would be actuated by a single signal. In addition, in pulse height analysis the amplitude is measured 1 μ sec after the initial rise. This would not in general be the maximum amplitude of the signal. In order to avoid these difficulties, the signal had to be shaped before admission to the analyzer.

A very simple circuit which is well suited to this application is the pulse stretcher. A schematic diagram of the circuit is shown in Figure 29. The device is essentially a half wave rectifier with two RC time constants.

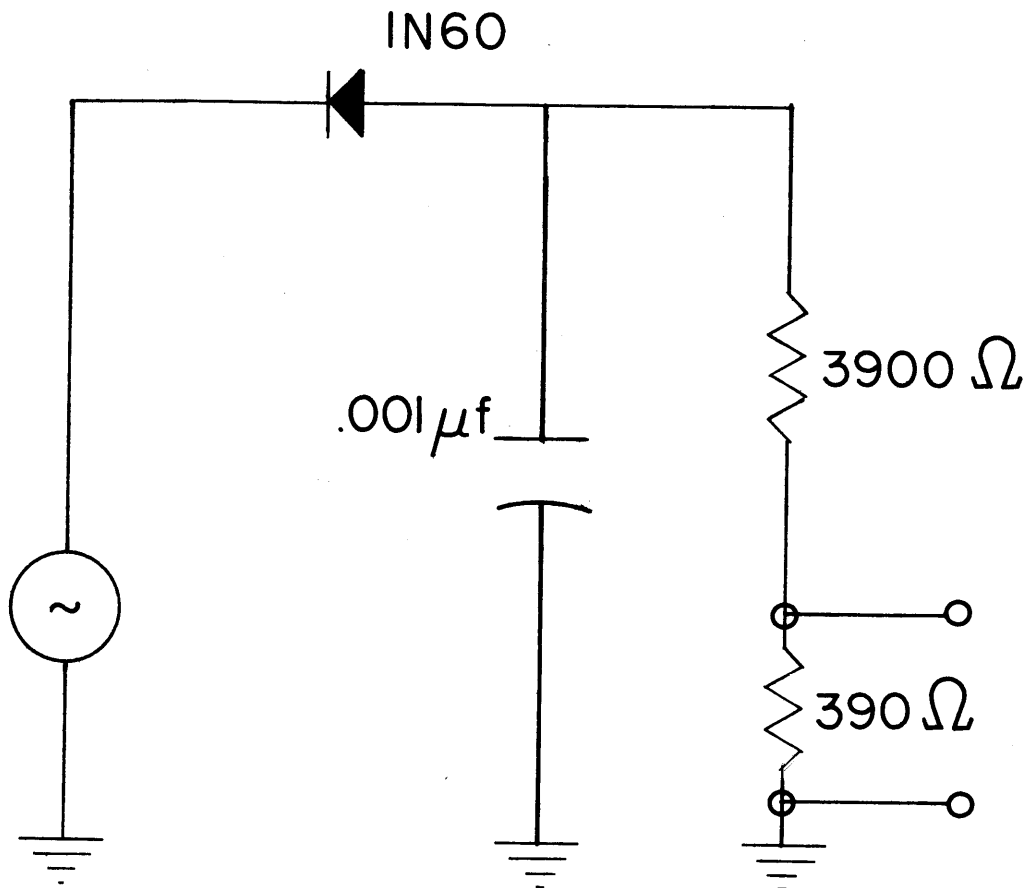


FIGURE 29. Schematic diagram of the shaping circuit.

The forward and reverse time constants are 0.2 and $5 \mu\text{sec}$, respectively, so that the device follows the initial rise with little distortion and peak to peak rectifies the rest of the pulse train. The resulting output is the envelope of the negative half of the signal.

Because the input to the shaper is into a diode, the signals had to be at a level of several volts. The attenuation necessary for admission to the analyzer was achieved with a simple voltage divider, shown in the schematic. Since the frequency content of the signals was observed to be fairly constant, such a purely resistive device was adequate. The diode in the circuit had another feature. The primary noise during the experiments was amplifier noise, which was very high frequency and fairly constant in level. This noise could be discriminated by simply reducing the gain until the noise level was just below diode cutoff. In pulse height analysis, consequently, the first few channels of information could not be used since they were in the nonlinear range of the diode.

APPENDIX III

METHOD FOR CALCULATING EVENT LOCATIONS

Suppose that an event occurs at a point x, y, z at time t . The arrival times of elastic waves are measured at six transducers in known locations. t_i is the arrival time at transducer i , located at x_i, y_i, z_i . Assuming a uniform velocity, v , these quantities are then related by the six equations

$$(x_i - x)^2 + (y_i - y)^2 + (z_i - z)^2 = [v(t_i - t)]^2 \quad (1)$$

Expanding equations 1 and collecting terms, we have

$$R_i^2 + R^2 - 2x_i x - 2y_i y - 2z_i z = v^2(t_i^2 - 2t_i t + t^2) \quad (2)$$

where

$$R_i^2 = x_i^2 + y_i^2 + z_i^2$$

If we now subtract the expression for transducer j from that of transducer i we obtain the set of equations

$$2(x_i - x_j)x + 2(y_i - y_j)y + 2(z_i - z_j)z + (t_i^2 - t_j^2)v^2 - 2(t_i - t_j)v^2t = R_i^2 - R_j^2 \quad (3)$$

which is a set of five equations in the five unknowns x, y, z, v, and t. If we consider v^2 and v^2t as the unknowns, we have a linear system in the form, in matrix notation

$$\underline{A} \underline{x} = \underline{b} \quad (4)$$

which can be readily solved. Due to the high relative errors of measurement, however, system 4 will not usually be compatible and solutions obtained by the usual method will not be well behaved. On the other hand if we multiply both sides of 4 by the transpose of A and then invert, the solution

$$\underline{x} = (\underline{A}^t \underline{A})^{-1} \underline{A}^t \underline{b} \quad (5)$$

will always be well behaved and will be the best solution in the least squares sense [Lanczos, 1962, p. 141]. This method was coded in Fortran II and the solutions obtained on an IBM 7094 computer. Matrix inversion was done with the gaussian elimination method.

In order to check the accuracy of the solution for each event, a station error at each transducer was calculated. This was done by finding the difference between the observed arrival time and the theoretical arrival time calculated from the solution of equation 5. This technique proved very useful in detecting erroneous first arrivals in low level signals.

APPENDIX IV

CREEP EXPERIMENTS

In Chapter 2 we derived an expression for transient creep of rock by extending the basic model to include the time dependence of microfracturing. In that analysis we found that the stress dependence of creep could be calculated from the results of the constant strain rate experiments reported in Chapter 1. In order to check that conclusion, a series of creep tests were performed using a sample of Westerly granite taken from the same block as that used in the constant strain rate experiments.

The tests were done in uniaxial compression in a conventional manner. The sample (Mogi's dogbone shaped specimen) was held at a series of constant stress levels with the same testing machine as used in the other studies. Stress was monitored during the experiments and maintained constant by manual adjustment. Strain in both axial and lateral directions was measured with electrical resistance strain gages in a similar manner to that used in the dilatancy study [Brace et al., 1966]. The strains were recorded with an Esterling Angus model strip chart recorder. The precision of measurement was 1×10^{-6} and the accuracy $\pm 2 \times 10^{-6}$. Unfortunately, it was not possible to monitor microfracturing during the experiments because the recorder employs a switch-

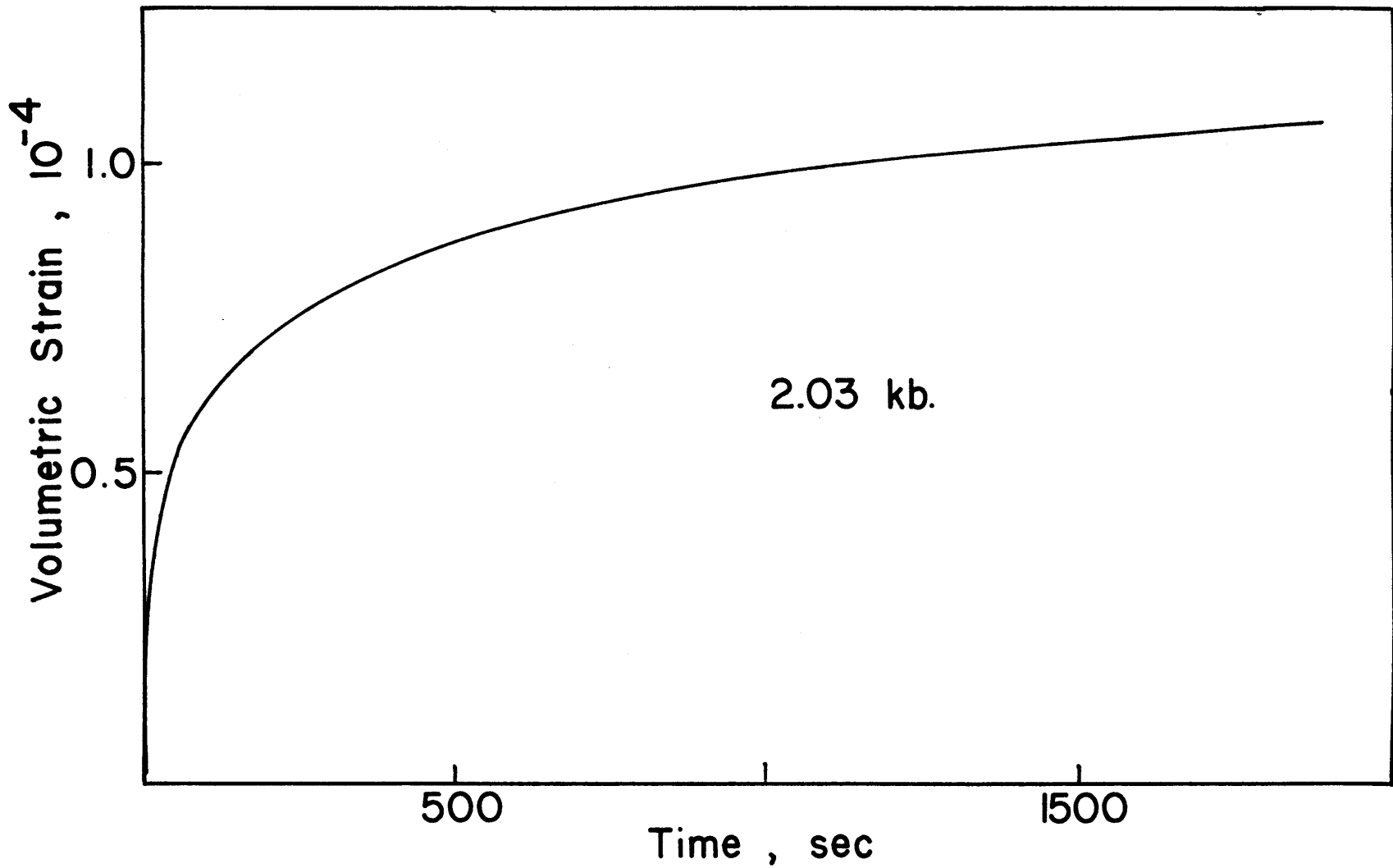


FIGURE 30. A typical volumetric creep curve obtained for Westerly granite in uniaxial compression. The curve is of transient (logarithmic) creep.

ing circuit which produced excessive interference.

Creep experiments with a duration of about 20 min were made at a series of successively higher stress levels. Volumetric creep strain was calculated for each of the experiments from the measured axial and lateral strains. A typical volumetric creep curve which was obtained is given in Figure 30. The stress dependence of volumetric creep rate has been given earlier in the main body of the thesis (Figure 17, Chapter 2).

BIOGRAPHY OF THE AUTHOR

I was born in February, 1943, at Pasadena, California, and was raised in the western part of the United States. I received my secondary education in Burlingame, California. My undergraduate studies were at the Mackay School of Mines, University of Nevada, where I received a B. S. in geological engineering in June, 1964.

My professional experience is as follows:

- 6/62 - 1/64 Physical Science Aid U. S. Bureau of Mines,
Reno Metallurgy Research Station, Reno, Nevada.
- 1/64 - 6/64 Research Assistant, Seismographic Station,
University of Nevada, Reno, Nevada.
- 6/64 - 9/64 Field exploration geologist, Hecla Mining Co.
Wallace, Idaho.
- 9/64 - 9/67 Research and Teaching Assistant, Massachus-
etts Institute of Technology, Cambridge, Mass.

Publications:

"Dilatancy in the Fracture of Crystalline Rocks",
J. Geophys. Res., 71 (16), 3939-3953, 1966. (with
W. F. Brace and B. W. Paulding).